

Connectivity analysis of the EHG during pregnancy and Labor

Noujoude Nader

▶ **To cite this version:**

Noujoude Nader. Connectivity analysis of the EHG during pregnancy and Labor . Signal and Image processing. UTC Compiègne; Université Libanaise (Liban), 2017. English. NNT : . tel-01544158

HAL Id: tel-01544158
https://hal.science/tel-01544158

Submitted on 23 Jun 2017

HAL is a multi-disciplinary open access archive for the deposit and dissemination of scientific research documents, whether they are published or not. The documents may come from teaching and research institutions in France or abroad, or from public or private research centers.

L'archive ouverte pluridisciplinaire **HAL**, est destinée au dépôt et à la diffusion de documents scientifiques de niveau recherche, publiés ou non, émanant des établissements d'enseignement et de recherche français ou étrangers, des laboratoires publics ou privés.

Noujoude Nader

« Sorbonne University, Université de technologie de Compiègne
Doctoral School « Sciences pour l'Ingénieur » and Lebanese University Doctoral School « Sciences et Technologie »

Titre:

Connectivity analysis of the EHG during pregnancy and Labor

Thèse Soutenue le 31-1-2017

Jury:

Régine LE BOUQUIN JEANNES	Prof. , Université de Rennes 1	**Reviewer**
Zaher DAWI	Prof., American University of Beirut	**Reviewer**
Sofiane BOUDAOUD	Assistant Prof., Université de Technologie de Compiègne	**Examiner**
Massimo MISCHI	Assistant Prof., Eindhoven University of Technology	**Examiner**
Mahmoud HASSAN	Dr., Université de Rennes 1	**Examiner**
Mohamad KHALIL	Prof., Université libanaise	**Supervisor**
Wassim FALOU	Prof., Université libanaise	**Co-Supervisor**
Catherine MARQUE	Prof., Université de Technologie de Compiègne	**Supervisor**

Université Libanaise
École Doctorale
Sciences et Technologies
Doyen

SORBONNE UNIVERSITES

COTUTELLE THESIS

To obtain the degree of Doctor in "**Computer Science**" issued by

Sorbonne University, Université de technologie de Compiègne
Doctoral School « Sciences pour l'Ingénieur »
and

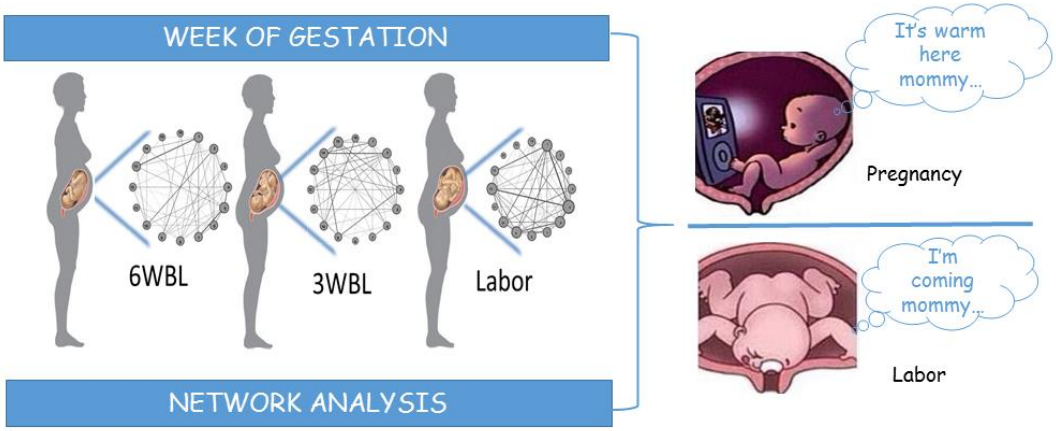
Lebanese University
Doctoral School « Sciences et Technologie »

Presented and publicly defended by

NADER Noujoud

31-1-2017

Title:



Connectivity analysis of the EHG during pregnancy and Labor

To…

RESUME FRANÇAIS

«Tout objet étudié par la biologie est un système de systèmes» (Jacob, 1976). Pour le système de systèmes complexe qu'est le corps humain, de nombreuses questions restent ouvertes, particulièrement en ce qui concerne l'utérus. Comment l'utérus fonctionne exactement? Comment reste-t-il au repos pendant la plus grande partie de la grossesse? Et comment se contracte-t-il d'une manière très organisée pendant le travail pour expulser un nouvel être humain dans ce monde? Les réponses à toutes ces questions pourraient sauver la vie de plus d'un million d'enfants qui sont morts parce que nés prématurément.

Donner naissance, ce miracle de la vie, peut se terminer tragiquement si l'enfant nait prématurément. En effet, l'accouchement prématuré survient quand une femme souffre de complications de sa grossesse et accouche avant la 37e semaine de gestation. Le risque de mortalité et de morbidité est le plus élevé pour les nouveau-nés qui naissent avant terme. La naissance d'un nouveau-né prématuré peut également entraîner des coûts économiques considérables et avoir des répercussions à court, moyen et long termes sur les services publics, tels que l'assurance maladie, l'éducation et d'autres systèmes de soutien social. Le fardeau économique social associé à la naissance prématurée était d'au moins 26,2 milliards de dollars en 2005 aux Etats-Unis (Behrman et al., 2007). Passer quelques jours de plus dans l'utérus peut cependant améliorer considérablement la maturation du fœtus. De ce fait, la détection précoce de l'accouchement prématuré est l'une des clés les plus importantes pour sa prévention et la diminution de ses conséquences.

L'un des marqueurs biologiques les plus prometteurs de la contraction utérine est l'activité électrique de l'utérus. Cette activité se reflète dans l'électrohystéogramme (EHG), qui représente la mesure non invasive de l'activité électrique utérine sur l'abdomen de la mère (Devedeux et al., 1993). Plusieurs études ont déjà été réalisées dans le contexte de la détection dude l'accouchement prématuré en analysant l'EHG (Euliano et al., 2009; Marque and Duchene, 1989; Planes et al., 1984). En fait, L'EHG est l'un des rares indicateurs accessibles de manière non-invasive, représentatifs de l'activité musculaire sous-jacente aux contractions utérines.

Le travail et l'accouchement sont précédés de deux phénomènes physiologiques: l'augmentation de l'excitabilité utérine et l'augmentation de la connectivité entre les cellules myométriales, suite à l'augmentation de la propagation du potentiel d'action initiateurs des contractions utérines (Devedeux et al., 1993).

Plusieurs études ont été réalisées pour caractériser la propagation utérine en étudiant la synchronisation entre les signaux EHG enregistrés à la surface de l'abdomen. Ces études se sont fondées sur différentes méthodes telles que: i) la connectivité/corrélation entre EHG (Euliano et al., 2009; Mahmoud Hassan et al., 2010; Marque and Duchene, 1989) où les méthodes ont été appliquées sur les contractions utérines segmentées manuellement, ii) la vitesse de propagation, quantifiée par analyse soit de la propagation du signal EHG entier (Lucovnik et al., 2011) (Mikkelsen et al., 2013), soit de pics isolés dans les bouffées d'EHG (Lucovnik et al., 2011; C. Rabotti et al., 2010)(Lau et al., 2014)(de Lau et al., 2013). L'analyse basée sur les pics isolés (en utilisant souvent des électrodes de petite taille) permettrait d'analyser plus précisément le processus de diffusion électrique.

L'analyse de connectivité a donné des résultats prometteurs en utilisant les signaux EHG pour l'identification du couplage statistique entre les contractions utérines enregistrées pendant le travail et/ou la grossesse, s'intéressant ainsi à la synchronisation globale de l'activité contractile., L'objectif principal de cette thèse est d'étudier cette synchronisation globale de l'activité électrique utérine en étudiant la connectivité entre différentes voies d'EHG enregistrées au cours de la grossesse et de l'accouchement. Concernant l'analyse globale, dans la plupart des études précédentes, les matrices de corrélation ont été réduites en ne gardant que leurs moyennes. Malgré les résultats encourageants obtenus, des informations pertinentes peuvent être manquées du fait de cette procédure de moyennage, ce qui peut expliquer les taux de classement relativement faibles obtenus jusqu'à présent. Pour caractériser précisément la matrice de corrélation et quantifier la connectivité associée, nous avons utilisé ici l'analyse basée sur la théorie des graphes., Ce type d'analyse, basée sur la théorie des graphes dans la caractérisation des matrices de corrélation (connectivité), s'est particulièrement développée récemment, notamment pour l'analyse des signaux électroencéphalographiques (EEG) (Bullmore and Sporns, 2009; Rubinov and Sporns, 2010; van den Heuvel and Sporns, 2013).

Intuitivement, un graphe peut être défini par un ensemble de nœuds connectés par des arrêtes. En utilisant l'analyse de graphe, la matrice de corrélation peut être représentée sous forme d'un graphe constitué d'un ensemble de noeuds (électrodes) interconnectés par des arêtes (valeurs de connectivité / corrélation entre les signaux recueillis par les électrodes).

Deux approches principales ont été utilisées dans cette thèse: i) L'estimation de la connectivité au niveau de l'abdomen (électrodes) et ii) L'estimation de la connectivité au niveau de la source utérine (après localisation des sources). Le schéma complet du travail de thèse est présenté figure 0.1.

Tout d'abord, les signaux EHG ont été enregistrés pendant la grossesse et le travail en utilisant une grille de 4 * 4 électrodes (Figure 0.1 A). Afin d'analyser ces signaux, nous avons étudié la corrélation (connectivité) entre les activités électriques utérines et leur quantification précise en se basant sur une nouvelle approche : la théorie des graphes. Les étapes suivies dans cette procédure sont les suivantes: (i) Estimation de la connectivité entre les signaux EHG (Figure 0.1 B) ; (ii) Quantification des matrices de connectivité obtenues à l'aide de la théorie des graphes (Figure 0.1 E) ; iii) Application clinique des mesures de graphe pour la surveillance de la grossesse ainsi que pour la classification entre grossesse et travail (Figure 0.1 E). Une comparaison avec les paramètres classiques de l'état de l'art pour la détection du travail prématuré a également été effectuée.

Pour s'affranchir du problème du volume conducteur dans l'estimation de la connectivité au niveau de la surface abdominale, nous avons proposé une nouvelle méthode appelée «connectivité des signaux EHG au niveau de la source» (Figure 0.1 C, D). Cette méthode consiste à identifier par méthode inverse les signaux des sources utérines puis à calculer le couplage statistique entre ces sources. Comme cette nouvelle méthode comprend deux étapes (identification des sources et analyse de conenctivité) pour lesquelles il n'existe pas de données bibliographiques sur les meilleures méthodes inverse/connectivité à utiliser pour l'EHG, nous avons analysé l'effet i) de l'algorithme utilisé dans la solution du problème inverse EHG et ii) de la méthode utilisée pour l'estimation de la connectivité, en utilisant des données simulées à partir d'un modèle biophysique développé dans l'équipe. Ensuite, comme au niveau de la surface, les matrices de connectivité obtenues au niveau source seront quantifiées en utilisant l'analyse basée sur la théorie des graphes (Figure 0.1 E).

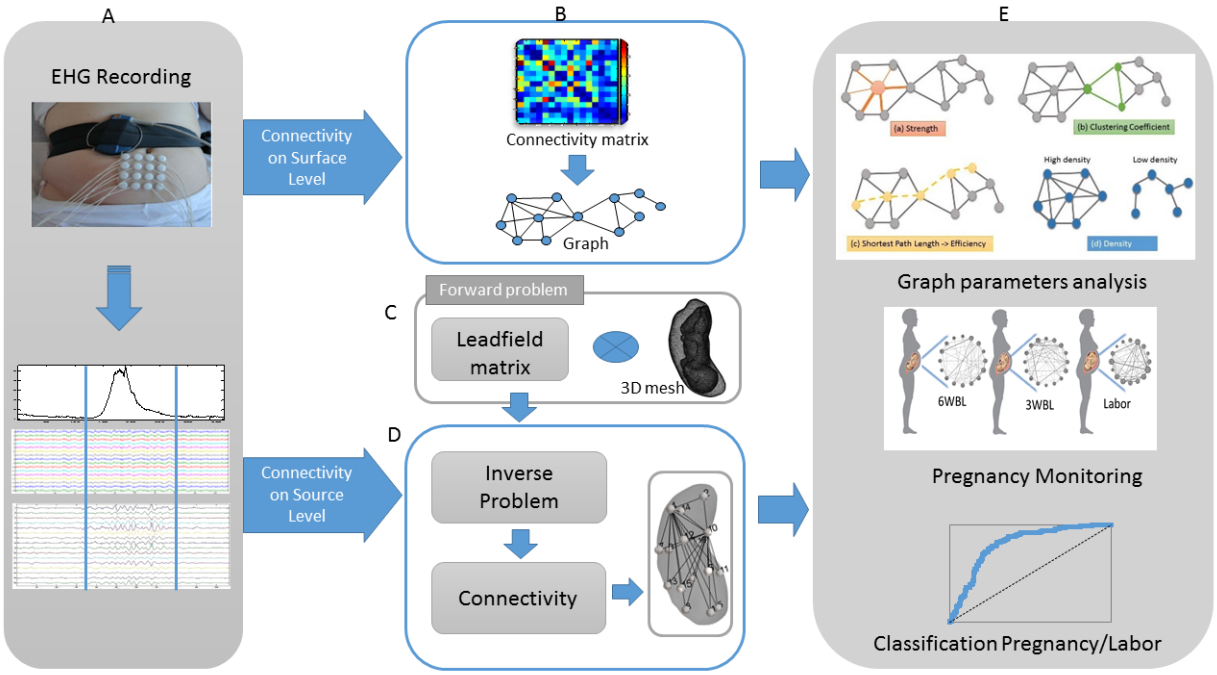


Figure 0.1 Schéma bloc complet de la thèse A. Enregistrement des signaux EHG B. Connectivité au niveau de la surface en utilisant les signaux EHG C. Problème Direct D. Connectivité au niveau de la source en utilisant les signaux EHG et la matrice du champ de dérivation estimée à partir du problème direct. E. Analyse de graphe et ses applications cliniques pour la surveillance de la grossesse ainsi que pour la classification entre grossesse et travail.

Le manuscrit est organisé comme suit:

Chapter 1 Dans ce chapitre, nous présentons l'état de l'art sur les bases anatomiques et physiologiques de l'utérus et de la contractilité utérine, en présentant les deux facteurs principaux qui la génèrent: l'excitabilité cellulaire et la propagation de l'activité électrique. Nous décrivons également les différentes études de propagation qui ont été déjà faites, ainsi que les principaux objectifs de la thèse et la nouvelle approche proposée.

Chapter 2 Dans ce chapitre, nous présentons les matériels et méthodes utilisés dans cette thèse. Nous décrivons tout d'abord les méthodes existantes utilisées pour analyser la propagation de l'activité électrique utérine. Une explication détaillée de la nouvelle approche proposée est également présentée. Pour l'analyse des signaux EHG, nous proposons d'utiliser une technique de mesure de la connectivité des réseaux basée sur la théorie des graphes.

Nous avons également utilisé cette nouvelle approche pour la connectivité au niveau de la source utérine. Ces méthodes ont été appliquées sur des données simulées et réelles. Nous allons également expliquer brièvement le modèle utilisé pour simuler l'activité utérine ainsi que le protocole expérimental utilisé pour enregistrer les signaux EHG réels.

Chapter 3 Nous présentons dans ce chapitre les résultats obtenus pour le calcul de la connectivité au niveau des EHG abdominaux. Nous avons d'abord comparé plusieurs méthodes de connectivité pour estimer la matrice d'adjacence représentée sous la forme d'un graphe. Nous avons ensuite évalué la performance de différentes mesures de graphe dans la classification des contractions de grossesse et de travail. Une comparaison avec les paramètres existants utilisés dans l'état de l'art pour la détection du travail et de la prévision du travail prématuré est également présentée.

Chapter 4 Dans ce chapitre, nous montrons les résultats préliminaires obtenus lors de l'étude de la connectivité au niveau des sources d'EHG identifiées au niveau du myomètre. Nous évaluons les différentes solutions inverses et les méthodologies de connectivité (pour calculer les couplages statistiques entre les sources reconstruites). Les réseaux obtenus par chacune des combinaisons sont comparés au réseau de référence généré par le modèle. Cette approche a également été appliquée à des signaux EHG réels.

Une conclusion générale et des perspectives sont enfin présentées au chapitre 5

Les résultats obtenus dans cette thèse nous ont permis de rédiger : 1 article de revue international en révision (un autre en préparation), 3 conférences internationales, 2 conférences nationales.

TABLE OF CONTENTS

General Introduction 12

Author's publication 16

Chapter 1: Background, problem statement and proposed approach 18

1.1 Preterm labor 18

1.2 Uterus anatomy and physiology 19

1.3 Uterine electrical activity 21

1.3.1 Cell excitability 21

1.3.2 Propagation of the uterine electrical activity 21

1.4 Pregnancy monitoring and preterm labor detection Methods 23

1.4.1 Pregnancy and Labor Monitoring Methods 23

1.4.2 Electrode number and position 25

1.4.3 Multichannel System for EHG Recording 28

1.5 Propagation analysis of the EHG signals 29

1.5.1 Proposed approach 34

Chapter 2: Materials AND Methods 36

2.1 Previously used methods 36

2.1.1 Propagation Velocity and Peak Frequency (PV+PF) 36

2.1.2 Conduction Velocity (CV) 37

2.1.3 Correlation analysis 37

2.2 Proposed approach 40

2.2.1 Imaginary part of coherence (*Icoh*) 40

2.2.2 Graph theory 41

2.2.3 Source localization 47

2.3 Data 50

2.3.1 Real EHGs 51

2.3.2 Simulated EHGs 54

2.4 Work Content 58

2.4.1 Connectivity on surface level 58

2.4.2 Connectivity at the source level 59

2.4.3 Statistical tests 61

2.4.4 Software 62

Chapter 3: EHG Connectivity analysis during pregnancy and Labor 63
3.1 Overview 63
3.2 Pregnancy vs. labor Classification 64
3.2.1 Graph measures 64
3.2.2 Graph visualization 68
3.2.3 Node-Wise Analysis 69
3.3 Pregnancy Monitoring 71
3.3.1 Graph Measures and Visualization 71
3.3.2 Node Wise Analysis 73
3.4 Longitudinal analysis per woman 75
3.5 Week of gestation 76
3.6 Discussion and conclusion 77
Chapter 4: EHG source connectivity analysis 81
4.1 Overview 81
4.2 Results on simulated data 82
4.3 Results on Real data 88
4.3.1 Node Wise Analysis 88
4.3.2 Edge Wise Analysis 89
4.4 Discussion and conclusion 93
Discussion and perspectives 97
References 119
Appendix A 102
Appendix B 105
Appendix C 109
Appendix D 111
Appendix E 113
Appendix F 114

TABLE OF FIGURES

General Introduction

Figure 0.1 Schéma bloc complet de la thèse A. Enregistrement des signaux EHG B. Connectivité au niveau de la surface en utilisant les signaux EHG C. Problème Direct D. Connectivité au niveau de la source en utilisant les signaux EHG et la matrice du champ de dérivation estimée à partir du problème direct. E. Analyse de graphe et ses applications cliniques pour la surveillance de la grossesse ainsi que pour la classification entre grossesse et travail. 5
Figure 0.1 Complete pipeline of the thesis A. EHG recording B. Connectivity at the surface level that uses the EHG signals C. Forward Problem D. Connectivity at the source level that uses the EHG signals and the leadfield matrix estimated from the forward problem. E. Network analysis and its clinical use for pregnancy monitoring as well as for the classification between pregnancy and labor..... 14
Figure 1.1: Preterm birth by region and week of gestation for 2010 (Blencowe et al., 2010) 19
Figure 1.2: Anatomy of pregnant woman uterus ("Stanford Children's Health")..... 20
Figure 1.3: The evolution of Gap junction number during gestation, birth and after delivery (Garfield et al., 1977)..... 22
Figure 1.4: Different techniques used to record EHG signals. 26
Figure 2.1 The seven Königsberg bridges problem 42
Figure 2.2 Definition of the graph. 43
Figure 2.3 The different graph types obtained from the types of connectivity. Functional connectivity leads to: (a) Unweighted (Binary) Undirected graph and (b) Weighted Undirected graph. Effective Connectivity leads to: (c) Unweighted (Binary) Directed graph and (d) Weighted Directed graph 44
Figure 2.4: Measures of network. (a) Strength: the sum of weights of links connected to the node (orange). (b) Clustering coefficient: triangle counts (green) (c) The Efficiency based on the shortest path length (yellow) (d) Density: fraction of present connections to possible connections (Gray and blue). 46
Figure 2.5 The grid of 4*4 electrodes system used for the uterine EHG measurement. (a) The grid position on the woman abdomen. (b) The recording system composed of the grid of electrodes, two references electrodes and the TOCO sensor. (b) The electrodes numbering on the grid when looking at the woman abdomen 52
Figure 2.6 : Segmentation and Denoising of the recorded EHG signals. (a) TOCO signal used for segmentation. (b) Monopolar raw EHGs. (c) Monopolar EHGs after denoising. 53
Figure 2.7: Uterine and fetal mesh (Yochum, Laforêt, and Marque 2016) 55
Figure 2.8: Simulated Uterine EHG signals from source cells 56
Figure 2.9 Example of an EHG signal recorded in the uterus of a monkey 57
Figure 2.10 The different scenarios network. (a) Ground truth of scenario 1. (b) Ground truth of scenario 2. (c) Ground truth of scenario 3. 58

Figure 2.11 Structure of the investigation. (a) Multichannel EHG recordings using a grid of 4x4 electrodes. (b) Segmentation and filtering of EHG signals. (c) Pair-wise connectivity matrix. (d) Characterization of connectivity matrices using network measures (e) Graphs used for pregnancy monitoring along week of gestation . (f) Statistical study based on the extraction of graph parameters. (g) Classification of labor/pregnancy. 59
Figure 2.12: Structure of the investigation. First, a given network is generated by the model and considered as the 'ground truth'. The statistical couplings are then computed between the original sources by using three different methods (R^2, h^2 and Icoh). By solving the forward problem, we generate synthetic EHGs. These signals are then used to solve the inverse problem in order to reconstruct the sources by using three different inverse solutions (MNE, wMNE, sLORETA). The statistical couplings are then computed between the reconstructed sources by using the same different methods (R^2, h^2 and Icoh). The identified network by each combination (inverse/connectivity) was then compared with the original network using a 'network similarity' algorithm. 60
Figure 3.1 ROC Curves for Icoh without and with using graph analysis. CC_icoh, Eff_icoh, strength_icoh represents respectively the results obtained with CC, Eff, Str parameters computed from the connectivity values obtained by Icoh. Icoh represents the roc curve of the results obtained using Icoh without graph. 64
Figure 3.2 ROC Curves for FW_h^2 without and with using graph. strength_Fw_h^2, Eff_Fw_h^2 and CC_Fw_h^2 represents respectively the results obtained with Str, Eff and CC parameters computed from the connectivity values obtained by Fw_h^2. Fw_h^2 represents the roc of the results obtained by Fw_h^2 without graph 65
Figure 3.3 ROC Curves for r^2 without and with using graph analysis. strength_r^2, Eff_r^2 and CC_r^2 represents respectively the results obtained with Str, Eff and CC parameters computed from the connectivity values obtained by Fw_h^2. R^2 represents the roc of the results obtained by R^2 without graph. 66
Figure 3.4 Roc Curves for the Comparison of CV, PV+PF and Icoh/Str. 66
Figure 3.5 Graph results using Icoh. (a) Mean pregnancy graph. (b) Mean labor graph 69
Figure 3.6 Boxplots of three parameter values in pregnancy and labor on 16 nodes (electrodes). All the differences are significant ($p<0.01$). (a) Str (b) Eff (c) CC 70
Figure 3.7 (a) Evolution of Icoh/Str with week before labor. Each point represents the Str value of one contraction for a given woman. Mean graph for: (b) 8WBL. (c) 6WBL. (d) 4WBL. (e) 3WBL. (f) 2WBL. (g) 1WBL. (h) Labor. 72
Figure 3.8 Boxplots of Str values for node 12 from with week before labor. Mean graph for: (b) 8WBL. (c) 6WBL. (d) 4WBL. (e) 3WBL. (f) 2WBL. (g) 1WBL. (h) Labor. 73
Figure 3.9 Evolution of Icoh/Str with week before labor for Woman W35. Each point represents the Str value of one contraction for this woman. 75
Figure 3.10 Mean graphs for woman W35 contractions in each term 76
Figure 3.11 Graph results for Woman W3. (a) Mean pregnancy graph (b) Mean labor graph 77
Figure 3.12 Mean graphs for EHGs recorded at 39WG: (a) Pregnancy, (b) Labor. 78

Figure 4.1 Complete network scenario. A) Uterine networks obtained by using the different inverse and connectivity methods, B) The original network (ground truth) and C) Values (mean ± standard deviation) of the similarity indices computed between the network identified by each combination and the model network. 85
Figure 4.2 One network scenario. A) Uterine networks obtained by using the different inverse and connectivity methods, B) The original network (ground truth) and C) Values (mean ± standard deviation) of the similarity indices computed between the network identified by each combination and the model network. 86
Figure 4.3 Two interconnected networks scenario. A) Uterine networks obtained by using the different inverse and connectivity methods, B) The original network (ground truth) and C) Values (mean ± standard deviation) of the similarity indices computed between the network identified by each combination and the model network. 87
Figure 4.4 Node-wise analysis for Strength metric. Only nodes showing significant differences between pregnancy/labor were visualized 90
Figure 4.5 Node-wise analysis for clustering coefficient metric. Only nodes showing significant differences between pregnancy/labor were visualized 91
Figure 4.6 Edge-wise analysis. Only edges showing significant differences between pregnancy/labor were visualized..... 92
Figure 4.7 Mean graph for pregnancy and labor by using wMNE/h^2..... 93

GENERAL INTRODUCTION

"Every object that biology studies is a system of systems" (Jacob, 1976). Among the complex system of systems of the human body, many questions remain open concerning the human uterus. How does the uterus exactly work as an organ? How does it remain quiescent during most of pregnancy? And how does it contract in a very organized way during labor to expulse a new human into this world? The answers of all these questions could save the life of more than one billion children who died because they were born too soon.

Giving birth, this miracle of life, can turn to death if preterm birth occurs. Indeed, preterm labor occurs when a woman suffers from complications of her pregnancy and gives birth before the 37^{th} week of gestation. The highest risk of mortality and morbidity is for those infants born at the earliest gestational ages. The birth of a preterm infant can also bring considerable economic costs and has implications for public-sector services, such as health insurance, educational, and other social support systems. The annual societal economic burden associated with preterm birth in the United States was at least $26.2 billion in 2005 (Behrman et al., 2007). However, more days in the uterus can improve the maturation of the fetus. For this reasons, the early detection of a preterm labor is one of the most important keys for its prevention.

One of the most promising biomarkers of uterine contraction is the electrical activity of the uterus. This activity is reflected in the Electrohysterography (EHG), which represents the noninvasive abdominal measurement of the uterine electrical activity (Devedeux et al., 1993). Several studies have already been realized in the context of preterm labor detection by processing EHG (Euliano et al., 2009, 2009; Laforet et al., 2013; Marque and Duchene, 1989; Planes et al., 1984). EHG is one of the few indicators that are measurable and representative of the underlying muscular activity of uterine contractions.

Labor and delivery are preceded by two physiological phenomena: increased excitability and increased connectivity between the myometrial cells, which results in an increase in the propagation of the action potentials that trigger the uterine contractions (Devedeux et al., 1993).

Several studies have been realized to characterize the uterine propagation by means of the synchronization between EHG signals recorded at the abdominal surface. These efforts were

based on various methods such as i) correlation/connectivity analysis (Euliano et al., 2009; Mahmoud Hassan et al., 2010; Marque and Duchene, 1989) where the methods were applied on the entire uterine burst manually segmented, and ii) propagation velocity quantified by analyzing either the propagation of whole bursts of EHG (Lucovnik et al., 2011) (Mikkelsen et al., 2013), or single spikes identified within bursts (Lucovnik et al., 2011; C. Rabotti et al., 2010)(Lau et al., 2014)(de Lau et al., 2013). The analysis based on spikes (often by using small and close electrodes) would permit to quantify the electrical diffusion process. The one made from whole bursts (with larger and more spaced electrodes) would focus more on the global synchronization of the uterus.

The connectivity analysis gave some promising results when using EHG signals for the identification of statistical coupling between uterine contractions recorded during labor and/or pregnancy. Thus the main objective of this thesis is to develop a new way to study the global synchronization of the uterine electrical activity by computing the connectivity between the recorded EHG signals. Concerning the global analysis (whole burst), in most previous studies, the EHG connectivity matrices were reduced by keeping only their average. Despite the encouraging results obtained, relevant information was missed due to this averaging which may induce the relatively low classification rate reported so far. To characterize precisely connectivity matrices and quantify the global uterine connectivity, we used here the graph theory based analysis. This field has shown a growing interest in the last years, especially to characterize brain networks (Bullmore and Sporns, 2009; Rubinov and Sporns, 2010; van den Heuvel and Sporns, 2013). According to this approach, a connectivity matrix can be represented as graphs consisting of a set of nodes (electrodes) interconnected by edges (connectivity/ correlation values between electrodes).

Two main approaches were used in this thesis i) Compute and quantify the connectivity at the abdomen (electrodes) level and ii) Compute and quantify the connectivity at the uterine source level. The complete pipeline of the thesis work is presented in Figure 0.1.

First, the EHG signals were recorded during pregnancy and labor by using a grid of 4*4 electrodes (Figure 0.1 A). To analyses these signals, we have computed the connectivity between the EHGs and quantified it by using graph theory approach. The processing pipeline includes i)

the estimation of the statistical dependencies between the different recorded EHG signals (Figure 0.1 B), ii) the quantification of the obtained connectivity matrices by using a graph theory-based analysis (Figure 0.1 E) and iii) the clinical use of network measures for pregnancy monitoring as well as for the classification of EHG bursts recorded during pregnancy or labor (Figure 0.1 E). A comparison with the existing parameters used in the state of the art for labor detection and preterm labor prediction was also performed.

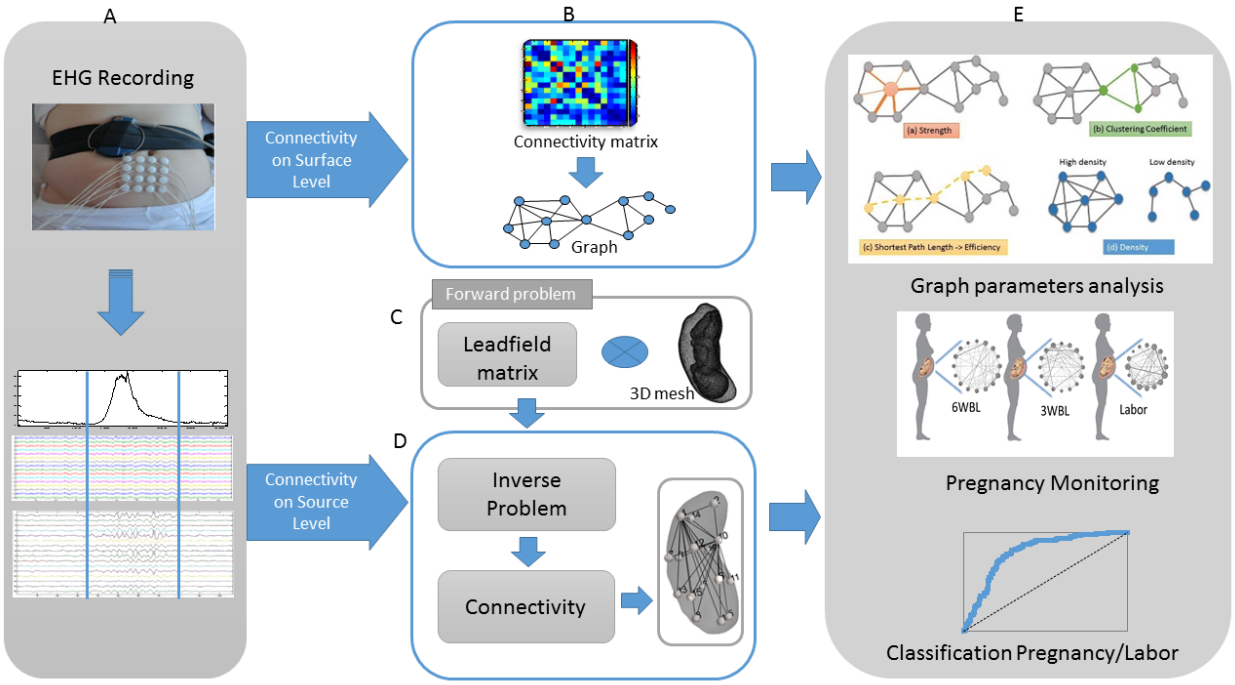


Figure 0.1 Complete pipeline of the thesis A. EHG recording B. Connectivity at the surface level that uses the EHG signals C. Forward Problem D. Connectivity at the source level that uses the EHG signals and the leadfield matrix estimated from the forward problem. E. Network analysis and its clinical use for pregnancy monitoring as well as for the classification between pregnancy and labor

To overcome the so-called problem of 'volume conduction' when computing the connectivity at the abdominal surface level, we have proposed a new method called 'EHG source connectivity' (Figure 0.1 C, D). This method consists of reconstructing the time series of the uterine sources associated to given EHGs and then computing the statistical coupling between these sources. As this new method involves mainly two steps and as there is no consensus about the inverse/connectivity method to be used, we analyzed the effect of the algorithm used in the solution of the EHG inverse problem as well as of the method used in the estimation of the

functional connectivity by using data simulated by using a model developed in our team (ground truth). As in the connectivity at the surface level, the obtained connectivity matrices at the source level have been be quantified based on the same graph theory analysis (Figure 0.1 E).

The manuscript is organized as follows:

Chapter 1 In this chapter, we present the state of the art of anatomical and physiological background of the uterus and its contractility with its two main factors: cell excitability and propagation of the electrical activity. We also describe the different propagation studies that have been done previously, as well as the main objectives of the thesis and the proposed new approach.

Chapter 2 presents the materials and methods used in this thesis. First we precise the existing methods used to analyze the propagation of the uterine electrical activity. A detailed explanation of our new proposed approach is also presented. For the analysis of the EHG signals, we propose to use a network measure technique based on graph theory. We have also used this new approach for the connectivity at the uterine source level. These methods were applied on simulated and real data. We will also briefly explain the model used for simulating uterine activity as well as the experimental protocol used to record real EHG signals.

Chapter 3 This chapter is dedicated to the results obtained when computing connectivity at the level of the electrodes. We first compared several connectivity methods to compute the connectivity matrix represented as a graph: a set of nodes (electrodes) connected by edges (connectivity values). We then evaluated the performance of different graph measures in the classification of pregnancy and labor contractions. A comparison with the existing parameters used in the state of the art of labor detection and preterm labor prediction is also presented.

Chapter 4 In this chapter, we show the first results obtained when studying the connectivity at the level of the EHG sources. We evaluate the different inverse solutions (to reconstruct the dynamics of uterine sources) and connectivity methods (to compute statistical couplings between reconstructed sources). Networks obtained by each of these combinations are

compared to the reference network (ground truth) generated by the model. This approach was also applied to real EHG signals.

A general conclusion and perspectives will finally be presented in chapter 5

AUTHOR'S PUBLICATION

Journal Paper

N. Nader, M. Hassan, W. Falou, A. Diab, M. Khalil, C. Marque, « Uterine muscle networks: Connectivity analysis of the EHG during pregnancy and Labor» ***in revision*** **(Computers in Biology and Medicine)**

N. Nader, M. Hassan, M. Yochum, S. Zahran, W. Falou, C. Marque, M. Khalil. « Electrohysterography source networksduring pregnancy and labor» ***under preparation***

International Conference papers

N. Nader, M. Hassan, W. Falou, A. Diab, S. Al-Omar, M. Khalil, et C. Marque, « Classification of pregnancy and labor contractions using a graph theory based analysis », in *2015 37th Annual International Conference of the IEEE Engineering in Medicine and Biology Society (EMBC)*, Milano, Italy, 2015, p. 2876−2879.

N. Nader, C. Marque, M. Hassan, N. Nader, W. Falou, A. Diab, et M. Khalil, « Pregnancy monitoring using graph theory based analysis », in *2015 International Conference on Advances in Biomedical Engineering (ICABME)*, 2015, p. 73−76.

N. Nader, C. Marque, M. Hassan, N. Nader, W. Falou, A. Diab, et M. Khalil. « A node-wise analysis of the uterine muscle networks for pregnancy monitoring» in 2016 *38th Annual International Conference of the IEEE Engineering in Medicine and Biology Society (EMBC)*, in Florida, USA

Al-Omar, S., Diab, A., **Nader, N.,** Khalil, M., Karlsson, B., Marque, C., 2015. Detecting labor using graph theory on connectivity matrices of uterine EMG. Conf. Proc. Annu. Int. Conf. IEEE

Eng. Med. Biol. Soc. IEEE Eng. Med. Biol. Soc. Annu. Conf. 2015, 2195–2198. doi:10.1109/EMBC.2015.7318826

National Conference papers

N. Nader, M. Hassan, M. Khalil, C. Marque, et W. Falou, « From EHG signals to graphs: A new method for predicting premature birth. », présenté aux Journées RITS 2015, pp 182−183.

N. Nader, M. Hassan, M. Khalil, C. Marque, et W. Falou, « Connectivity Graph: A New Method for the Classification of Labor-Pregnancy EHG », LAAS 2015

CHAPTER 1: BACKGROUND, PROBLEM STATEMENT AND PROPOSED APPROACH

This chapter starts by a definition of the preterm labor problem, which represents the main cause of infant mortality and morbidity. We then briefly describe the anatomical and physiological background of the uterus and the uterine contractility with its two main factors: cell excitability and propagation of the electrical activity. An overview of the different pregnancy monitoring techniques available to record the uterine activity is then reported. Finally, we present an overview of the studies that were reported in the context of analyzing the propagation of the uterine activity. We conclude by the main objective of this thesis and the proposed new approach.

1.1 PRETERM LABOR

Preterm birth, which occurs before week 37 of pregnancy, is the major cause of newborn deaths and the second biggest cause of deaths in children under five years old. The premature birth is extremely preterm when it happens before week 28, very preterm between weeks 28 and 32, moderate to late preterm from 32 to 37 weeks ("WHO | Preterm birth,").

An estimated 15 million babies are born preterm every year which is more than 1 in 10 babies. One million children die each year due to complications of preterm birth with an increasing rate of preterm birth in most countries. Studies in 184 countries reported that the rates of preterm birth across these countries range between 5% and 18%. More than 80% of preterm births occur between 32 and 37 weeks of gestation as shown in Figure 1.1. Preterm newborns are at increased risk of illness, disability and death. Many preterm survivors face a lifetime of disability, including learning disabilities, visual and hearing problems (Blencowe et al., 2013).

The immediate neonatal intensive care incurs large economic costs of preterm birth, including long-term complex health needs (Blencowe et al., 2013). Indeed, the medical, physiological and socioeconomic consequences of preterm labor are important. However, more days in the uterus

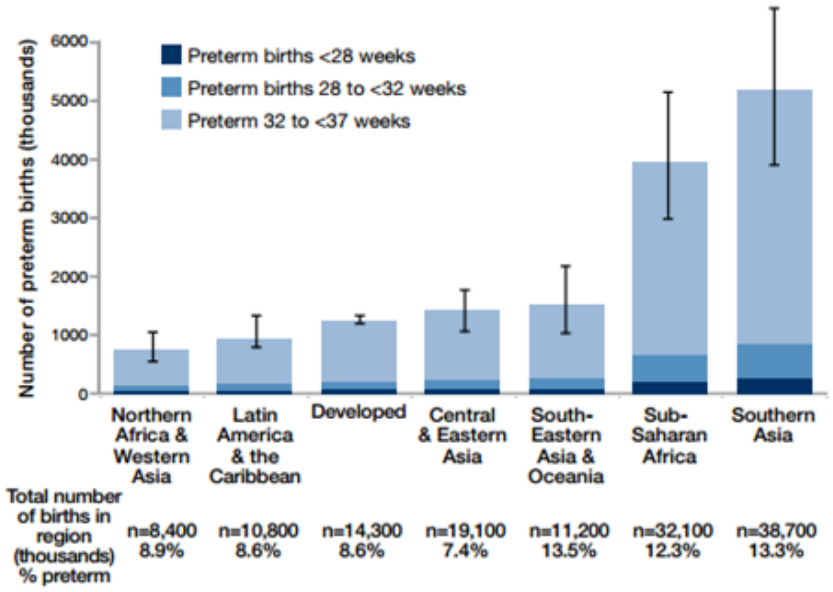


Figure 1.1: Preterm birth by region and week of gestation for 2010 (Blencowe et al., 2010)

can improve the maturation of the fetus. For this reasons, the early detection of a preterm labor is one of the most important keys for its prevention.

1.2 UTERUS ANATOMY AND PHYSIOLOGY

As a dynamic female reproductive organ, the uterus is responsible for several reproductive functions, including menses, implantation, gestation, labor, and delivery ("Uterus Anatomy," 2015). The uterus, which is a hollow muscular organ, is where the fetus is developing during pregnancy.

Three parts can be differentiated the uterus:

- The fundus, which corresponds to the upper portion
- The corpus, which is the main part of the uterus including uterine cavity
- The narrow, which is the lower section and is called the cervix.

The uterus is located above the vagina, midway between the bladder and the rectum. The non-pregnant uterus measures approximately 7.5 cm in length, 4 to 5 cm in width at its upper portion, and 2 to 3 cm in thickness, and it weighs 50 to 70 g (Ellis, 2005) . At term, it measures approximately 32 cm in length, 23 cm in width, and weights about 1000 g, with an inner volume of 4-5 liters, for a mono-fetal pregnancy.

The anatomy of the thick uterine wall consists of three tissue layers (Chard, 1994). The inner layer, or endometrium, is the most active layer. This layer responds to cyclic ovarian hormone changes since it consists of glandular cells that produce secretions. This membrane thickens to prepare the uterus for implantation of a fertilized egg. The middle layer, or myometrium, is a muscular layer composed of smooth muscle cells and forms the larger part of the uterine wall. It increases by two procedures: either by hypertrophy of the existing cells, or by multiplication of the cell number. It is well known that the myometrium has an active role during pregnancy. During the last stage of gestation, the smooth cells reach a maximum length of 300 μm and a maximum width of 10 μm (Csapo, 1962). The interaction of myosin and actin filaments produces the contractions of smooth muscle cells. When delivery occurs, the electrical activity generated by the smooth muscle cells, produces rhythmic contractions, which lead to birth. The outer layer of the uterus, the serosa or perimetrium, is a thin layer of tissue made of epithelial cells that envelops the uterus.

In Figure 1.2 we present the anatomy of a pregnant woman uterus. The amniotic sac, a thin-walled sac filled with amniotic fluid is called the amnion. It surrounds the fetus during

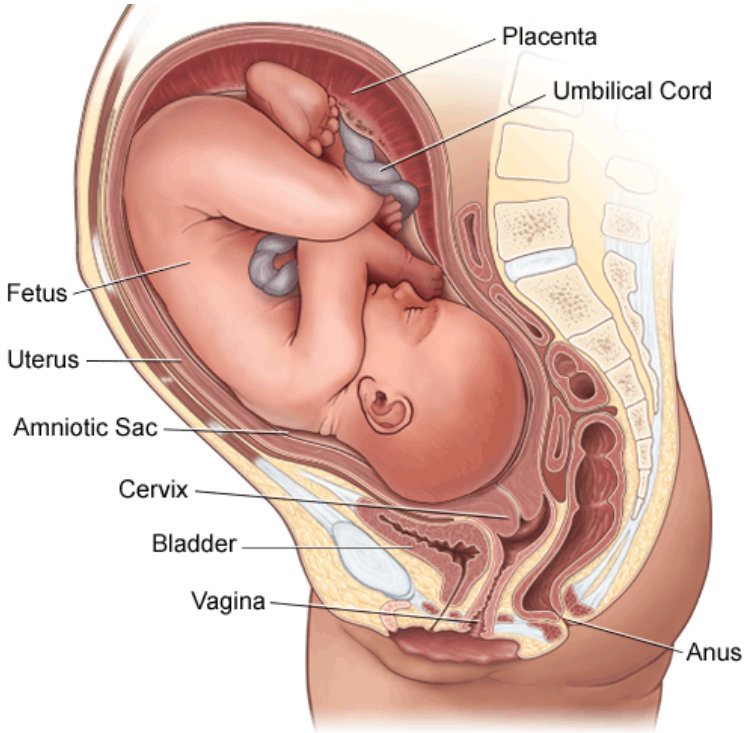


Figure 1.2: Anatomy of pregnant woman uterus ("Stanford Children's Health")

pregnancy. The placenta only grows during pregnancy and provides a metabolic interchange between the fetus and mother. The umbilical cord connects the fetus to the placenta. The umbilical cord contains two arteries and a vein, which carry oxygen and nutrients to the fetus and waste products away from the fetus ("Stanford Children's Health").

1.3 UTERINE ELECTRICAL ACTIVITY

One of the most promising markers of uterine contraction is the electrical activity of the uterus. This activity is reflected in the electrohysterogram (EHG), which is a noninvasive abdominal measurement of the uterine electrical activity (Devedeux et al., 1993). Labor and delivery are preceded by two physiological phenomena: increased excitability and increased connectivity between the myometrial cells which results in an increase in the propagation of the action potential that underlie uterine contractions (Devedeux et al., 1993).

1.3.1 Cell excitability

Two types of potential describe the electrical activity of cells: the resting potential and the action potential. The resting potential is the difference between the negative inside and the positive outside of a resting cell. The resting potential is unstable when recording the electrical activity of a membrane. It presents slow waves of low amplitude that describe the electrical base line. The potential difference across the cell membrane reverses, when a cell depolarizes. Then, the trans-membrane potential increases. An action potential is generated when a given threshold is reached. For uterine cells, action potentials are often grouped by bursts. The physiological electrical activity is composed of irregular bursts of action potentials during pregnancy. While term and labor uterine electrical activity is composed of regular bursts composed of regular trains of action potentials (Sanborn, 1995), generated spontaneously. .

1.3.2 Propagation of the uterine electrical activity

The uterus is known as a myogenic organ, therefore the myometrium is able to contract by itself without nervous or hormonal inputs (Shmygol et al., 2007; Wray, 1993). The electrical activity is controlled by changes in the membrane potential of the smooth muscle cell of the myometrium (Kuriyama and Suzuki, 1976; Ohya and Sperelakis, 1989; Wray, 1993).

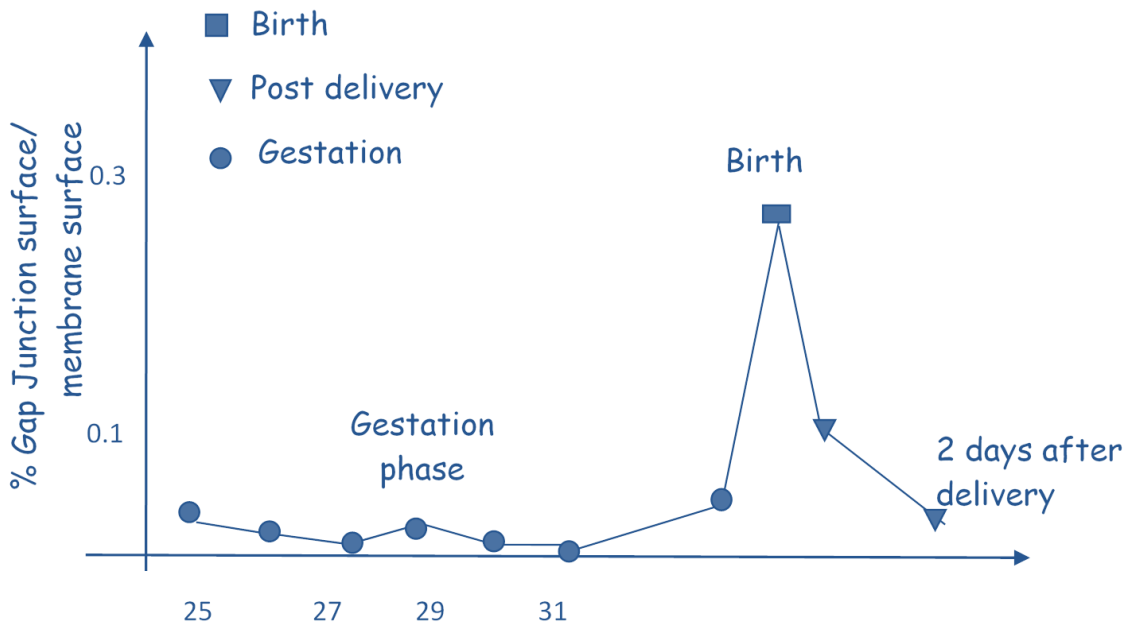


Figure 1.3: The evolution of Gap junction number during gestation, birth and after delivery (Garfield et al., 1977)

The uterine myometrial cells can either generate their own potential; these cells are called pacemaker cells, or can be excited by the action potential from its neighbor cell; these cells are called pacefollower cells. However, myometrial cells may alternatively be pacemaker or pacefollower cells.

Several studies were recently devoted to understand the propagation phenomena of the uterine electrical activity during pregnancy and labor (Rabotti and Mischi, 2015). Many studies focused on locating the pacemaker area of the uterine muscle during pregnancy and labor. However, uterine pacemakers have been mostly observed to appear randomly throughout the tissue and to change their location during a single contraction or several successive contractions even during labor (Lammers et al., 1994; Marshall, 1959; Parkington et al., 1988).

In addition, myometrial cells are coupled together electrically by gap junctions (Garfield et al., 1977; Devedeux et al., 1993; Garfield and Maner, 2007). These gap junctions are areas where the membranes of two adjacent cells form pores allowing electrical coupling. They form a pathway for the passage of action potentials by forming a low-resistance electrical contact between the cells (Miller et al., 1989) (Garfield et al., 1977). Many studies indicated that during most of pregnancy phases, the cell-to-cell gap junctions are absent or present in very low density

(Garfield et al., 1977). On the other hand, a large number of gap junctions between myometrial cells is observed during labor (Garfield et al., 1977; Garfield and Hayashi, 1981) ensuring the development of a synchronized muscle activity (Figure 1.3) due to electrical diffusion.

1.4 PREGNANCY MONITORING AND PRETERM LABOR DETECTION METHODS

Detection and evaluation of the uterine contractions are of major importance. One of the aims of pregnancy monitoring is to differentiate normal pregnancy contractions, which are inefficient to those, efficient, which could cause a dilation of the cervix, thus inducing a premature birth. For this reason, many studies focused on pregnancy monitoring techniques to assess the key risk factors and allow the prediction of preterm labor.

1.4.1 Pregnancy and Labor Monitoring Methods

Typical clinical practice involves the use of different methods.

One of the most efficient methods is the use of Intrauterine Pressure (IUP), it provides the best information concerning the contractile state of the uterus (Garfield et al., 2001). A catheter is inserted into the uterine cavity and connected to a pressure sensor, that gives different information on the duration, amplitude and frequency of appearance of the contractions (Garfield et al., 1998a). The main drawback of this method is its invasiveness which can increase the risk of infection and requires rupture of the membranes (Garfield et al., 2001). Obviously, it cannot therefore be used during pregnancy.

Being external and non-invasive, the most widely used device for monitoring uterine contractions during pregnancy is the "Tocodynamometer". It is used in over 90% of all hospital births. This device is an external pressure measurement device formed by a force sensor placed on the mother's abdomen, usually over the uterine fundus. This sensor detects changes in abdominal stiffness as an indirect indication of uterine contraction (Garfield et al., 1998a). The main primary advantage of a tocodynamometer is its non-invasiveness which allows the device to be used for most pregnancies without any risk to the fetus or the mother. Nevertheless, the success of this device depends on the subjectivity of the examiner. In addition of being uncomfortable, its main disadvantage is its inaccuracy. Different variables could affect its

accuracy such as instrument placement, amount of subcutaneous fat, uterine wall pressure, mother's motion…. Many other variables could be detected as uterine contractions such as body movements, gastric activity, and other non-labor induced stresses (Garfield et al., 2001). This technique could only permit to detect the number of contractions over a given time interval (usually 10 mm).

Many clinicians prefer to rely on different indicators such as cervical dilation and effacement, vaginal bleeding, or ruptured membranes in order to detect preterm labor. However, since these parameters are subjective and have a high variability within and between observers, this technique has a low predictive value (Creasy, 1993). Other biological tests, such as fibronectin, have been clinically used for the diagnosis of premature births (Iams, 2003), but they have a low predictive value.

A noninvasive technique named light-induced auto fluorescence (LIF) has been also proposed for labor monitoring (Garfield et al., 1998b). This technique attempts to measure cervical tissue changes during gestation and labor. Many studies have proved its capability for estimating the cervical status. Although this technique could provide useful information for preterm labor prediction, it is not used yet in clinical practice.

Another technique used for the labor detection consists of measuring the cervix length via endovaginal ultrasonography. This method gives good predictive values but only after the appearance of symptoms of preterm labor (Romero et al., 1992). Therefore, the success to detect preterm labor is limited when using this technique. Additionally, the measurement of the cervical length using this technique is not reliable because it is influenced by the varying amount of urine in the bladder (Iams, 2003).

The Magnetomyography (MMG) is a noninvasive technique permitting to measure the magnetic fields associated with the uterine action potentials. It is also used for uterine activity recording. MMG recordings of spontaneous uterine activity were recorded for the first time by Eswaran et al. (Escalona-Vargas et al., 2015; Eswaran et al., 2004). This method is presently only used as a research tool due to its high cost and the need of very special (and not easy to set-up) equipment.

The electrohysterography (uterine electromyography, EHG) permits to overcome the limitations of the MMG. This method permits to record the uterine activity non invasively, with affordable and simple equipment. The electrohysterography permits to derive quantitative information on the myometrium from the analysis of its electrical activity collected on the mother's abdomen. EHG consists of the summation of the electrical activity generated by the active uterine muscle cells, plus the noise related to corrupting electrical and mechanical activities. The analysis of the EHG was shown to be one of the most promising tools to monitor the efficiency of uterine contractions during pregnancy (Marque et al., 2007).

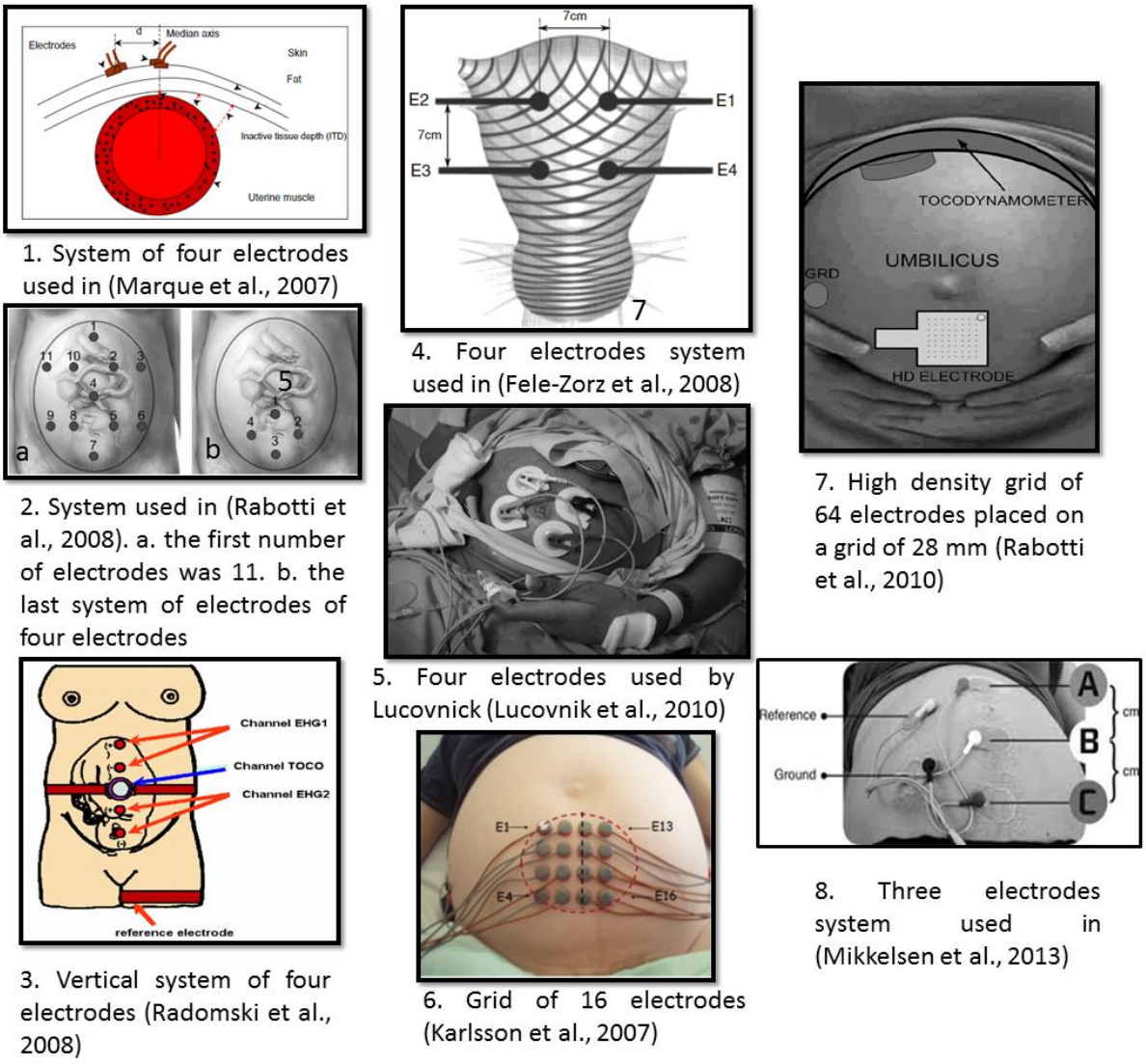
EHG signals, recorded externally using electrodes placed on the women's abdomen, has been demonstrated to be representative of the uterine electrical activity (Devedeux et al., 1993; Mansour et al., 1996). The EHG is composed of two main components, a low wave (which is synchronous to the IUP) and a fast wave. The fast wave is also divided into two frequency components: Fast Wave Low (FWL) and Fast Wave High (FWH). It has been proposed that FWL is related to propagation and FWH is related to excitability of the uterine cells (Gondry et al., 1993) .

According to these results, we can expect that this noninvasive recording of the EHG will provide information not only on the excitability of myometrial cells but also on the propagation of the uterine electrical activity. Therefore, EHG analysis could be used clinically for pregnancy monitoring, labor detection and preterm labor prediction. However, the performance of the EHG analysis depends on the electrodes number as well as on their positions (Rabotti et al., 2008). In the following section we will present the different systems used so far for the uterine electrical activity recordings.

1.4.2 Electrode number and position

Most of the early studies used two to five electrodes to invasively record uterine electrical activity. Therefore they focused mainly on the excitability of the uterus (Schlembach et al., 2009) (M. Hassan et al., 2010).

Marque et al. (Marque et al., 2007) used 4 Ag/AgCl electrodes (8 mm diameter spaced by 2.5 cm), forming 2 bipolar leads, to record EHG signals and a reference electrode was positioned on the hip of the patients as shown in Figure 1.4.1. Terrien et al. (Terrien et al., 2006) used four electrodes, a pair positioned in the middle of the median axis near the umbilicus and another one positioned 5cm left of the middle electrode. In order to identify a suitable electrode configuration, Rabotti et al (Rabotti et al., 2008) proposed two measurements for 15 min in labor. They first used 11 active electrodes placed on the abdomen (Figure 1.4.2 a). They measure then the average SNR in each electrode. In this preliminary study, they evidenced the highest



1. System of four electrodes used in (Marque et al., 2007)

2. System used in (Rabotti et al., 2008). a. the first number of electrodes was 11. b. the last system of electrodes of four electrodes

3. Vertical system of four electrodes (Radomski et al., 2008)

4. Four electrodes system used in (Fele-Zorz et al., 2008)

5. Four electrodes used by Lucovnick (Lucovnik et al., 2010)

6. Grid of 16 electrodes (Karlsson et al., 2007)

7. High density grid of 64 electrodes placed on a grid of 28 mm (Rabotti et al., 2010)

8. Three electrodes system used in (Mikkelsen et al., 2013)

Figure 1.4: Different techniques used to record EHG signals.

average SNR on the lower vertical median line of the abdomen, in particular on the region immediately below the umbilicus. They explained these results by means of two main hypotheses. First, the distance between the recording site, on the skin, and the signal source, in the myometrium, is reduced with respect to the more lateral sites. Second, the position of the uterus relative to the abdominal wall is constant even during contractions, in the region surrounding the umbilicus, which results in a better SNR. According to the results obtained in this preliminary analysis, they used four unipolar contact Ag–AgCl electrodes placed on the abdomen (figured in Figure 1.4.2 b). The common reference for these electrodes was placed on the right hip.

A system containing two bipolar electrode pairs was used in Randomski et al. (Radomski et al., 2008). In addition, they used one Tocographic probe and a reference electrode attached to the left hip (Figure 1.4.3). The distance between the electrodes forming the bipolar channels was fixed at 5 cm. The electrodes were attached in the vertical median axis of the woman's abdomen because they indicate that this position provides a suitable SNR due to a closer contact and during contractions, more invariant position of the uterus in relation to the abdominal wall (Graczyk et al., 1995).

In other studies, (Baghamoradi et al., 2011; Fele-Zorz et al., 2008; Fergus et al., 2013), authors used 4 AgCl electrodes to record EHG. These electrodes were placed in two horizontal rows, symmetrically under and above the umbilicus, spaced 7 cm apart (Figure 1.4.4). Therefore, three bipolar EHG were obtained in these studies.

Two electrodes placed on the abdominal wall of the women were used in (Terrien et al., 2010). The interelectrode distance was 2.1 cm and they were placed on the uterine median axis, midway between the fundus and the symphysis. They used also a reference electrode placed on the hip of the women.

Four electrodes were used by Lucovnik et al. (Miha Lucovnik, 2010) positioned around the umbilicus in a form of square shape. The distance between each two electrodes vertically and horizontally is fixed at 2.5 cm (measured from center to center) (Figure 1.4.5). For EHG recording they use differential, bipolar electrode pairs.

Several studies indicated that this small number of electrodes used was not sufficient for adequate analysis of the propagation in this complex environment represented by the uterine muscle and abdominal anatomy of a pregnant woman (Devedeux et al., 1993; Garfield and Maner, 2007). Therefore, a high number of electrodes is required. In this context, Karlsson et al (Karlsson et al., 2007) proposed a new recording system consisting of a grid of 16 monopolar electrodes (4 x 4) to study the propagation of the uterine electrical activity (Figure 1.4.6). The inter-electrode distance was 2.1 cm. They positioned the grid on the abdomen of the pregnant woman where the third electrode column of the grid is always on the uterine median vertical axis, and the 10-11th electrodes are midway between the symphisis and the uterus fundus. They used also two reference electrodes placed on each of the women's hip. In order to increase the signal to noise ratio, authors used the vertical bipolar signals (BPi), giving thus a 3 x 4 signal matrix.

Rabotti et al (Chiara Rabotti et al., 2010; C. Rabotti et al., 2010) used a Refa system made of a multichannel amplifier for electrophysiological signals and a grid of 64 (8×8) high density electrodes (1mm diameter, 4 mm spaced). They used this system in order to estimate non-invasively the conduction velocity of the EHG-action potentials (Figure 1.4.7).

Finally, Mikkelsen et al. used three surface electrodes placed abdominally along the median vertical axis (Mikkelsen et al., 2013) (Figure 1.4.8). The inter-electrode distance was of 6.5–11.2 cm.

1.4.3 Multichannel System for EHG Recording

A high spatial resolution is always needed in order to obtain a precise mapping of underlying electrical activity. In a labor room, the placement of a large number of electrodes for measuring EHG takes time and is difficult to perform. To tackle this problem, from 2007, a collaborative group from France and Iceland, involving biomedical researchers, engineers and medical doctors, created a new design that reduces the inconvenient of multiple electrodes positioning. They defining a standard position (also their size and number) for the recording electrodes. The main goal of this project was to better record and analysis the propagation and the characteristics of the uterine electrical activity during contractions. More details about this protocol will be described in the next chapter.

Usually, a single bipolar signal is obtained by subtracting the signals recorded by two close electrodes. The results from a preliminary study showed a very acceptable SNR (signal to noise ratio) on bipolar signals (Alexandersson et al., 2015). On the other hand, this configuration introduces a bias for studying the propagation, as two adjacent bipolar signals can share a same electrode.

Therefore, monopolar EHG could be more interesting to get rid of this bias as well as to increase the spatial resolution when processing signals. For this reason, Hassan et al (Hassan et al., 2011) developed a specific denoising method to denoise monopolar EHG. Thus we obtain a correct SNR permitting to study the propagation of the electrical uterine activity from monopolar EHG. This method is based on combination of canonical component analysis (CCA) and on Empirical Mode Decomposition (EMD). In this work, we used this denoising method to obtain noise-free monopolar signals to study the synchronization of uterine activity.

1.5 PROPAGATION ANALYSIS OF THE EHG SIGNALS

Numerous studies have shown that the analysis of the propagation of the uterine electrical activity is a powerful tool to characterize and to discriminate pregnancy and labor contractions (Lammers, 2013; Miha Lucovnik, 2010; Rabotti et al., 2009) . This propagation phenomenon can be studied at a micro level when using invasive recordings but also can be studied at the skin level with abdominal electrodes. Some of these studies focused on the propagation pattern or on the velocity of the uterine activity in the uterus during pregnancy and labor. Others studied the propagation phenomenon by looking at the statistical couplings and delays (also called correlation/connectivity) between the different electrodes. In this section we will explain these different approaches.

Propagation pattern

Earlier studies on the propagation of the uterine electrical activity in labor (women or animal) found a predominant downward propagation where the origin of the burst is in the upper/ovarian region of the uterus in women and in the guinea-pig (Lammers et al., 2008; Mikkelsen et al., 2013; Norwitz and Robinson, 2001; Planes et al., 1984; Rabotti et al., 2009). In other studies, on women, upward and multidirectional propagation patterns have been reported (Lange et al.,

2014; Mikkelsen et al., 2013; Rabotti et al., 2009), while, a predominant upward direction of the uterine activity was revealed into women who delivered successfully vaginally (Buhimschi, 2009; Euliano et al., 2009).

In addition, many studies based their analysis on single spikes manually identified from the EHG bursts and not on the whole EHG burst. It was proven that the propagation of single spikes is more relevant to the prediction of labor than the analysis of the whole burst (Miha Lucovnik, 2010; Lammers et al., 1994; Lammers, 1997; Melton and Saldivar, 1964; Miller et al., 1989).

This propagation of the uterine electrical activity was studied not only on women but also on different species. In (Lammers et al., 1994) authors used a two-dimensional high-density grid in order to study the propagation in an isolated preterm rat myometrium as well as in the intact guinea-pig uterus at term (Lammers et al., 2008). In these studies, authors reported that the propagation of single spikes is unpredictable and can propagate spontaneously in a circular way. Sparse and fractionated spike propagation was reported in the uterus of the guinea pig at term when recorded in the placental insertion area (Lammers et al., 2008). Miller et al (Miller et al., 1989), when studying rat uterine strips, reported a progressive recruitment in the axial direction preterm and not at term. Authors used an array of six extracellular glass-pore surface electrodes (3 mm apart). Other studies were done on the intact uterus of pregnant ewes using pairs of stainless-steel wires sewn into the myometrium of their uterus. They evidenced that individual spikes do not propagate among electrodes when their inter-distance is over 3 cm apart along the longitudinal as well as along the circumferential layer of the myometrium (Parkington et al., 1988).

Another way to analyze the propagation phenomenon is to measure the statistical coupling between recorded signals. This coupling analysis can be associated with the detection of a time delay. Duchene et al. were the first to study the correlation between EHG envelopes recorded at several sites in the uterus of delivering macaques (Duchene et al., 1990). More recently Diab et al. showed that the correlation of the uterine electrical activity spreads to the whole matrix and in all directions but remains more concentrated down, towards the cervix, when approaching labor (Diab, 2014).

Other studies focused their analysis on the activity of the uterus on the placental region. Weaker potentials, slower propagations, and a shorter length constant were found in microelectrode recordings in the placental region, in rat myometrium (Kanda and Kuriyama, 1980). Research on the pregnant cat showed that the placental region was less excitable and showed little or no spontaneous activity by using extracellular recordings (Daniel, 1960).

Propagation Velocity

Recently, an increasing number of studies on animals and women evidenced that the propagation of single electrical spikes in the myometrium is linear. This observation permits to measure the propagation velocity (Lammers et al., 1994; Lammers, 1997; Lammers et al., 2008; Miha Lucovnik, 2010; Rabotti and Mischi, 2010) . The propagation velocity of electrical spikes in the uterus was for the first time quantified in (Bozler, 1970) for the guinea-pig, the rabbit and the cat. Later, many studies have focused on the propagation velocity by using different recording methods on different species like guinea-pig (Bozler, 1970), cat (Bozler, 1970; Daniel, 1960), rat (Kanda and Kuriyama, 1980; Miller et al., 1989) and ewe (Parkington et al., 1988) . They reported values of propagation velocity for guinea-pig ranging from 0.1 to 0.3 cm/s (Bozler, 1970), and for the cat, 6 cm/s in (Bozler, 1970), 9-10 cm/s in vivo and 8-12 in vitro in (Daniel, 1960). For the rat, authors in (Kanda and Kuriyama, 1980) obtained values of 6.6 ± 2.2 cm/s (at 7 days gestational age (GA)), 12.3 ± 3.2 cm/s (at 15 days GA), 33.4 ± 4.1 cm/s (at 22 days GA) in non-placental regions; and 1.3 ± 0.4 cm/s (at 15 days GA), 2 ± 0.9 cm/s (at 22 days GA) in placental regions. In (Miller et al., 1989) the values were 9.2 ± 0.6 cm/s (in the longitudinal layers), 2.3 ± 0.7 cm/s (in the circumferential directions) in pregnancy, while the values in labor were 10.5 ± 1.3 cm/s (in the longitudinal layers) and 4 ± 0.8 cm/s (in the circumferential directions).

Also in the intact uterus of pregnant ewes, Parkington et al. found that the propagation velocity in the longitudinal direction significantly increased from pregnancy (7.2 ± 0.3 cm/s) to labor (13.3 ± 0.7 cm/s) (Parkington et al., 1988).

The MMG was also used to determine the uterine contractions propagation velocity (Escalona-Vargas et al., 2015). Results indicated that the propagation was multidirectional and ranged from

1.9-3.9 cm/s. Authors in (Wikland and Lindblom, 1985) reported a velocity ranging between 1 and 2 cm/s using biopsies technique of the myometrium. In labor, Wolfs & van Leeuwen (Wolfs and van Leeuwen, 1979) estimated a slightly higher propagation velocity by using intrauterine technique (2.5-5 $cm.s^{-1}$). Using a two-dimensional flexible grid comprising 64 electrodes, others authors quantified the propagation velocity (PV) by analyzing either the propagation of whole bursts of EHG (Lucovnik, 2010) (Mikkelsen et al., 2013), or single spikes identified within bursts (Lucovnik, 2010)(C. Rabotti et al., 2010)(Lau et al., 2014)(de Lau et al., 2013). These studies reported a speed of 5.30 ± 1.47 cm/s for pregnancy and 8.65 ± 1.90 cm/s for labor.

The combination of PV and peak frequency (*PF*) reported so far the highest classification rate (96%) to discriminate labor and non-labor contractions (Lucovnik, 2010). On a larger population of pregnant women, much higher figures of PV than the aforementioned studies have been reported in (Lucovnik, 2010). In these studies, authors used only two couples of standard bipolar surface electrodes.

Mikkelsen et al. (Mikkelsen et al., 2013) used three electrodes placed on the median vertical axis of the abdomen and used as reference the center of mass of the EHG burst envelop for the calculation of the interchannel delay. By analyzing separately, the upper and the lower uterine segments, authors found average values equal to 2.15 and 1.53 cm/s respectively, with a variability between 0.66 and 13.8 cm/s and between 0.58 and 6.7 cm/s for the upper and lower uterine segment respectively (Mikkelsen et al., 2013). Recently, Lange et al. used two-dimensional electrode grids of 16-channels for the EHG recordings. The estimated average propagation velocity was 2.18 (±0.68) cm/s for 35 contractions (Lange et al., 2014).

None of the above reported studies is clinically used so far. Thus, advanced techniques for analyzing the propagation of the EHG are required. In the next section, we show that more recent studies used the correlation/connectivity between EHG signals as a new feature to analyze the propagation phenomenon.

Connectivity/Correlation

Studying the correlation/coupling between signals recorded from different channels is not new. It is widely used for EEG signals. This approach has been reported in different studies based on human or animal EHG recordings. Indeed, looking at the connectivity at the electrode level could

provide important information on the synchronization of the uterine activity. Marque et al. have used the linear correlation coefficient (r^2) and noticed more correlation in low than in high frequencies (Marque, 1987). Duchêne et al. used autocorrelation, cepstrum and deconvolution function in order to study the uterine EMG propagation (Duchene et al., 1990). Their results show that no linear propagation can be evidenced from all developed methods.

The linear inter-correlation has been also used for EHG propagation analysis by Karlsson et al. (Karlsson et al., 2007). They used 16 electrodes for the EHG recording. They present both an animation of the evolution of the electric potential, as well as a temporal correlation presentation and they observed complex activation patterns.

Mansour et al. used the inter-correlation function to analyze the propagation of the internal uterine EMG of a monkey using four internal electrodes (Mansour et al., 1996). The signals were first filtered into FWL and FWH frequency bands. Their results indicate that the correlation during labor is higher for FWL than for FWH.

Other studies used the nonlinear correlation coefficient to estimate the relationships between 16 EHG signals recorded by a matrix of 4x4 electrodes placed on the woman's abdomen (Hassan et al., 2010) (Hassan et al., 2013; Muszynski et al., 2012). Authors showed a significant difference between pregnancy and labor contractions (Hassan et al., 2013) as well as an increase in the correlation of EHGs as labor approaches (Muszynski et al., 2012).

Very recently, a comparative study was performed between several correlation measures applied to EHG signals (Diab et al., 2014). Authors used the nonlinear correlation coefficient (h^2), General synchronization (H) and the Granger causality (GC). Authors tested the sensitivity of these methods to some characteristics of the signal (nonstationarity, frequency content) or of the recording protocol (bipolar or monopolar recording), in order to improve the performance of the coupling detection methods for the classification of EHG bursts recorded during pregnancy and labor. They processed EHG signals recorded from 48 women during pregnancy (174 contractions) and labor (115 contractions), with a 16 electrode matrix (4x4). The h^2 coefficient did not demonstrate any monotonic increase from pregnancy to labor. Therefore, authors tried to improve the performance of this method. They retained only the low frequency band of the EHG (FWL), which is supposed to be more related to the propagation of EHG, and proposed a time-

varying approach. Using the combination of these two preprocessing steps, the obtained Filtered Windowed-h^2 (FW-h^2) demonstrated good performance with an increase from pregnancy to labor.

Again, none of the above reported studies is clinically used so far.

1.5.1 Proposed approach

Preterm birth remains a major problem in obstetrics. Therefore**,** it has been a topic of interest for many researchers. As presented in the overview above, the uterus is a complex organ. Understanding how this organ works would be important to detect the onset of labor as well as to predict preterm labor. Among the many methods used to record the uterine contractility, the most used is the abdominal EHG, as being an easy to use and a non-invasive tool. Many studies have reported that the use of this signal could be a very powerful tool to monitor pregnancy and to detect labor. It indeed permits to access the uterine excitability (with only one EHG signal, monovariate approach) as well as the synchronization of the uterine activity, by using multiple signals (bivariate approach).

It has been shown that the connectivity analysis gave promising results when using EHG recordings in clinical application, such as the classification labor/pregnancy contractions. Thus this thesis focuses on the analysis of the uterine synchronization by mean of the study of the connectivity between the recorded EHG signals

However, in almost all previous studies, reported above, about the synchronization of uterine electrical activity (Diab, 2014; Hassan et al., 2013), authors estimated the correlation between multiple EHG signals by using different connectivity methods. On the one hand, EHG correlation matrices were often reduced keeping only their mean and standard deviations. Despite the encouraging results obtained, relevant information may have been missed due to this averaging, which may induce the relatively low classification rate reported so far. To characterize precisely the correlation matrix and quantify the associated connectivity, we propose in this thesis to use a network measure technique based on graph theory. This field has shown a growing interest in the last years, especially to characterize brain networks (Bullmore and Sporns, 2009; Rubinov and Sporns, 2010). According to this approach, the obtained correlation

matrix can be represented as graphs consisting of a set of nodes (electrodes) interconnected by edges (connectivity/correlation values between electrodes). On the other hand, recent works on the synchronization of the uterine activity used always a small database. In this thesis, we tackle this issue by using a larger database of multichannel EHG signals recorded from women during pregnancy and labor from two different clinical sites.

The new framework, to analyze the EHG signals recorded during pregnancy and labor, proposed in this thesis is based on the characterization of the correlation between the uterine electrical activities and on its precise quantification by using graph theory approach. The processing pipeline includes i) the estimation of the statistical dependencies between the different recorded EHG signals, ii) the quantification of the obtained connectivity matrices using graph theory-based analysis and iii) the clinical use of network measures for pregnancy monitoring as well as for the classification between pregnancy and labor EHG bursts. A comparison with the already existing parameters used in the state of the art for labor detection and preterm labor prediction will also be performed. We also investigate a new method to study the EHG source connectivity, to overcome the problem of computing the connectivity at the abdominal surface level.

CHAPTER 2: MATERIALS AND METHODS

In this chapter we present the materials and methods used in this thesis to study uterine connectivity, by using the graph theory applied to the electrode then to the source levels. We first present the previously used methods in the literature. Then we describe our new approach based on the graph theory where we use also a new correlation method. We also applied this new approach to uterine sources identified from the real EHGs, after source localization (uterine level). We thus describe both kinds of data used in this work: real and simulated EHGs. Simulated data were generated from a computational EHG model developed in our team. Then, we describe the experimental protocol used to record real EHG signals, the data acquisition and the different preprocessing steps. A short synthesis finally describes the network-based analysis approach by using graph theory, for the two levels of our analysis: surface-level (abdominal electrodes) and source-level uterine networks (after a source localization step).

2.1 PREVIOUSLY USED METHODS

The propagation of the uterine electrical activity has been studied with different approaches, and on different species. We report here the main results presented in the literature for the monitoring of pregnancy and the detection of preterm labor.

2.1.1 Propagation Velocity and Peak Frequency (PV+PF)

Lucovnik et al. explored on pregnant women the performance of the Propagation Velocity (*PV*) in the differentiation between nonlabor and labor EHGs (Lucovnik et al., 2011). After estimating the distance *d* that the propagating signals travels, and the time *t* needed for crossing this distance, *PV* can be estimated by dividing the distance *d* by the time *t*. For a given EHG, after computing the Peak Frequency (*PF*) from its power spectral density, the obtained *PF* value is then combined with its *PV* values by a simple summation of their values.

2.1.2 Conduction Velocity (CV)

The Conduction Velocity (*CV*) was proposed by Rabotti et al. (Rabotti et al., 2009; C. Rabotti et al., 2010). Authors estimated the velocity and the direction of the propagation of individual spikes identified in EHG signals recorded on women. The delay of time between two electrodes on a given row is t_r and on a given column is t_c. The velocity v and the angle of propagation Θ were computed using the equations:

$$v = f_s \frac{dcos(\theta)}{\tau_r}$$
$$v = f_s \frac{dsin(\theta)}{\tau_c} \qquad (1)$$

where *fs* is the sampling frequency. For more details, see (C. Rabotti et al., 2010).

PV and *CV* were mainly applied to single spikes identified within bursts, not to whole uterine burst. In this work, we have computed *PV* and *CV* on the whole EHG burst to process the same signals as with the other methods used in this thesis, and to be able to compare their results. Furthermore, these spike-based methods address only le local propagation, that can be related to close electrical tissue diffusion. In our work, we are interested in the analysis of the global synchronization of the uterine activity. For this global approach, the whole burst based connectivity measure is more pertinent. Moreover, the processing of the whole burst needs no a priori concerning which peak is supposed to be propagating, only tools for the burst segmentation (Khalil, 1997). Its use will therefore be more convenient for clinical purpose than the peak-based one.

2.1.3 Correlation analysis

Here, we refer to the correlation with the term ‘connectivity’ which represents the statistical couplings between two time series. Functional connectivity is defined as a temporal correlation between different signals recorded from different channels without any other information about the correlation direction, whereas effective connectivity describes the influence or causal effects that one signal exerts on another one (Friston, 1994), taking thus into account the direction of the information flow between the 2 signals (Lehnertz, 2011). In our work, we are interested in the

functional connectivity methods. In this section, we introduce different measures of functional connectivity. The classical linear (R^2) and nonlinear (h^2) correlation coefficients (Hassan et al., 2013), its modified version *(FW-h^2)* proposed by (Al-Omar et al., 2015; Diab, 2014) (this last method being chosen as demonstrating the highest performance for uterine EHG) as well as the imaginary part of the coherence (*Icoh*) proposed by (Nolte et al., 2004) will be presented in this section.

2.1.3.1 The cross-correlation coefficient (R^2)

The cross-correlation method measures the linear correlation between two variables X and Y in the time domain. The estimation of this coefficient for the two-time series *X(t)* and *Y(t)* is performed by using the following equation:

$$R^2 = \max_{\tau} \frac{cov^2(X(t), Y(t+\tau))}{var(X(t))var(Y(t+\tau))} \qquad (2)$$

where *var* and *cov* denote respectively the variance and covariance between the two-time series *X(t)* and *Y(t).*τ denotes the time shift (Ansari-Asl et al., 2004). R^2 was calculated by maximizing τ. R^2 varies between 0 (X and Y are independent) and 1 (X and Y are fully correlated).

2.1.3.2 The nonlinear correlation (h^2)

The nonlinear correlation coefficient (h^2) is a bivariate method that estimates the degree of dependence between two variables. The method is computed from the signals *X (t)* and *Y (t),* by considering that the value of *X* is seen as a function of the value of *Y*. Then the value of *Y* can be predicted according to a nonlinear regression curve when given *X*. The variance of *Y* according to this regression curve is termed as the explained variance, since it is explained or predicted by the knowledge of *X*. The unexplained variance is estimated by subtracting the explained variance from the original one. The correlation ratio, h^2, describes the reduction of variance of *Y* that can be obtained by predicting the *Y* values from those of *X*, according to the regression curve, as h^2 = (total variance - unexplained variance)/total variance.

In practice, to estimate the nonlinear correlation coefficient h^2, we study a scatter plot of *Y* versus *X*. We subdivide the values of *X* into bins; for each bin, we calculate the average value of

X (*pi*) and the average value of *Y* (*qi*). The regression curve is approximated by connecting the resulting points (*pi*, *qi*) by straight line segments (Pereda et al., 2005). Then, the nonlinear correlation coefficient between the two signals *X* and *Y* is calculated as follows:

$$h^2_{Y/X} = \frac{\sum_{k-1}^{N} Y(k)^2 - \sum_{k-1}^{N} (Y(K) - f(X_i))^2}{\sum_{k-1}^{N} Y(k)^2} \quad (3)$$

The estimator $h^2_{Y/X}$ ranges from 0 (*Y* is independent of *X*) to 1 (*Y* is fully determined by *X*) and the nonlinear correlation coefficient is asymmetrical so $h^2_{Y/X} \neq h^2_{X/Y}$ and thus permits to give information on the direction of the information (Hassan et al., 2013; Wendling et al., 2001). This asymmetry feature is not explored in our work as we are interested only in the presence or not of a nonlinear relationship between two signals.

2.1.3.3 Filtered Windowed h^2 (FW-h^2)

The ***Filtered Windowed h^2*** is the modified version of the nonlinear correlation coefficient h^2 proposed by Diab et al (Diab, 2014). This method showed highest performance in labor detection when compared to other methods. When trying to improve the performance of nonlinear correlation method, Diab et al. (Diab, 2014) focused on overcoming some of the weaknesses in the methodology, as well as on getting free from the natural filtering effect due to inter-individual varying fat thickness during signal recording. Based on the hypothesis that the propagation of EHG in more related to low frequency bands (FWL: 0.1 - 0.3 HZ) (Gondry et al., 1993), this new method consists of filtering the data in the low frequency bands. The contractions will be then segmented by using the bivariate piecewise stationary signal pre-segmentation (bPSP) algorithm proposed in (Terrien et al., 2008). This algorithm uses an automatic segmentation procedure of the EHG that search for the longer locally adapted stationary parts.

Authors (Diab, 2014) found that using a combination of these two preprocessing steps, the obtained Filtered-Windowed- h^2 (FW-h^2) yielded the best results in the classification between labor and pregnancy with a clear increase from pregnancy to labor. Although the encouraging results obtained in this study, the processing time of the segmentation is very long.

The above classical R2 and h^2 as well as the recent FW-h^2 correlation-based methods will be compared with the features reported in the state of the art for the propagation of the uterine electrical activity. We remind here that none of the previously used methods gave results consistent enough to be used for clinical diagnosis of preterm labor. New approaches are thus needed to improve the robustness of the results.

2.2 PROPOSED APPROACH

2.2.1 Imaginary part of coherence (*Icoh*)

Volume Conduction problem

One major problem when estimating the interactions between surface-level signals is the so-called 'volume conduction' problem. This term is used to describe the effects of recording and processing an electrical activity at a distance from its source generator. As an example, the diffusion process through this volume conduction (different tissues layered between the source and the recording electrodes) can induce a correlation between several signals even if the single sources are independent. This effect mainly occurs because the activity of a single source is mapped simultaneously by many sensors. In fact, the volume conduction plays a significant role in almost all noninvasive electrophysiological recordings, since the sensors are never in direct contact with the sources generating the signals (Westdrop, 1993). Therefore, volume conduction substantially affects the results of connectivity measures. This problem has been clearly defined and partly tackled in the context of brain network analysis using EEG (Holsheimer and Feenstra, 1977; Nunez et al., 1997; Srinivasan et al., 2007; van den Broek et al., 1998). Several methods have been proposed to deal with this problem such as the imaginary part of the coherence (ICOH) proposed by Nolte et al. (Nolte et al., 2004).

Coherence is a measure that has been widely used to detect the relationships between time series in the frequency domain. The weakness of coherence is that it is strongly affected by volume conduction. Recently new methods have been proposed in order to solve this problem by taking only the imaginary part of the coherence (Nolte et al., 2004). The hypothesis behind this method is that the real part of the coherence function reflects the zero lag interactions between signals which means a fake interaction and thus the imaginary part of the coherence may reflects the true interactions which the real correlation between signals (Nolte et al., 2004). The ICOH, a

promising tool for functional connectivity measurement of the EEG signals, has not been used yet for the EHG connectivity analysis. We thought that it could be interesting to test it on our signals and to compare it with the other methods.

The coherence (*C*) function gives the linear correlation between two signals *X* and *Y* as a function of the frequency. It is defined as their cross-spectral density function C_{XY} normalized by their individual auto-spectral density functions C_{XX} and C_{YY}. The imaginary part of coherence (*Icoh*) is then defined as:

$$Icoh = \frac{|ImC_{XY}(f)|}{\sqrt{|C_{XX}(f)||C_{YY}(f)|}} \quad (4)$$

Icoh varies between 0 (X and Y are independent) and 1 (X and Y are fully correlated). This new connectivity analysis will be tested in this work and compared to the previously used method. To quantify the connectivity computed with these different methods over the whole matrix of EHG signals, we will use the graph theory approach.

2.2.2 Graph theory

The "Graph theory" started with the scientist Euler in 1936 when he tried to find a solution for the question: "What is the best path across the seven Köningsberg bridges?" (Figure 2.1(1)) (Boccaletti et al., 2006). This path that was called later "Eulerian path" should cross over each of the seven bridges exactly once (Figure 2.1(2-3)). From such problems, the field of graph theory has developed numerous algorithms that can be applied into many domains. Later on, this approach has been largely used in several fields such as biological system, internet networks and social groups (Newman, 2002).

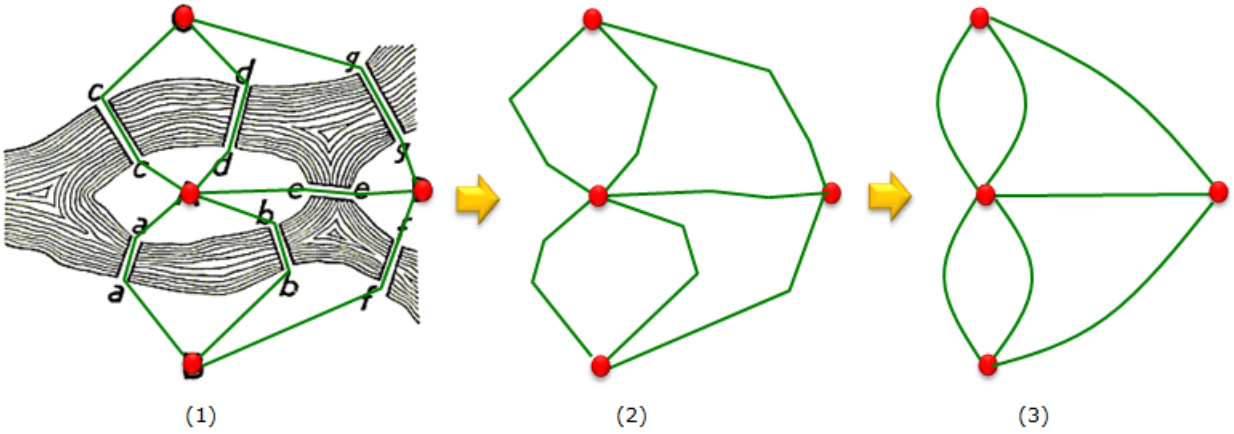


Figure 2.1 The seven Köningsberg bridges problem

In biology and medicine, network analysis includes different application such as drug target identification, determining a protein or gene function, designing effective strategies for treating various diseases or providing early diagnosis of disorders (Pavlopoulos et al., 2011). Protein-protein interaction (PPI) networks (Pellegrini et al., 2004), biochemical networks, transcriptional regulation networks, signal transduction or metabolic networks (Jeong et al., 2000) are the highlighted network categories in systems biology often sharing characteristics and properties. Graph theory has also been recently applied in neuroscience, and is nowadays considered as a promising research frontier topic in the field of brain connectivity analysis (Bullmore and Sporns, 2009; Rubinov and Sporns, 2010).

2.2.2.1 Definitions

A graph is an abstract representation of a complex system, consisting of a set of nodes (*N*), sometimes called vertices, associated with a set of connections, links or edges (E) (Figure 2.2). The edges in a graph can have different meaning, depending on the measured connectivity. Indeed, depending on the connectivity method, different types of graph can be obtained, which are related to the presence or absence of directions and weights for the edges. The weight can represent the strength of the connection, or some physical distance between the two connected vertices. According to this, four different types of graphs can be defined:

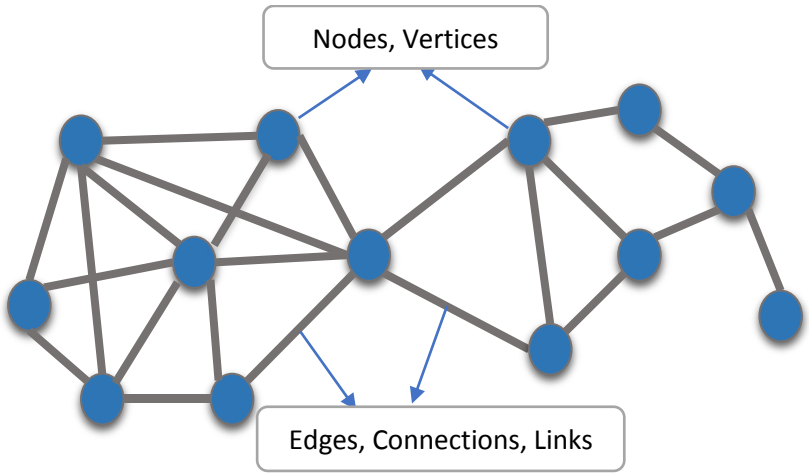


Figure 2.2 Definition of the graph.

- Binary (or unweighted) undirected: where there is no information about direction of information flow and weights of connection; the edges are absent (0) or present (1). (Figure 2.3a)
- Weighted undirected: there is information about edges weight but not about their directions (Figure 2.3 b).
- Binary (or unweighted) directed: when we know the direction of edges, but not about their weights. Edges direction represents the fact that one vertex exerts some influence on its neighbor (Figure 2.3 c).
- Weighted directed: there are information about both direction and weights of the edges (Figure 2.3 d).

The graphs obtained from a functional connectivity are undirected while from effective connectivity the graphs are directed. A graph can also be represented by a square matrix (N x N) called the "adjacency matrix". This adjacency matrix indicates if there is an edge between each pair of nodes in a graph. For undirected graphs the adjacency matrix is symmetrical (Bullmore and Sporns, 2009) (Boccaletti et al., 2006). In our case, the nodes represent the electrodes (N=16) and the edges represent the value of the connectivity measure.

A weighted graph $G^W = (N, L, W)$ consist of a set $N= \{n_1, n_2,..,n_3\}$ of nodes, a set $L=\{l_1,l_2,,....,l_k\}$ of links (or edges), and a set of weights $W= \{w_1, w_2,....., w_k\}$ that are real numbers attached to the

links. A weighted graph can be drawn as in Figure 2.3b with the thicknesses of the links representing their weights.

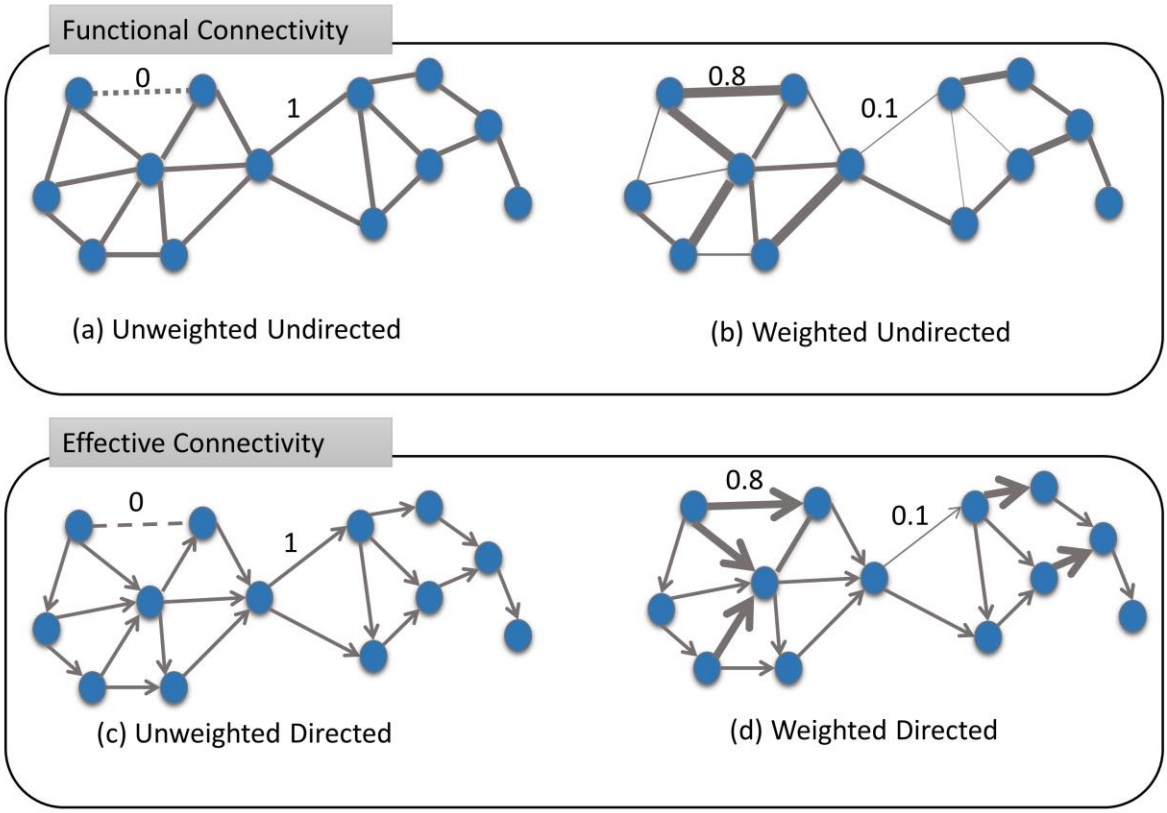


Figure 2.3 The different graph types obtained from the types of connectivity. Functional connectivity leads to: (a) Unweighted (Binary) Undirected graph and (b) Weighted Undirected graph. Effective Connectivity leads to: (c) Unweighted (Binary) Directed graph and (d) Weighted Directed graph

2.2.2.2 Graph parameters

Several metrics can be extracted from a graph:

1) Strength

The strength shows the importance and the contribution of each node with respect to the rest of the network. The strength of a node is the sum of the weights of the edges connected to this node and can be defined as:

$$S_i = \sum_{j \in N} w_{ij}. \qquad (5)$$

where *i*, *j* denotes respectively the i^{th} , j^{th} nodes and w_{ij} is the value (weight) of the relation between nodes *i* and *j* (Rubinov and Sporns, 2010). The average strength value over all the nodes can be also computed, indicating the overall characteristic of the network (Figure 2.4 a).

2) Density

The network density is the actual number of edges in the graph as a proportion of the total number of possible edges. Connection weights are ignored in the calculation. It is one of the basic estimator of the physical cost of a network (Bullmore and Sporns, 2009). The density can be estimated as follow:

$$D = \frac{\sum_{j \in N} a_{ij}}{n}. \qquad (6)$$

where a_{ij}=1 if there a link between nodes *i* and *j (*Figure 2.4 *d).*

3) Clustering Coefficient

Clustering coefficient is a graph measure introduced by Watts and Strogatz (Watts and Strogatz, 1998). This measure captures the degree to which the neighbors of a given node link to each others. For a node *i* with degree k_i the local clustering coefficient is defined as the fraction of triangular connection around the node.

$$C_i = \frac{2t_i}{k_i(k_i-1)}. \qquad (7)$$

where t_i denotes the number of triangular connections around the node and $k_i(k_i-1)$ the maximum possible number of edges in the graph (Muñoz-Martínez, 2000; Watts and Strogatz, 1998).

The clustering coefficient is a measure between 0 (none of the neighbors of node *i* link to each other's) and 1 (the neighbors of node *i* form a complete graph, i.e. they all link to each other's). C_i is the probability that two neighbors of a node link to each other. Consequently, C = 0.5 implies that there is a 50% chance that two neighbors of a node are linked.

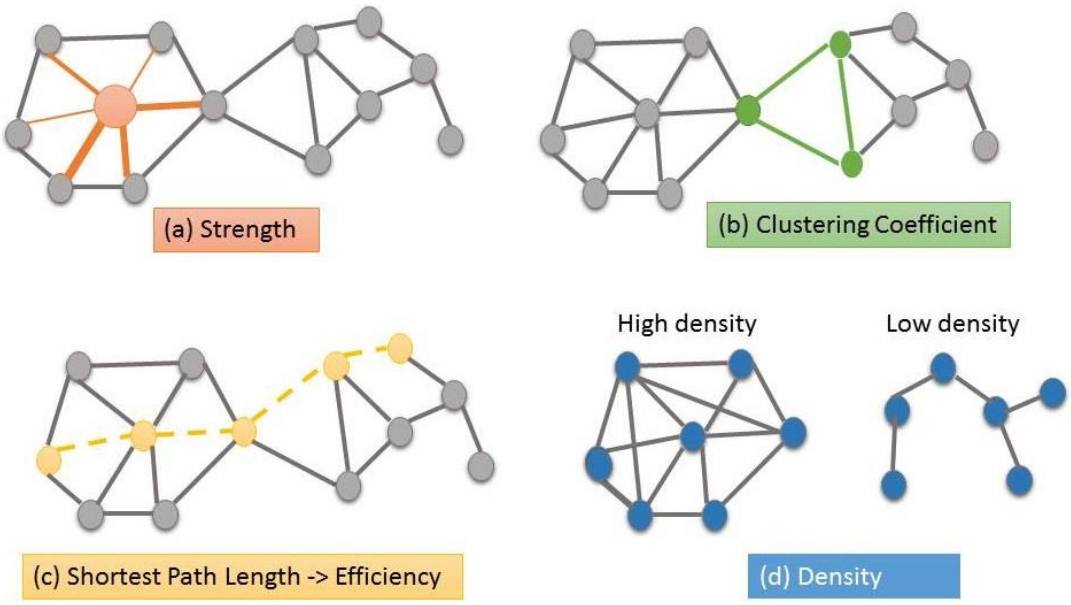


Figure 2.4: Measures of network. (a) Strength: the sum of weights of links connected to the node (orange). (b) Clustering coefficient: triangle counts (green) (c) The Efficiency based on the shortest path length (yellow) (d) Density: fraction of present connections to possible connections (Gray and blue).

To sum up, C_i measures the network's local link density: The more densely interconnected the neighborhood of node *i*, the higher is its clustering coefficient (Figure 2.4 b).

4) Local efficiency

Local efficiency is an alternative measure of the clustering properties of a graph (Boccaletti et al., 2006). It is the inverse of the shortest path parameter between a pair of nodes.

$$E = \frac{1}{N(N-1)} \sum_{i,j \in N,\, i \neq j} \frac{1}{d_{ij}}. \qquad (8)$$

where *i*, *j* denotes respectively the i^{th} , j^{th} nodes, d_{ij} is the value of the shortest path length between nodes i and j (Freeman, 1978) (Figure 2.4c).

2.2.3 Source localization

Another original feature of this work is to study the uterine connectivity first, classically at the abdominal surface level, where the methods (connectivity measures) are applied to the EHGs, and then at the uterine level, where the analysis is applied to the uterine electrical sources. These uterine sources have first to be estimated from the surface-level recordings, the EHGs, by solving the so-called inverse problem. Generally speaking, this inverse problem consists of estimating the internal sources S(t) from the surface signals X(t) (here the EHGs). The main advantage of this approach is to analyze directly to the sources that generate the EHG signals. Source reconstruction has been widely applied to EEG (Hassan et al., 2013)(Hassan et al., 2014) (Becker et al., 2014; Hassan et al., 2014, 2016; Hauk, 2004; López et al., 2014; Montes-Restrepo et al., 2014) and MEG (Hauk et al., 2011; Mattout et al., 2006). To our knowledge, the source localization has been applied on uterine EHG very recently, for the first time, by Marque et al. (Marque et al., 2015). Source localization requires two processing steps: i) the forward problem, to model the path from the source to the surface signals; ii) the inverse problem, going from real surface signals to the estimated sources.

2.2.3.1 Forward problem

The forward problem is used to define the path of signal propagation from the sources (here the uterine muscle) to the recorded sites (here the electrodes on the abdominal skin) (Mideksa et al., 2013). This problem involves calculating the electric potentials generated by known current sources for a given anatomical model.

Forward modeling is done in our case based on a volume-conduction model that describes the geometrical and electrical properties of the tissue in the abdomen above the uterus. The volume conduction often requires a geometrical description of the tissue boundaries contained in the abdomen (Mideksa et al., 2013).

The volume conductor model that we first used in this work for the forward problem, assumes that the abdomen above the uterus consists of a set of 3D meshes, made of triangulated surfaces, representing the uterine muscle, the abdominal muscles, the fat, and the skin. If the conductivities for each of these regions are isotropic and constant, the electric potentials can be expressed in terms of surface integrals. Thus, the forward EHG problems can be solved numerically using the boundary-element method (BEM) (Gramfort et al., 2010; Hall, 1994;

Kybic et al., 2005). The BEM is a numerical technique for estimating the surface potentials generated by known sources. This method is still widely used because of its low computational needs. The method was first used in the field of electrocardiography (Hallez et al., 2007)., then in the field of EEG source localization in (Hallez et al., 2007). BEM provides a solution by calculating, for a given predefined volume, the potential values at the interfaces and boundary of the volume, induced by a given current source simulated by a current dipole. The interfaces separate regions of differing conductivity within the volume, while the boundary is the outer surface separating the non-conducting air with the conducting volume (Hallez et al., 2007). In our case, BEM calculates the potentials/fields of the non-intersecting homogeneous regions bounded by the uterine muscle, abdominal muscle, fat, and skin surface boundaries, giving thus a representation of the links existing between any point of the uterine muscle, as a possible source (dipole), and any point of the skin surface recording possible for EHG recording. This link, known as the leadfield matrix, will then be used for the inverse problem.

2.2.3.2 Inverse problem

As for other biological signals, the uterine activity can be estimated from surface EHGs by solving an ill-posed inverse problem that is regularized using anatomical and mathematical constraints (Grech et al., 2008). An increasing interest in current dipole reconstruction algorithms has occurred during the past few years. All these algorithms have in common that elementary dipoles are distributed on regular grids (Fuchs et al., 1999). The calculation of the strengths and position of these dipoles usually leads to a highly under determined system of equations – the number of unknown dipole P components (the sources) is greater than the number of channels M (the recorded EHGs).

According to the linear discrete equivalent of current dipole model, EHG signals X(t) measured from M channels can be expressed as linear combinations of P time-varying current dipole sources S(t) as follow:

$$X(t) = G.S(t) + N(t) \tag{9}$$

where *G* is the leadfield matrix of the dipolar sources and *N(t)* an additive noise.

The inverse problem consists of finding an estimate $\hat{S}(t)$ of the dipolar source parameters (typically, the position, orientation and magnitude), given the EHG signals *X(t)* and given the

gain matrix ***G*** already computed from a multiple layer uterus model (volume conductor) and from the position of electrodes by using BEM by means of the forward problem step.

Several algorithms have been proposed to estimate the sources moments based on different spatial and temporal assumptions (Groetsch, 1993; Vogel, 2002). Here we chose to evaluate 3 of the most commonly used algorithms (in the context of brain sources localization): the Minimum Norm Estimate (*MNE*), the weighted Minimum Norm Estimate (*wMNE*) and the standardized Low Resolution brain Electromagnetic Tomography (*sLORETA*), presented below.

1) Minimum Norm Estimate (MNE)

The Minimum Norm Estimate was proposed by Hämäläinen and Ilmoniemi in (Hämäläinen and Ilmoniemi, 1994) Its concept is to search for the solution with the minimum power. This type of estimations is well suited to distributed source models where the dipole activity is likely to extend over some areas of the surface.

A common equation for MNE resolution matrix is written as follow:

$$\hat{S}_{MNE} = (G^T G + \alpha I)^{-1} G^T X \tag{10}$$

where *I* is the identity matrix and α is the regularization parameter that weights the influence of priors in the solution.

2) Weighted Minimum Norm Estimate (wMNE)

The Weighted Minimum Norm Estimate compensates for the tendency of MNE method to favor weak and surface sources. This algorithm concept is to modify the general expression of the MNE method by introducing a weighting matrix W, giving thus:

$$\hat{S}_{wMNE} = (G^T W G + \alpha I)^{-1} G^T W X \tag{11}$$

where *W* adjusts the properties of the solution by reducing the bias inherent to MNE solutions. Generally, *W* is a diagonal matrix that is estimated from matrix G, with non-zero terms inversely proportional to the norm of the lead field vectors.

3) Standardized low resolution brain electromagnetic tomography (sLORETA)

Standardized low resolution brain electromagnetic tomography (sLORETA) (Grech et al., 2008) is a method in which the localization is based on images of standardized current density. As input, the sLORETA uses the current density estimate evaluated by the minimum norm estimate $\hat{S}_{\mathrm{wMNE}}$ then it standardizes it, based on its variance.

$$\hat{S}_{sLORETA} = \hat{S}_{MNE,I}^{T}\{|V_D|_{II}\}^{-1}\hat{S}_{MNE,I} \tag{12}$$

where:

- $\hat{S}_{MNE,I}^{T}$ is the current density estimate at the I^{th} voxel given by the minimum norm estimate
- V_D is the variance of the estimated current density $\hat{S}_{MNE,I}^{T}$
- $\{|V_D|_{II}\}$ is the I^{th} diagonal block of V_D defined as $G^T[GG^T + \alpha I]^{-1}$.

The choice of α is important and many approaches have been proposed for its estimation. Although there is no agreement on any optimal solution, our focus in this study is to compare different methods for our new approach based on inverse solutions and connectivity estimates. We thus choose to use the same value of 0.28 for the three inverse algorithms, as the inverse of the signal to noise ratio of our abdominal EHG real signals.

We used these three inverse problem methods in order to estimate the uterine sources from real EHG signals. Connectivity methods and graph theory parameters will then be extracted from these estimated signals, as they are extracted from surface EHGs.

2.3 DATA

We first applied our new approach, developed for the quantification of the uterine activity connectivity (connectivity measures associated to graph theory), to real EHG signals (abdominal level). These signals have been recorded on women, during pregnancy or during labor, preprocessed, and used to test the clinical power of this new quantification of uterine contractility, for the monitoring of pregnancy and the detection of preterm labor.

We also applied this new approach to uterine sources identified from the real EHGs, after source localization (uterine level). We have had thus to use simulated EHG signals, in order to first test and compare the efficiency of the different source localization presented above, before using them for source localization from real EHGs.
We describe in this section both kind of data used in this work: real and simulated EHGs.

2.3.1 Real EHGs

Experimental protocol

We used a standard protocol, defined in a previous study, to record the electrical activity of the uterine muscle. This protocol uses a grid of 16 monopolar electrodes (4x4 matrix) placed on the woman's abdominal skin, with two reference electrodes on each of her hips. The hip is chosen as the reference site as there is little electrical activity under the electrode and the distance from the reference electrodes to the abdominal electrodes is small. The standardized system uses Ag/AgCl electrodes (8mm diameter, with 17.5 mm distance between the centers of two adjacent electrodes), an alignment frame, a double-sided hypoallergenic adhesive sheet and a silicone backing. The alignment frame was used to align and attach the double-sided adhesive sheet to the silicone backing. The electrodes were then placed into the holes of the silicone backing and attached to the adhesive sheet. The abdominal skin of the woman was carefully prepared by using an abrasive paste and cleaned with alcohol solution. The electrode holes are filled with electrode gel and then the electrode matrix is placed on the abdomen.

The grid position on the abdomen is standardized as: the third column of the electrode grid has to be located on the median vertical axis of the uterus; the 10th–11th pair of electrodes has to be located midway between the uterine fundus and pubic symphysis (Figure 2.5a). We avoid the navel by moving the matrix up or down whilst staying as close as possible to the desired position. We also prepare the skin over the iliac crests on both sides in the same procedure as for the abdomen. A ground electrode and a reference electrode with electrode gel were then attached on each side using adhesive washers. A tocodynamometer (TOCO) was also attached to the abdomen during recordings. The measurements were performed using a 16 channels multi-purpose physiological signal recorder (Embla A10). A typical example of the electrodes and

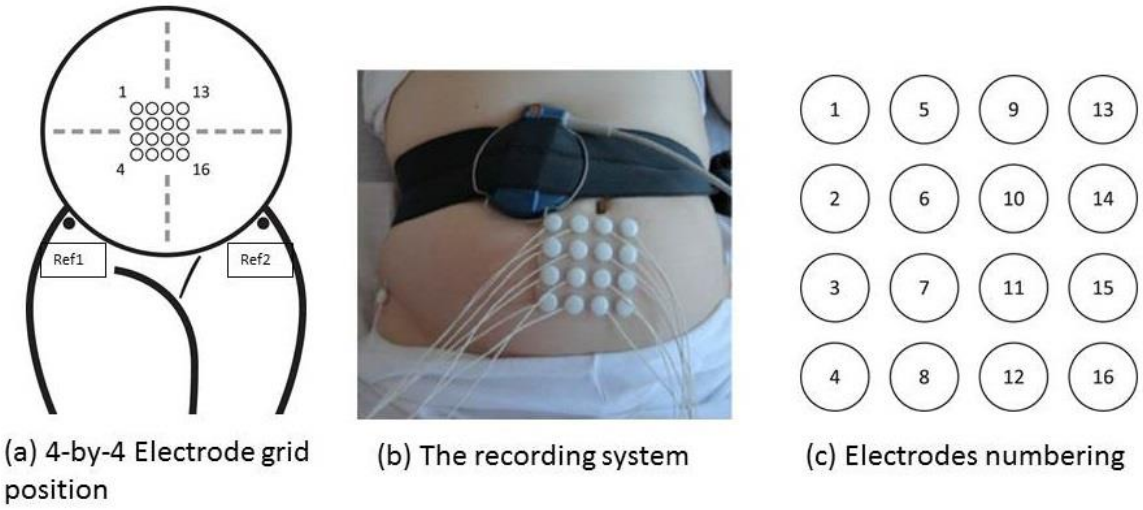


*Figure 2.5 The grid of 4*4 electrodes system used for the uterine EHG measurement. (a) The grid position on the woman abdomen. (b) The recording system composed of the grid of electrodes, two references electrodes and the TOCO sensor. (b) The electrodes numbering on the grid when looking at the woman abdomen*

tocodynamometer sensor placement is illustrated in Figure 2.5b. The electrode numbering repartition, as seen when looking at the abdomen of the woman is as presented in Figure 2.5c.

If the woman was in pregnancy, she was asked to seat in recliner chairs and a support, such as a small pillow, was positioned under the right side of the participants to prevent potential aorto-caval compression syndrome. For labor recordings, the woman was lying on her bed in the maternity room. The woman was asked to sign an informed consent form and the declaration of Helsinki was respected in all aspects. The duration of a pregnancy recording was about one hour and the duration of a labor recording was at least half an hour (depending on the delivery conditions).

After the recording, we followed the pregnant women in order to label their signals as either pregnancy or labor. Women were considered in labor if they were measured a maximum of 24 hours before delivery, thus their EHGs were labeled “labor”. If the delivery occurred later, the signals were labeled “pregnancy”. The sampling frequency was 200 Hz, after using an antialiasing filter (Low-pass 100 Hz). The data were recorded at the Landspitali university hospital (Reykjavik, Iceland) using a protocol agreed by the Icelandic ethical committee (VSN02-0006-V2) and at the Center for Obstetrics and Gynecology (Amiens, France), using a protocol agreed by the French ethical committee (ID-RCB 2011-A00500-41).

Data Pre-processing

The bursts of EHG related to uterine contraction (muscle activity) were segmented manually based on the tocodynamometer trace recorded simultaneously. The tocodynamometer paper trace (reflecting the mechanical activity of the abdomen) was digitalized in order to ease the segmentation of the uterine contractions (figure 2.6a).

The EHGs are corrupted by different artifacts, such as the mother cardiac activity, electronic noises, drip pump noise… Thus, the segmented bursts were then denoised by using a CCA-EMD method, developed in the team (Hassan et al., 2011). This algorithm is a combination of blind source separation using canonical correlation analysis (BSS_CCA) and empirical mode decomposition (EMD) methods, permits to efficiently denoise monopolar EHGs. An example of the obtained signals is illustrated in Figure 2.6. The figure presents the digitized TOCO trace

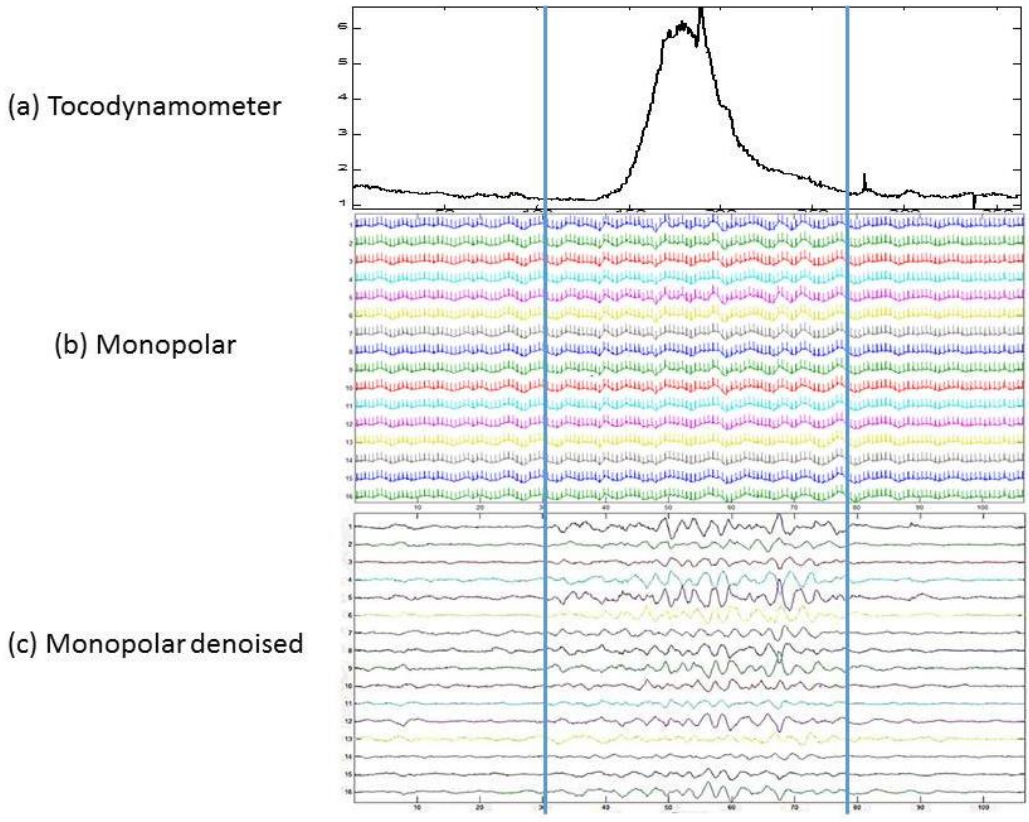


Figure 2.6 : Segmentation and Denoising of the recorded EHG signals. (a) TOCO signal used for segmentation. (b) Monopolar raw EHGs. (c) Monopolar EHGs after denoising.

(Figure 2.6a), the monopolar recorded signals (Figure 2.6b) and the monopolar signals after denoising (Figure 2.6c). After segmentation and denoising, we obtained 183 labor and 247 pregnancy bursts. These contractions were extracted from 35 healthy women. Detailed information on the women enrolled in our study is presented in Table A. 1 (Appendix A).

2.3.2 Simulated EHGs

Studying the global synchronization of the uterus at the source level, by using noninvasive signals (recorded real EHGs) could be a very important tool for clinical purpose. In this part of our work, we used simulated EHGs signals to test and compare the efficiency of the different source localization and connectivity methods, in order to then use the best ones for processing the real EHGs. As source localization from real EHGs is based on solving the inverse problem, the performance of the different inverse problem should be first tested on simulated network obtained. For this aim, we used a realistic model developed in our team, to simulate EHGs (Yochum et al., 2016). This model permits us to control the number, position and activity of the uterine sources (network of sources) used to simulate the EHGs. The original simulated network is called the "ground truth". This ground truth will then be compared with the estimated, one after application of the different methods, in order to identify the best inverse/connectivity combination to be applied to real EHGs. We present in this section the uterine model and the different simulated networks, based on this model, used as ground truth to test the methods.

EHG model

The model is multi-scale. It combines different sub-models of the uterine smooth muscle behavior, going from the electrical activity, generated at the cellular level, to the abdominal level where the EHGs are simulated. This model is also multiphasic. It computes also the mechanical force generated by the muscle, and from these forces, the deformation of the uterine tissue.

The electrical model, adapted from the Hodgkin-Huxley model, describes, at the cell level, the ionic currents involved in the uterine cell activity, as well as the diffusion of the electrical activity to the neighboring cells. As outputs of this model we get first Vm, the cell electrical potentials at the uterine muscle surface. These Vm propagate through the volume conductor

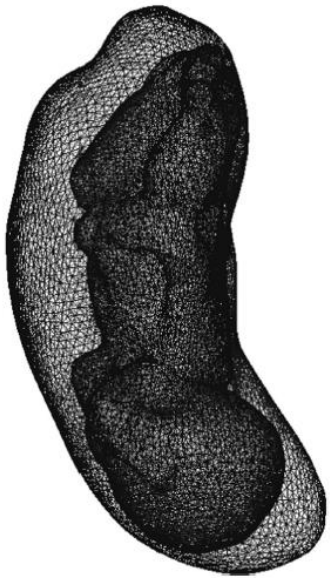


Figure 2.7: Uterine and fetal mesh (Yochum, Laforêt, and Marque 2016)

model (modeling the 3 layers: abdominal muscle, fat, and skin) and are then integrated via the electrode model to simulate the EHGs.

The second output of interest of the cellular electrical model is the intracellular calcium concentration, which is then used as an input parameter of the force model that gives the force generated by each active cell. The last step is to simulate the deformation of the uterine muscle at the tissue and organ levels. This is done by moving the cells depending on their generated force, by using a simple visco-elastic model of the tissue behavior, based on the classical Kelvin-Voight model (Yochum et al., 2016).

The co-simulation of the electrical and the mechanical models is done on a realistic 3D uterine mesh. Figure 2.7 presents the uterine mesh that we used for the simulations. This mesh was obtained from the FEMONUM project (http://fmonum.telecom-paristech.fr/) that offers the scientific community 3D fetal, uterine and abdominal meshes extracted from MRI imaging (Bibin et al., 2010). This figure displays the original mesh including the fetus mesh (head downwards), seen from the mother's left side. This mesh contains 99 084 vertices, where the surface of each vertex is 1.74 mm^2. Each vertex is associated with an electrical and a force models. Each edge of this mesh is associated to an electrical diffusion process and to a Kelvin Voight model, in order to be able to co-simulate the electrical propagation and the tissue deformation. As illustrated in Figure 2.8 we were able to generate delayed uterine activity in

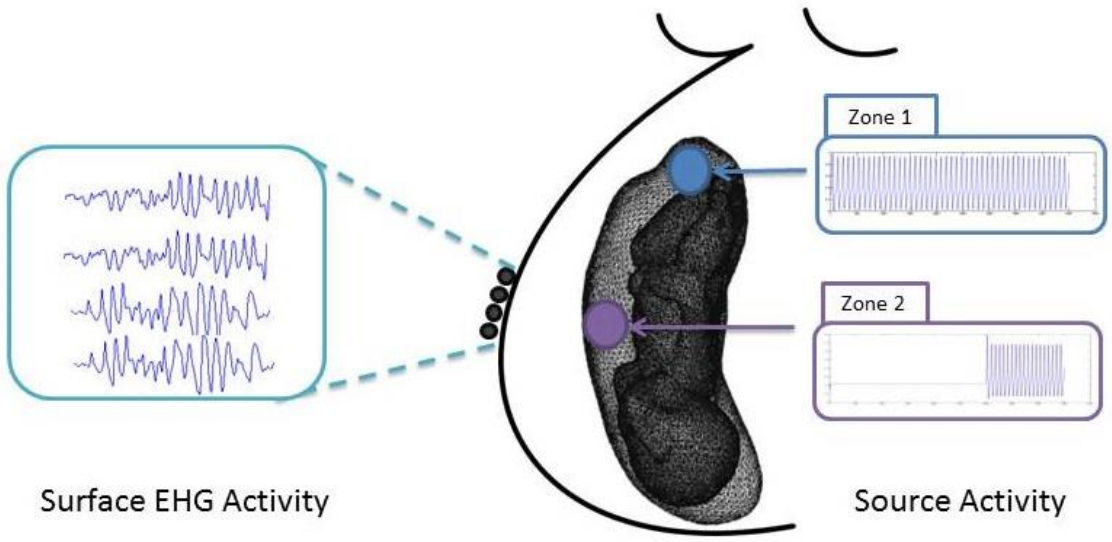


Figure 2.8: Simulated Uterine EHG signals from source cells

multiple zones just by introducing short delays between the simulation start times of the activated zones. A noise was also added to the simulated source signals. This noise was obtained based on real signals recorded from monkeys (Terrien, 2005). An example of the monkey uterine EHG signals is presented in Figure 2.9. We use these signals to estimate the SNR value (3.59 db) that permitted us to define the level of noise added to the simulated source signals.

The simulation time was 45 seconds (the average period of a real contraction) and the sampling frequency was 200 Hz. In our case we have activated 1000 cells. We have considered in our work three different scenarios, described below.

Scenario 1

In this scenario a single network fully connected was generated. We have activated 1000 regions that were grouped into sixteen zones depending on their Euclidian distance. We have labeled these zones by their number (from 1 to 16). In this scenario, signals of 45 s at 200 Hz were simulated. All regions are activated at the same start time (t_0=0s). After simulation, a noise is added to these signals. (Figure 2.10a) .

Scenario 2

In the second one we have generated an interconnected network. As in the first case, the regions are grouped into sixteen zones. In this case, only four zones were activated (zones 1, 3, 5 and 6). The signals of zones 1 and 6 started at t0=0s, while a time delay was added to signals of zones 3 and 5. The zones 3 and 5 were highly correlated with zones 1 and 6, but with a delay (30s). (Figure 2.10b).

Scenario 3

In this case, we have activated created two interconnected networks. The signals of zone 1, 2, 3, 4, 5 and 14 were activated. Thus we created two interconnected networks that are also connected to each other together. (Figure 2.10c).

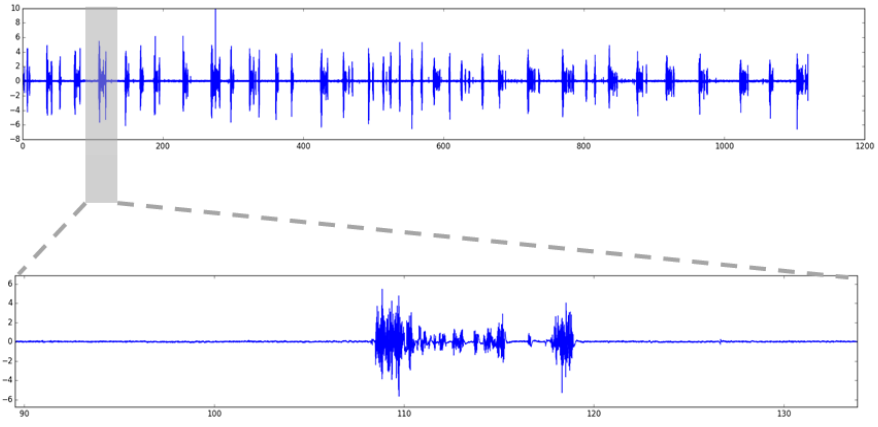


Figure 2.9 Example of an EHG signal recorded in the uterus of a monkey

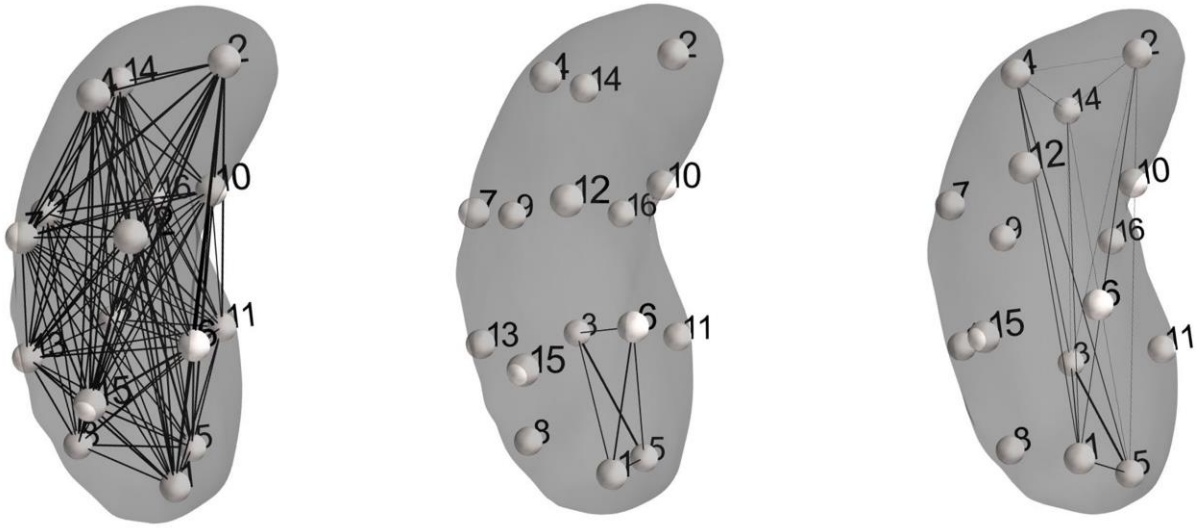


Figure 2.10 The different scenarios network. (a) Ground truth of scenario 1. (b) Ground truth of scenario 2. (c) Ground truth of scenario 3.

2.4 WORK CONTENT

The work in this thesis in divided into two main parts i) the analysis of the connectivity at the level of abdominal sensors (EHG) and ii) the analysis of the connectivity at the level of uterine sources.

2.4.1 Connectivity on surface level

The complete pipeline of our approach is presented in Figure 2.11 The first step consists in recording the uterine contractions by using a grid of 4x4 electrodes (Figure 2.11a). The EHG signals are then segmented and denoised (Figure 2.11b). The third step is to compute the connectivity between the denoised signals using different connectivity methods (Figure 2.11c).

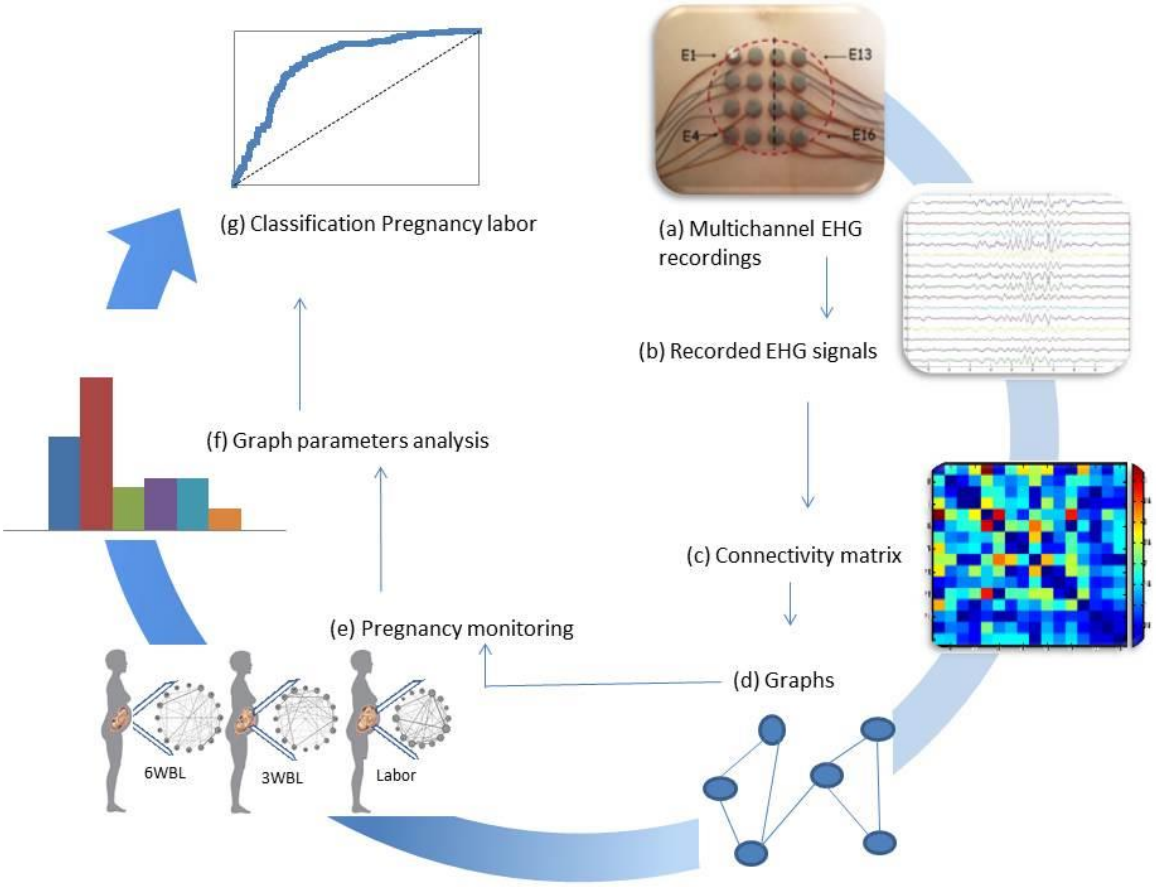


Figure 2.11 Structure of the investigation. (a) Multichannel EHG recordings using a grid of 4x4 electrodes. (b) Segmentation and filtering of EHG signals. (c) Pair-wise connectivity matrix. (d) Characterization of connectivity matrices using network measures (e) Graphs used for pregnancy monitoring along week of gestation . (f) Statistical study based on the extraction of graph parameters. (g) Classification of labor/pregnancy.

The connectivity matrix obtained with each method can be represented by a graph (Figure 2.11d). These graphs are computed from uterine pregnancy and labor EHG contractions at different term (Figure 2.11e). Several measures can be extracted from the obtained graphs based on graph theory (Figure 2.11f). These measures are then used to evaluate the clinical impact of the proposed approach in the classification between labor and pregnancy contractions and for pregnancy monitoring (Figure 2.11g).

2.4.2 Connectivity at the source level

The main objective in this second part is to estimate a corresponding graph for the electrical activity of the uterus at the source level. Therefore, it is important to find the best combination

inverse problem/connectivity methods. We based this analysis on the simulated networks described previously. We explain the complete pipeline of this analysis below.

As illustrated in Figure 2.12, a given simulated network was generated at the source level. Surface EHG signals were obtained by solving the forward problem with the uterine model previously described. The volume conductor contains: the myometrium (where the source is located) with conductivity = 0.2 S/m and depth = 0 (the source are supposed to be located at the surface of the uterine muscle); the abdominal muscle with conductivity 0.3 S/m, and thickness = 0.936 cm; fat with conductivity = 0.04 S/m and thickness = 2 cm; and skin with conductivity =

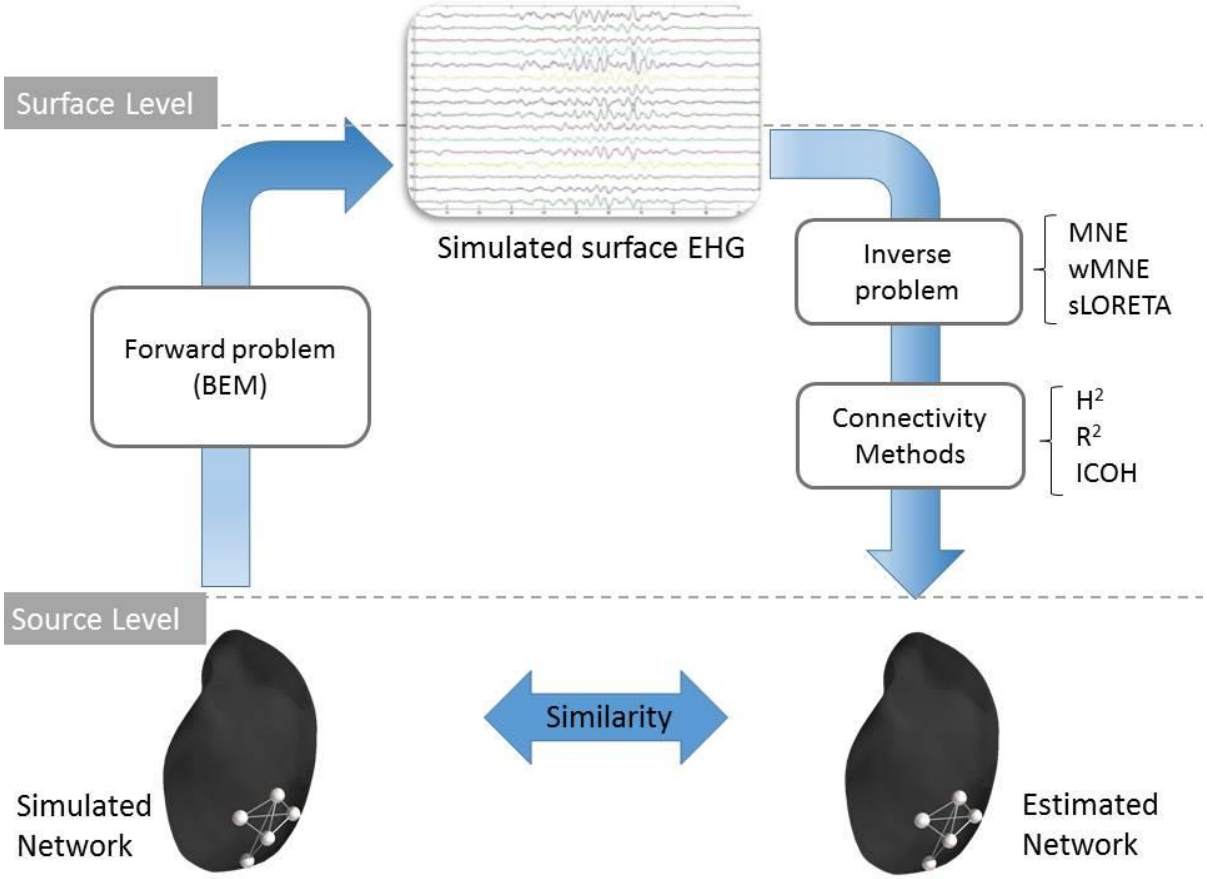


Figure 2.12: Structure of the investigation. First, a given network is generated by the model and considered as the 'ground truth'. The statistical couplings are then computed between the original sources by using three different methods (R^2, h^2 and Icoh). By solving the forward problem, we generate synthetic EHGs. These signals are then used to solve the inverse problem in order to reconstruct the sources by using three different inverse solutions (MNE, wMNE, sLORETA). The statistical couplings are then computed between the reconstructed sources by using the same different methods (R^2, h^2 and Icoh). The identified network by each combination (inverse/connectivity) was then compared with the original network using a 'network similarity' algorithm.

0.5 S/m and thickness = 0.2 cm. The corresponding leadfield is computed by using the Boundary Element Method (BEM) with OpenMEEG (Gramfort et al., 2010). After the estimation of EHG signals we added to these signals different SNR values. From these simulated EHG signals, source activity was estimated by using three inverse algorithms (wMNE, sLORETA and MNE).

After the reconstruction of sources, functional connectivity was estimated by using three methods (R^2, h^2, *Icoh*). In all the scenarios (scenario 1, 2 and 3), the connectivity matrices were 16x16. These matrices were thresholded by saving edges with the highest weight values. We have tried different threshold values in order to investigate the effect of threshold on the results. Threshold value ranged from 50% to 5%. These thresholds were applied on the matrices obtained with all the combinations (inverse/connectivity).

In order to compare the reference uterine network, simulated from the ground truth modeled in each scenario, with the network identified from simulated surface EHG by each of the inverse/connectivity combination, we used the simNet algorithm (Mheich et al., 2015). The main advantage of this algorithm is that it takes into account the spatial location (3D coordinates) of the nodes when comparing two networks. The algorithm provides a normalized Similarity Index (SI) between 0 (totally different graph) and 1 (same graph).

Once identified the best methods, the source localization was applied, for real EHG, on the segmented contractions (see section 2.3.1) using the best inverse/connectivity combination methods. The same thresholding procedure was also applied for the 16x16 connectivity matrices

2.4.3 Statistical tests

We used the Wilcoxon test in order to test the significance differences obtained between different situations. The Wilcoxon test is a nonparametric test used without a constraint about the distribution to be normal. This test can be also applied when the samples have unequal size (Wilcoxon, 1992).

To evaluate the classification performance of the different features, we used the Receiver Operating Characteristic (ROC) curve analysis (Metz, 1978; Zweig and Campbell, 1993). ROC curve is a fundamental tool for diagnostic classification test evaluation. In a ROC curve the true positive rate (Sensitivity) is plotted in function of the false positive rate (100-Specificity) for

different cut-off points of a parameter. Each point on the ROC curve represents a sensitivity/specificity pair corresponding to a particular decision threshold. The area under the ROC curve (AUC) is a measure of how well a parameter can distinguish between two diagnostic groups (in our case labor/pregnancy).

In our case if we are looking if a woman is in the labor phase or not, the definition of specificity and sensitivity will be then as follows:

Specificity is the probability that a test result will be negative when the patient is not in labor (true negative rate, expressed as a percentage).

$$Specificity = \frac{TN}{FP + TN} \tag{13}$$

Sensitivity is the probability that a test result will be positive when the patient is in labor (true positive rate, expressed as a percentage).

$$Sensitivity = \frac{TP}{TP + FN} \tag{14}$$

where TP, TN, FP and FN stand respectively for True Positive, True Negative, False Positive and False Negative values.

2.4.4 Software

On real data, we used the matlab based Brain Connectivity Toolbox (BCT) for the calculation of graph parameters (Rubinov and Sporns, 2010). For the surface-level graph visualization, we used 'GEPHI' software (Bastian et al., 2009). For the simulated data, we used Python programming language using the 'Pycharm Edu 2.0.3' software (www.jetbrains.com). For the network visualization, we used 'mayavi' toolbox on the same software.

CHAPTER 3: EHG CONNECTIVITY ANALYSIS DURING PREGNANCY AND LABOR

3.1 OVERVIEW

In most previous studies, the EHG correlation matrices were reduced by keeping only their average. Despite the encouraging results obtained, relevant information was missed due to this averaging. To characterize precisely the correlation matrix and quantify the associated connectivity, we used here analysis tools based on graph theory. As presented in Chapter 2 section 2.4.1, the aim of this work is to characterize the connectivity between the noise-free EHG signals using different connectivity methods and the graph theory. The obtained connectivity matrix is thus represented by a graph where electrodes represent the nodes and the edges represent the connectivity values. These graphs are computed from pregnancy and labor uterine contractions at different terms. Several measures are then extracted from the obtained graphs by using graph theory. These measures are used to evaluate the clinical impact of the proposed approach in the context of classification between labor and pregnancy contractions.

A total number of 247 pregnancy and 183 labor contractions were segmented from 35 women. In order to differentiate between these two groups, we have computed three connectivity methods: r^2 (Ansari-Asl et al., 2004), FW_h^2 (Diab, 2014) and *Icoh* (Nolte et al., 2004). r^2 has been used in (Marque et al., 1987); authors noticed more correlation in low than in high frequencies. FW_h^2 has been chosen as demonstrating the highest performance for uterine EHG in (Diab, 2014). The imaginary part of the coherence (Icoh), proposed in (Nolte et al., 2004) was shown to reduce efficiently the effect of volume conductor (in the context of brain connectivity). These methods are bivariate, thus they should be computed over all the pair-wise combinations of the 16 channels. We obtain a connectivity matrix (graph) for each contraction and each method. We have then tested the performance of each method for the classification between pregnancy and labor contractions. To investigate the added value of the graph measures, we have compared the

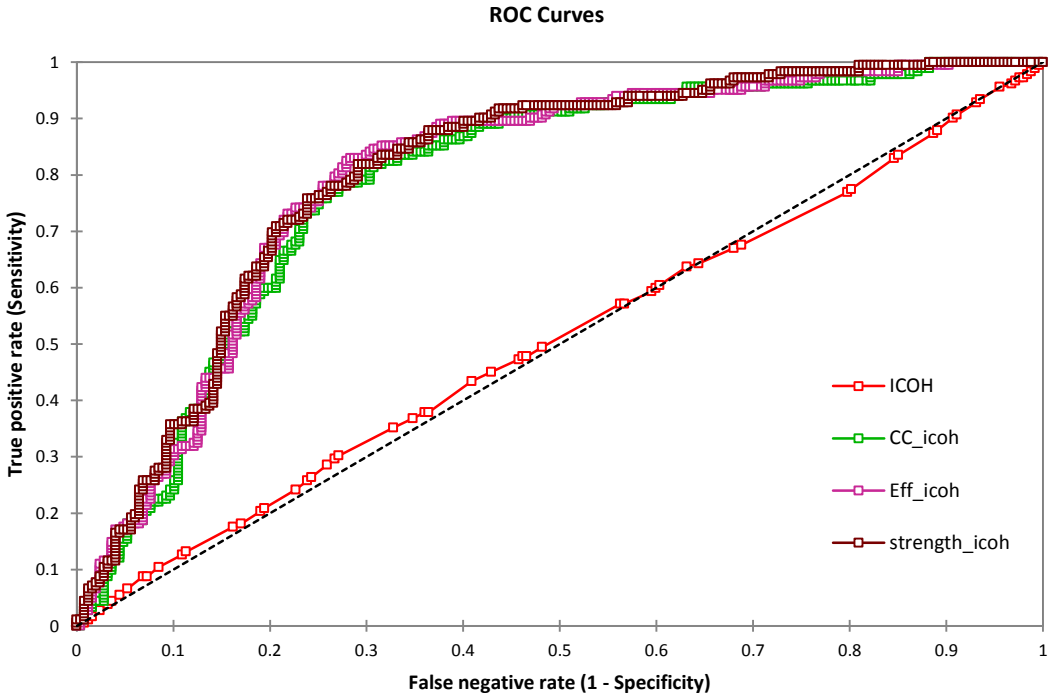


Figure 3.1 ROC Curves for Icoh without and with using graph analysis. CC_icoh, Eff_icoh, strength_icoh represents respectively the results obtained with CC, Eff, Str parameters computed from the connectivity values obtained by Icoh. Icoh represents the roc curve of the results obtained using Icoh without graph.

results given by each graph metric with the ones obtained by the approach previously used in the context of EHG correlation analysis (average of the values of each connectivity matrix). The results are also compared to the metrics mostly used in the literature, mainly *PV+PF* (Lucovnik et al., 2011) and *CV* (de Lau et al., 2013; Rabotti et al., 2009) by using ROC curves. We used here three graph metrics, described in the previous chapter,: *Str*ength (*Str*), *Eff*icency (*Eff*), Clustering Cofficient (*CC*) (Boccaletti et al., 2006; Rubinov and Sporns, 2010). We have also used the density parameter when visualizing the graphs.

3.2 PREGNANCY VS. LABOR CLASSIFICATION

In this section, the contractions are grouped into two groups: pregnancy and labor.

3.2.1 Graph measures

We present the ROC curves obtained for the different tested methods.

Figure 3.1 shows the ROC curves obtained for the imaginary part of coherence (*Icoh*) without/with graph measures. The area under curve (AUC) was higher when using the graph parameters for *Icoh*. For instance, AUC increases from 0.504 (*Icoh*) to 0.801 (*Icoh*/*Str*). *CC*, *Eff* and *Str* showed a good classification rate, with the highest AUC for *Str*. *Eff* presents an (AUC) of 0.797, with 82% sensitivity and 72% specificity, while *CC* has an AUC of 0.785, with 78 % sensitivity and 73% specificity. *Str* presents the highest AUC (0.801), with 82 % sensitivity and 71 % specificity

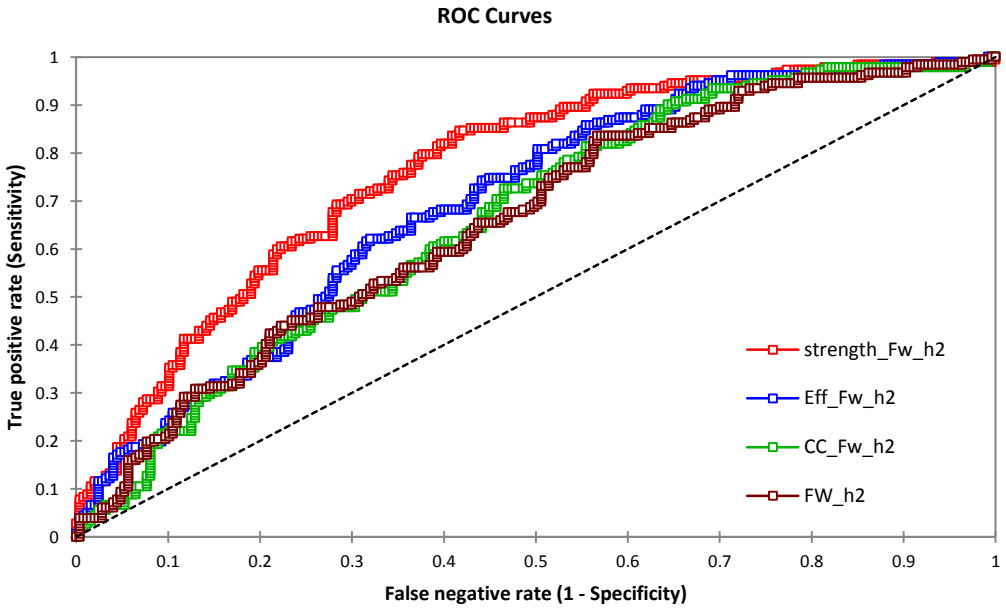


Figure 3.2 ROC Curves for FW_h^2 without and with using graph. strength_Fw_h^2, Eff_Fw_h^2 and CC_Fw_h^2 represents respectively the results obtained with Str, Eff and CC parameters computed from the connectivity values obtained by Fw_h^2. Fw_h^2 represents the roc of the results obtained by Fw_h^2 without graph

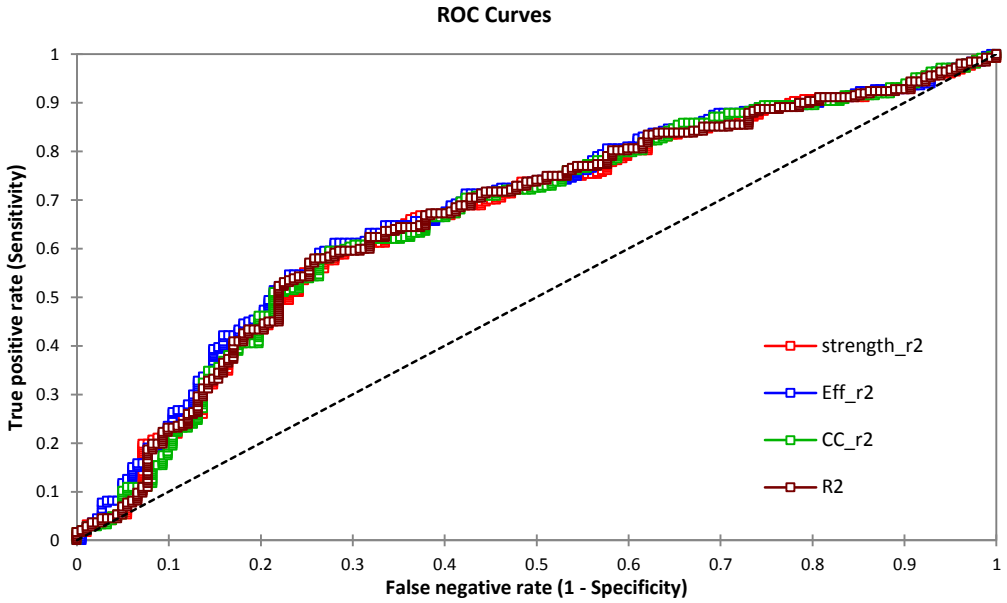


Figure 3.3 ROC Curves for r^2 without and with using graph analysis. strength_r^2, Eff_r^2 and CC_r^2 represents respectively the results obtained with Str, Eff and CC parameters computed from the connectivity values obtained by Fw_h^2. R^2 represents the roc of the results obtained by R^2 without graph.

In Figure 3.2 we present the results obtained by using the filtered windowed h^2 (*Fw_h^2*). In this

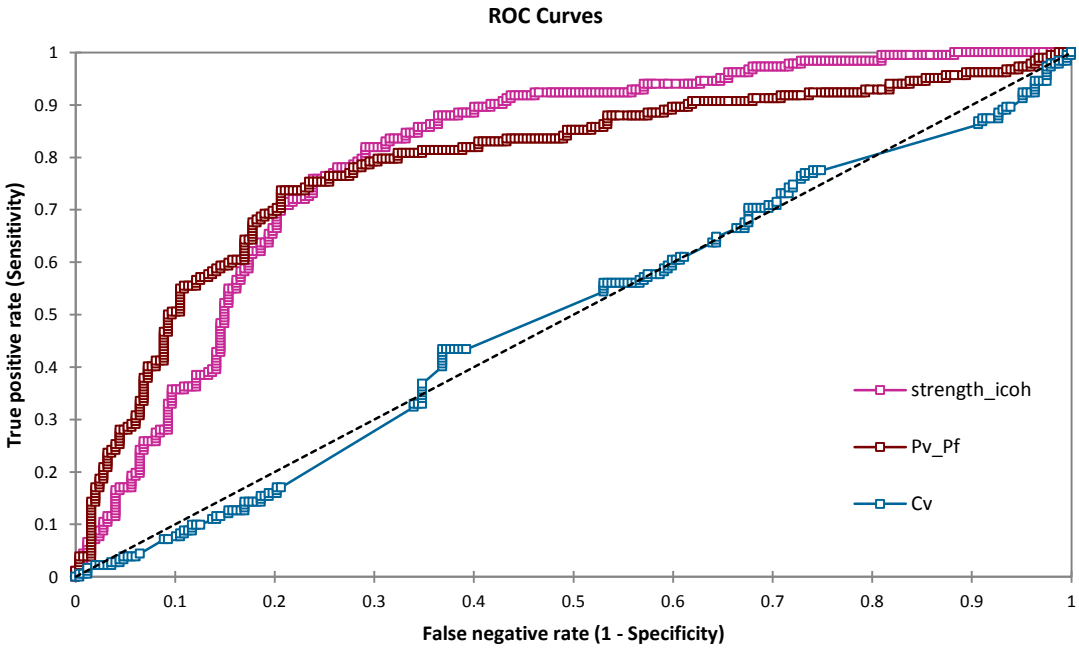


Figure 3.4 Roc Curves for the Comparison of CV, PV+PF and Icoh/Str.

case, the AUC increases from 0.658 when using only FW_h^2 to 0.77 when using graph measure (*Str*). *Eff* presents an (AUC) of 0.693, with 80% sensitivity and 49% specificity, while *CC* has an AUC of 0.661, with 72 % sensitivity and 53% specificity. *Str* presents the highest AUC (0.762), with 84 % sensitivity and 58 % specificity.

The results obtained when using the linear correlation (r^2) are presented in Figure 3.3. The AUC when using only r^2 (AUC (r^2) =0.669) is very close to the ones obtained when using graph measures. The AUC of r^2/*Eff* is 0.676, with 61% sensitivity and 71% specificity. *CC* has an AUC of 0.664, with 59 % sensitivity and 72%. *Str* gives AUC of 0.664, with 59 % sensitivity and 70 % specificity.

Finally, we compare the results obtained with the parameters mostly used in the literature: the peak frequency combined with the propagation velocity (PF +*PV*) and the conduction Velocity (*CV*), both computed from the whole bursts. The results of this comparison are presented in Figure 3.4. The AUC obtained with the *CV* was 0.495, with sensitivity and specificity 54% and 55 % respectively, while for *PV*+*PF* the AUC was 0.789, with 73% as sensitivity and 79 % as specificity. *Icoh*/*Str* presents the best AUC (0.801) when computed these 3 methods from the whole EHG burst.

Table 3.1 summarizes the results obtained from this first analysis. The best overall performances are obtained by using the strength parameter computed from the connectivity obtained by using the Icoh connectivity method. This observation confirms the interest of this new connectivity method, Icoh less sensitive to the volume conductor effect. It confirms also the interest of using graph parameters rather than the average of the whole connectivity matrix. The results are better when using the graph parameters, except for r^2 that always gives poor classification results. We will thus use this combination of methods, *Icoh + Strength (Icoh/Str)*, in the following work.

TABLE 3.1 COMPARISON OF SIGNIFICATIVITY IN LABOR VERSUS PREGNANCY CLASSIFICATION FOR DIFFERENT PARAMETERS

	Sensitivity (%)	*Specificity (%)*	*AUC*
ICOH	*30*	*72*	*0.504*
Icoh / Eff	*82*	*72*	*0.797*
Icoh / CC	*78*	*73*	*0.785*
Icoh / Str	***82***	***71***	***0.801***
FW_h^2	*83*	*43*	*0.658*
FW_h^2 / Eff	*80*	*49*	*0.693*
FW_h^2 / CC	*72*	*53*	*0.661*
FW_h^2 / Str	*84*	*58*	*0.762*
r^2	*57*	*74*	*0.667*
r^2 / Eff	*61*	*71*	*0.676*
r^2 / CC	*59*	*72*	*0.665*
r^2 / Str	*59*	*70*	*0.665*
CV	*54*	*55*	*0.495*
PV+PF	*73*	*79*	*0.789*

3.2.2 Graph visualization

Figure 3.5 shows the graphs averaged on the 247 pregnancy (a-c), and the 183 Labor (b-d) contractions when using *Icoh* as connectivity method. The difference between densities over all contractions of labor and pregnancy groups is not significant (Wilcoxon test, p=0.384).

In Figure 3.5a and Figure 3.5b, we represent each graph in a topographic way, as the grid of 4x4 nodes (electrodes) located on the woman's abdomen during recoding. The edges present the connectivity values between two electrodes. Figure 3.5c and Figure 3.5d, illustrate the same graphs in a circular layout. The thickness of each edge depends on its weight (here the *Icoh* values). The size of a node depends on its *Str* value. This representation permits to synthetize in a more visual way the connectivity values and graph parameters between all nodes. Figure 3.5c and 3.5d show that the nodes 1, 5 and 12 have the highest *Str* values, and that the weights are the highest (thickest edges) between nodes 1-5 and nodes 5-12 for the labor graph.

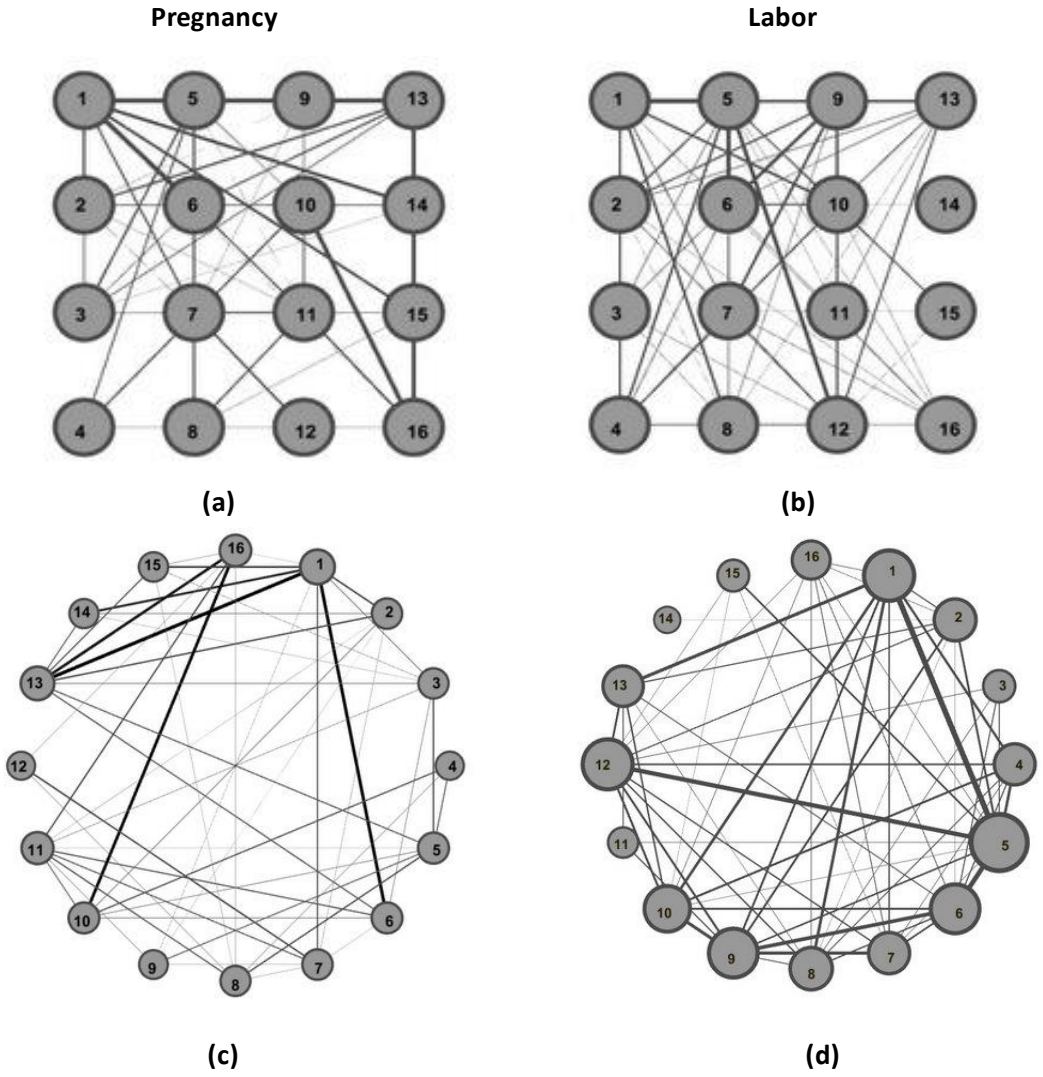
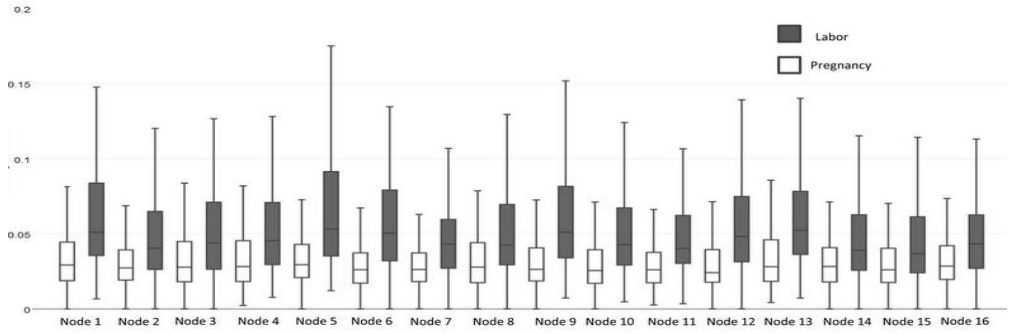


Figure 3.5 Graph results using Icoh. (a) Mean pregnancy graph. (b) Mean labor graph

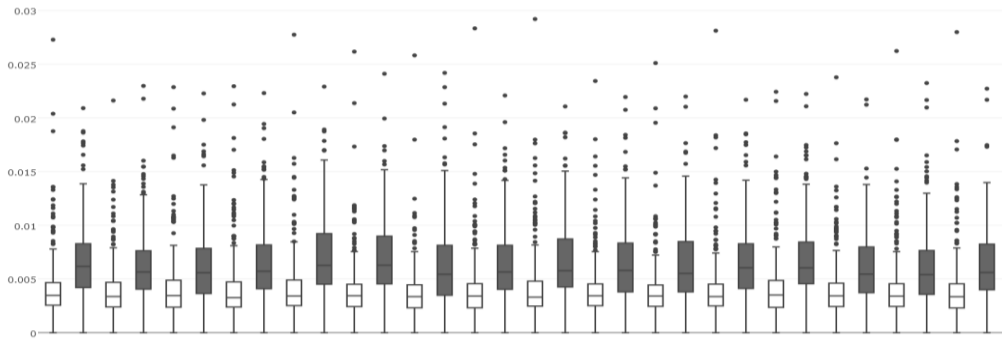
3.2.3 Node-Wise Analysis

In this analysis we computed the graph measures for each electrode and then performed a statistical test at the level of each node, in order to test if some electrode locations are more efficient than others to discriminate between pregnancy and labor contractions. To investigate the possible difference between pregnancy and labor, we plotted a boxplot for these two classes on each electrode when using the three parameters described above. Figure 3.6a, show an increase in the *Str* values from pregnancy to labor with noticeable differences for all the electrodes. We

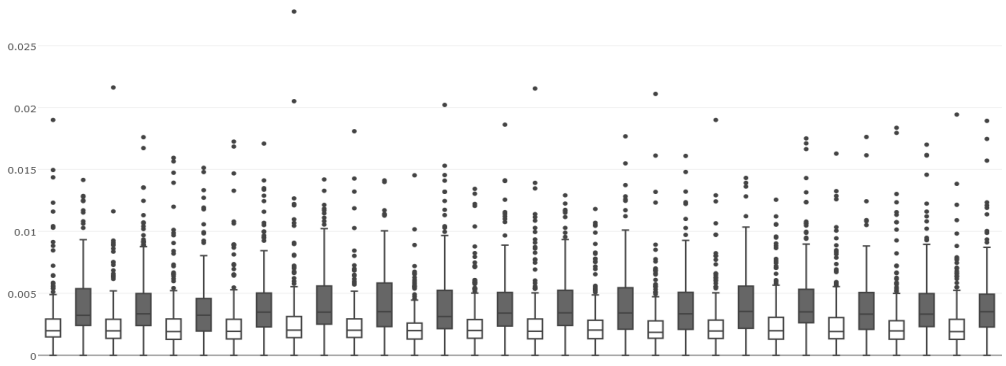
used the Wilcoxon test in order to test the significance of these differences. The results for *Str* parameter are shown in Table 3.2. These results indicate that all the differences between labor and pregnancy *Icoh*/*Str* are significant (p<0.01, corrected for multiple comparison using Bonferroni method), whatever the electrode. The same results are obtained with *Icoh*/*CC*



(a) Str



(b) Eff



(c) CC

Figure 3.6 Boxplots of three parameter values in pregnancy and labor on 16 nodes (electrodes). All the differences are significant (p<0.01). (a) Str (b) Eff (c) CC

(Figure 3.6b) and *Icoh*/*Eff* (Figure 3.6c). There is always an increase in these parameter values from pregnancy to labor for all the electrodes. The differences between labor and pregnancy of these parameters are significant (p<0.01, corrected for multiple comparison using Bonferroni method), whatever the electrode.

We can conclude from this analysis that there is no obvious preferred location of the electrode for the discrimination between pregnancy and labor contractions when using the *Strength* graph parameter computed from the *Icoh* connectivity values.

TABLE 3.2 WILCOXON TEST RESULTS BETWEEN LABOR AND PREGNANCY AT EACH NODE (ELECTRODE) FOR ICOH/STR PARAMETER

Nodes	***p_value***	***Nodes***	***P_value***
Node 1	5.76E-11	Node 9	6.94E-11
Node 2	1.33E-07	Node 10	1.72E-08
Node 3	6.53E-05	Node 11	8.69E-10
Node 4	7.14E-08	Node 12	2.79E-10
Node 5	4.93E-13	Node 13	8.66E-08
Node 6	1.15E-11	Node 14	0.00111
Node 7	8.71E-09	Node 15	0.000119
Node 8	7.69E-07	Node 16	0.000322

3.3 PREGNANCY MONITORING

3.3.1 Graph Measures and Visualization

To investigate the evolution of the uterine muscle connectivity all along pregnancy until labor, we have parted the uterine contractions in weeks before labor (WBL). For more details, see Chapter 2 section 2.2.2. The performance of the proposed approach for the monitoring of pregnancy evolution along term is presented in Figure 3.7. Figure 3.7a shows the evolution of the average *Str* values for each woman at each WBL. There is no clear evolution for all the terms before labor (8WBL to 1WBL), while an increase between 1WBL and Labor groups is clearly

noticed. The *Str* value for the most of the contractions (170/197) remains under 0.04 during pregnancy, unlike for the labor group. The regression curve of these results follow the same trends: almost no evolution between weeks before labor, with a noticeable increase between 1WBL group and labor group.

Figure 3.7b-h presents the corresponding averaged circular graphs for the different terms. We can notice that the number of significant edges in the averaged labor graph (Figure 3.7h) is higher than for the different terms. In terms of node *Str*, no clear difference can be noticed between all the pregnancy groups (Figure 3.7b-g), unlike in the Labor graph where the nodes are larger than those of the other graphs. The same remark applies to edges thickness where edges in labor graph are the thickest.

Table *3.3* summarizes the density values for the different graphs. The density value is the highest (0.5) for the Labor graph and ranges between 0.425 (8WBL) and 0.475 (4WBL) with a mean

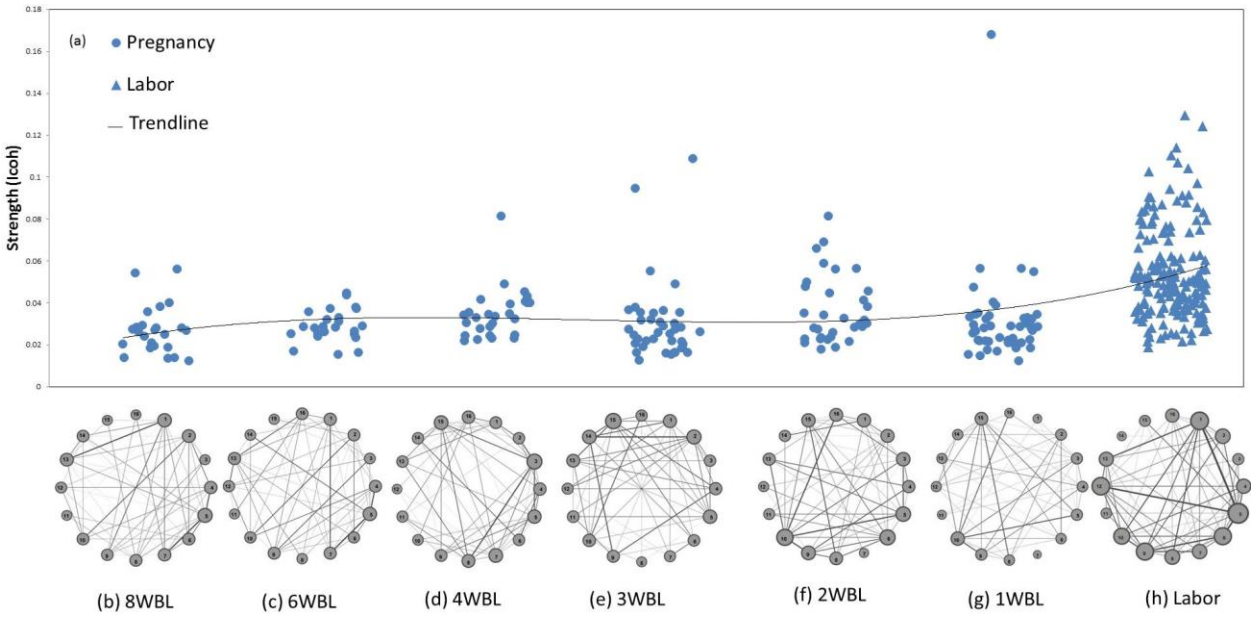


Figure 3.7 (a) Evolution of Icoh/Str with week before labor. Each point represents the Str value of one contraction for a given woman. Mean graph for: (b) 8WBL. (c) 6WBL. (d) 4WBL. (e) 3WBL. (f) 2WBL. (g) 1WBL. (h) Labor.

value of 0.433 ±0,024.

Table 3.3 Density values for each group

Group	***Density value***	***Group***	***Density value***
8WBL	0.425	2WBL	0.442
6WBL	0.433	1WBL	0.417
4WBL	0.475	**Labor**	**0.5**
3WBL	0.408		

3.3.2 Node Wise Analysis

To evaluate, for a given electrode, the evolution of *Icoh*/*Str* along term, we have computed the value of *Icoh*/*Str* for each node and each available week of gestation group. We showed the results for node number 12 in Figure 3.8. Node 12 has a higher *Str* value in labor than in

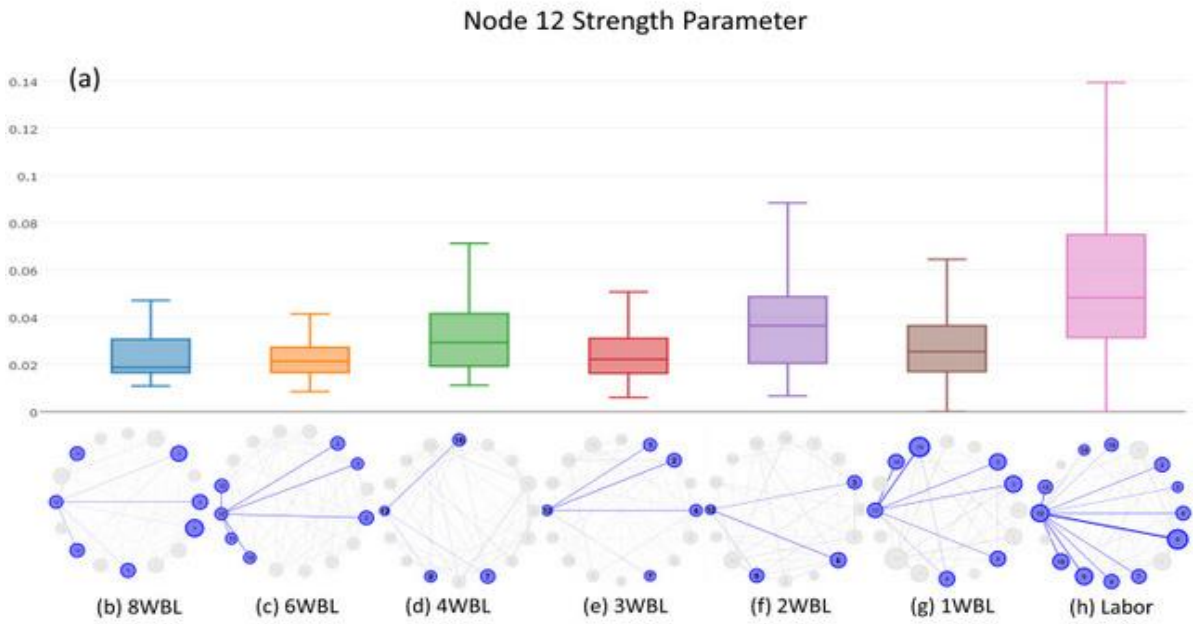


Figure 3.8 Boxplots of Str values for node 12 from with week before labor. Mean graph for: (b) 8WBL. (c) 6WBL. (d) 4WBL. (e) 3WBL. (f) 2WBL. (g) 1WBL. (h) Labor.

pregnancy and a very low Wilcoxon p value between labor and pregnancy.

Figure 3.8a shows that all the *Str* values during pregnancy stay relatively small. There are no clear differences between the term groups from 8WBL to 1WBL, while an increase between 1WBL and Labor groups is noticeable. We present in Figure 3.8b-h the corresponding averaged graphs for each of the term groups. We highlighted in each graph only node 12 and the nodes to which it connects. As usual, the thickness of the edge represents the weight (*Icoh* value) and the diameter of a node represents its *Str*. We can notice in the labor graph that node 12 is associated to a higher number of significant edges (Figure 3.8h). It is indeed connected to 11 nodes over the 15 possible, unlike during pregnancy, where node 12 connects to a maximum of 6 nodes, whatever the pregnancy group (Figure 3.8b-g). In terms of *Str* (diameter of the node), no clear difference can be noticed between all the WBL graphs.

However, during labor node 12 is clearly larger (higher *Str*) than for all the pregnancy groups. We then computed the statistical differences between all the terms by using the Wilcoxon test. results are presented in Table 3.4. No significant difference was observed between the pregnancy groups ($p>0.01$), except between 8WBL and 2WBL ($p=0.009$). A significant difference was always obtained between labor and all the other groups ($p<0.01$ corrected for multiple comparison using Bonferroni).

Table 3.4 Statistical analysis of the difference between weeks before labor and labor groups at each node for Str parameter

	8wbl	6wbl	4wbl	3wbl	2wbl	1wbl	Labor
8wbl		0.576	0.025	0.672	**0.009**	0.427	**< 0.0001**
6wbl	No diff		0.017	0.547	0.02	0.296	**< 0.0001**
4wbl	No diff	No diff		0.067	0.457	0.131	**0.0001**
3wbl	No diff	No diff	No diff		0.037	0.748	**< 0.0001**
2wbl	**diff**	No diff	No diff	No diff		0.029	**0.005**
1wbl	No diff	No diff	No diff	No diff	No diff		**< 0.0001**

Labor	**diff**	**diff**	**diff**	**diff**	**diff**	**diff**	

3.4 LONGITUDINAL ANALYSIS PER WOMAN

Some women (N=14) in our database have been recorded several times all along pregnancy. For these women, we have computed the *Icoh*/*Str* values at each week. The performance of the proposed approach for the monitoring of pregnancy evolution along term is presented for each woman. For example, woman W35 has been recorded four times at: 7WBL (11 contractions), 4WBL (7 contractions), 3WBL (9 contractions) and 1WBL (9 contractions).

In Figure 3.9 we present the evolution of the average *Str* values after using the *Icoh* as connectivity method for Woman W35 for her recorded terms. No clear difference can be noticed between the *Str* values. No significant difference was observed between these groups (p>0.01). We present the evolution of the same parameter for the other women that have been recorded several times in Appendix B. We have also computed the mean graph at each term for this woman. Results are presented in Figure 3.10. It is clear that there is no difference between the mean graphs of 7WBL, 4WBL and 3WBL while a slight difference is noticed in 1WBL graph in

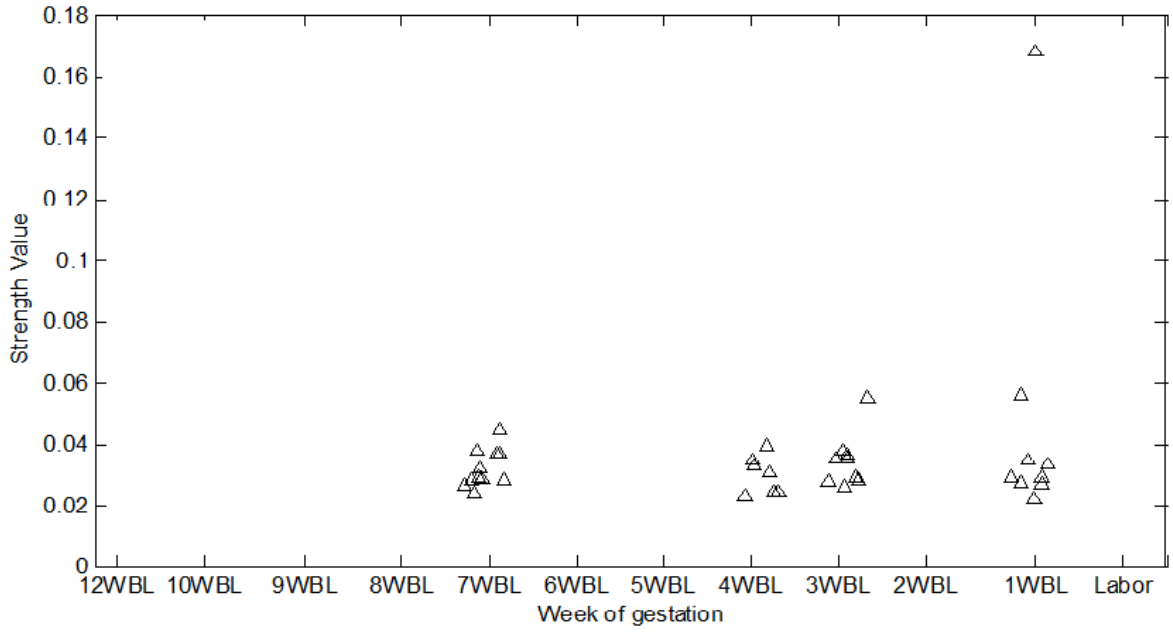


Figure 3.9 Evolution of Icoh/Str with week before labor for Woman W35. Each point represents the Str value of one contraction for this woman.

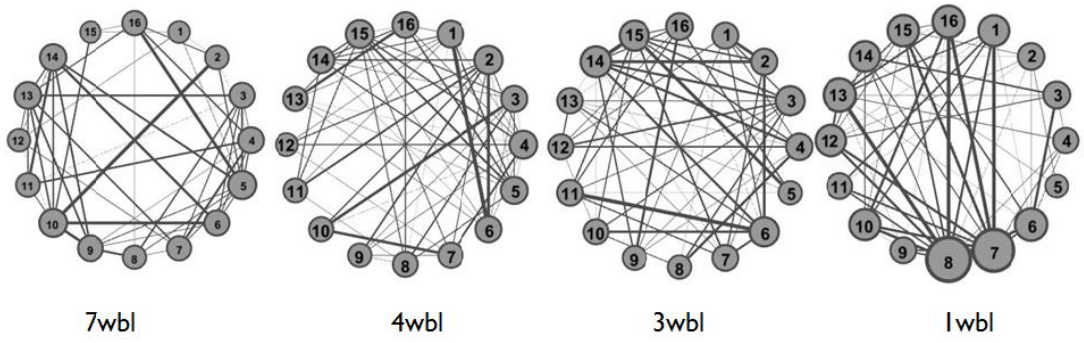


Figure 3.10 Mean graphs for woman W35 contractions in each term

terms of edges thickness and nodes diameter. The density of these graphs slightly increases from 0.417 (7WBL) to 0.492 (1WBL).

In our database we could record women not only in their pregnancy phase but also in labor. To investigate if this network reconfiguration is related to the labor process and not only resulted from the simple evolution of gestation, we selected contractions from the same women recorded in pregnancy and labor. A typical example is presented in Figure 3.11 for woman W3. This woman has 9 contractions during pregnancy (5WBL, 2WBL, 1WBL) and 10 contractions in Labor. A clear difference is noticed between the mean pregnancy graph (Figure 3.11a) and the mean Labor graph (Figure 3.11b). Edges in labor graph are more frequent and thicker and nodes are larger; which mean high values in term of edges weight and node *Str*s.

3.5 WEEK OF GESTATION

In order to investigate the possible usefulness of this approach for a clinical practice, we used the term count used in clinical practice, the Weeks of Gestation, WG (counted from the time of the last menstrual period). This term counting permits to test if the pregnancy evolution differs from labor for the same given WG term. We selected contractions from women recorded at the same term, 39 WG, but some being already in labor (labor group) and the others having delivered later (pregnancy group). We have 11 contractions from 5 women in the pregnancy group, and 41 contractions from 5 women in labor. We present in Figure 3.12 the difference in the connectivity networks for these two groups recorded at 39WG. A clear difference is noticed between the mean graph of Pregnancy (Figure 3.12a) and the mean graph of Labor (Figure 3.12b) in term of edges number, weight and node strength. All these values are higher in the Labor group. Results

in other weeks of

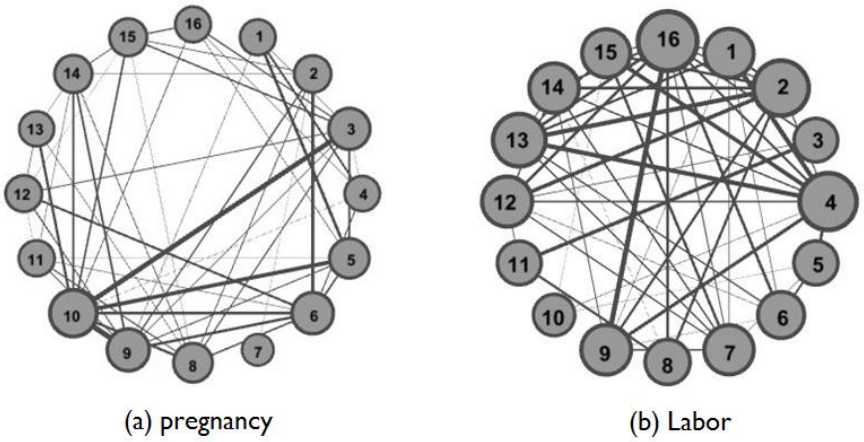


Figure 3.11 Graph results for Woman W3. (a) Mean pregnancy graph (b) Mean labor graph

gestation (37, 38 and 40) are presented in Appendix C. Mean graphs for all the contractions of each week of gestation are presented in Appendix D. The contractions in the weeks under 37 week of gestation are in pregnancy and in 41 and 42 week of gestation they are in labor.

3.6 DISCUSSION AND CONCLUSION

In this chapter, we have presented the results of a novel approach aiming at characterizing the functional connectivity of the uterine electrical activity. We investigated the ability of the EHG network-based analysis to characterize the evolution of uterine contractions from pregnancy to labor and to discriminate pregnancy and labor contractions. Previously, the connectivity matrices computed between EHGs were usually transformed into a single value per contraction, by averaging the connections weights of each matrix, for instance in (Hassan et al., 2013). Consequently, useful information was certainly lost. The graph theory based analysis used here is indeed a better way to characterize the whole connectivity matrix, taking into account all the characteristics of the network. In this study, the graph theory based analysis has been proven to be more efficient to quantify connectivity matrices for normal pregnancy and labor contractions than the previous averaged classical quantification of the connectivity. However, the method showed lower performance for pregnancy monitoring, as no significant changes were observed between the different pregnancy weeks before labor. These results are more specifically discussed hereafter.

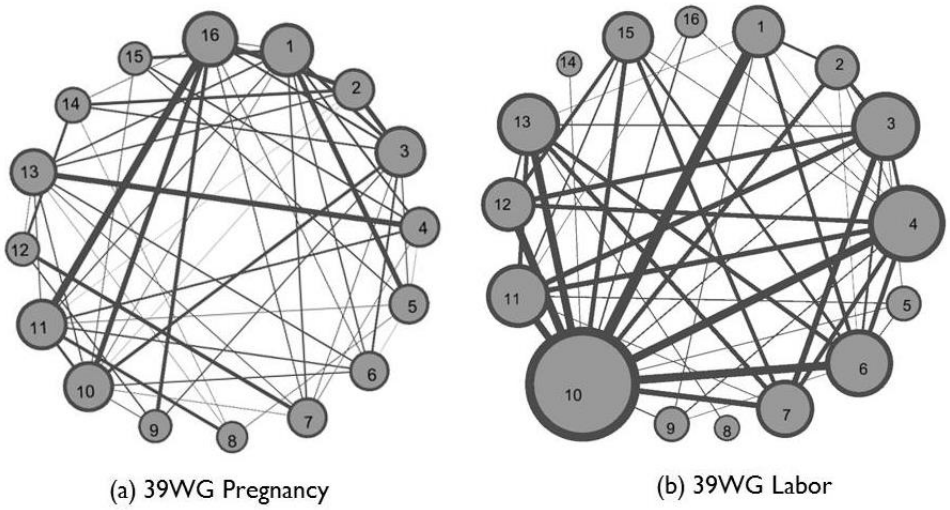


Figure 3.12 Mean graphs for EHGs recorded at 39WG: (a) Pregnancy, (b) Labor.

Increase of synchronization with term

This network-based approach has improved the classification between pregnancy and labor. The results obtained with *Icoh/Str* (AUC=0.801) were higher than those obtained by *PF+PV* (AUC = 0.789), as well as by *CV* (AUC=0.495). It is however difficult to compare these results with the reported good performance of *PV/CV* in previous analysis (Lucovnik et al., 2011); (de Lau et al., 2013; Rabotti et al., 2009) as these metrics were computed differently. *PV* and *CV* were usually applied to single spikes not to whole uterine burst which may explain the reported poor results of both methods in our study. We have computed *PV* and *CV* on the whole burst to standardize the computation way, and to be able to compare with the correlation-based methods. These poor results of *CV* and *PV* do not put any doubt about the high performance of *CV* and *PV* when used on single spikes as reported in (C. Rabotti et al., 2010). But, with the whole burst approach, getting free from spike identification may present a huge advantage from the applicative clinical point of view.

Nevertheless, a classification rate of 80% between labor and nonlabor groups is still not clinically sufficient. A possible improvement of these results is, first the use of the EHG source connectivity approach (as realized recently in the context of brain connectivity) (Hassan et al., 2014) and the possible combination of different features related to different physiological phenomena.

One of the results obtained from this work based on graph theory, and on whole burst analysis, is that we did not evidence any increase in synchronization with increasing pregnancy term, but an abrupt increase during labor. This increase in the *Str*, *Eff*, and *CC* values from pregnancy to labor was noticeable for all the electrodes. This finding disagrees with the previously reported results using EHG when using the nonlinear correlation coefficient on a smaller dataset (Hassan et al., 2013) or MMG-based studies where authors showed an increase in synchrony as the women approach active labor (Govindan et al., 2015). A possible explanation for this increase in connectivity only during labor can be related to the propagation phenomenon, associated with the appearance of a large number of gap junctions just prior to labor (Garfield and Hayashi, 1981). It could be also related to as the electromechanical coupling proposed by Young as one of the synchronization process appearing before and during labor (Young, 2007).

It is important to notice that all women included in our study gave birth at term (none of the births was premature). Our study showed the possible use of a new promising approach to first characterize the uterine bursts during pregnancy and labor and secondly, to classify normal pregnancy and labor contractions. To validate the clinical impact of the approach, the method should be applied to data from women with premature labors. In addition, different steps in our approach, such as the manual burst segmentation also should be automatized in order to bring this approach the clinical use.

Limitations

First, a classical and still unsolved difficult question relates to the setting of threshold values applied to the connectivity matrices/measures. In this study, the same threshold value was used for each method/WBL or WG to standardize the analysis (10% of the maximum connectivity values). Other threshold values were also investigated (10% to 50%) and gave the same differences between methods and conditions.

Other approaches can be also explored like those based on surrogate data, but they require a higher computation time.

Another unsolved question that presents a big limitation for this study is that we cannot record always the same woman in all pregnancy and labor phases, due to the hospital and subject availability. Only few women (14) of our database have been recorded several times. Indeed, it is difficult to record contractions during pregnancy as the contraction number is very low during

most of pregnancy. Furthermore, the women being available for recording only when present at the hospital (for standard follow up, or hospitalization for risk pregnancy), due to the short duration of their availability, we got very few contractions for most of recordings. Nevertheless, results on women recorded in different terms gave similar conclusion than the results on the whole database. An increase in labor was also shown for a woman that was recorded in pregnancy and labor phases.

It is also important to keep in mind that the estimation of the functional connectivity at the electrode (surface abdomen) level can be affected by the volume conduction influence. The volume conduction induces that different channels actually measure the activity of a same uterine source. To tackle this problem, we used in this work the imaginary part of the coherence function, as it was proven to have a high performance to reduce this effect in the context of brain connectivity (Nolte et al., 2004). Moreover, in the context of electroencephalography, the connectivity analysis at the brain source level showed a considerable reduction of the effect of the volume conduction when compared to the scalp level (Hassan et al., 2015). One possible improvement to the results reported in this study is to adapt the 'source connectivity' approach to the uterine muscle, by localizing the sources of the EHG at the uterine muscle level, which is the subject of the next chapter.

In conclusion, we showed that network-based approach can be used successfully to first characterize uterine electrical activity during pregnancy and second classify pregnancy and labor contractions. We speculate that this new approach could have a clinical impact for detecting alterations in the uterine networks connectivity in relation with the contractions recorded during preterm labor threat in order to detect as soon as possible preterm labor.

CHAPTER 4: EHG SOURCE CONNECTIVITY ANALYSIS

This chapter presents the results obtained when studying the connectivity at the level of the source identified from the EHG. We started by evaluating the effect of the two key steps involved in EHG source connectivity processing: i) the algorithm used in the solution of the inverse problem and ii) the method used for the estimation of the functional connectivity. We evaluate three different inverse solutions (to reconstruct the dynamics of uterine sources) and three connectivity measures (to compute statistical couplings between the reconstructed sources). The networks obtained by each combination of the inverse/connectivity methods were compared to a reference network (ground truth) generated by the model. This approach was then applied to real EHG signals.

4.1 OVERVIEW

In this chapter, we evaluate the performance of the new approach called "EHG source connectivity" where the objective is to estimate the functional networks of the uterine electrical activity after source localization. This approach contains mainly two steps: first, solving EHG inverse problem and second, source connectivity estimation. Therefore, it is crucial to find the best combination (inverse/connectivity) that may give the best results. To do so, we used data generated by means of the EHG model previously described (see Chapter 2 Section 2.3.2).

We first generated simulated data at the source level for each defined scenario. Then we simulated the related surface EHGs by solving the forward problem. The leadfield corresponding to each simulated scenario was computed using the Boundary Element Method (BEM), OpenMEEG software (Gramfort et al., 2010). From these simulated EHGs, the source activity was estimated by using three different classical algorithms for solving the inverse problem: wMNE (Hämäläinen and Ilmoniemi, 1994), sLORETA (Grech et al., 2008) and MNE (Hämäläinen and Ilmoniemi, 1994).

Then we used three connectivity methods, R^2 (Ansari-Asl et al., 2004), h^2 (Pereda et al., 2005), *Icoh* (Nolte et al., 2004) to compute the connectivity matrices both from the simulated sources

(reference network) and from the reconstructed sources. These matrices were then thresholded with different threshold values, by keeping a proportion of the highest connectivity values.

In order to compare the reference network and the network identified after reconstruction of the sources, by using each one of the inverse/connectivity combination, we used the simNet algorithm (Mheich et al., 2015). This algorithm takes into account the spatial location (3D coordinates) of the nodes when comparing two networks. It provides a normalized Similarity Index (SI) between 0 (totally different graph) and 1 (same graph).

The source connectivity approach was also applied to real EHG data, (see Chapter 2 section **Erreur ! Source du renvoi introuvable.**).

4.2 RESULTS ON SIMULATED DATA

1) Scenario 1

The results obtained in the case of the first network scenario are illustrated Figure 4.1 for the 9 different combinations of the source reconstruction and functional connectivity methods. Visual inspection of these results permit to say that the networks identified by using the different combinations fit more or less with the reference network (Figure 4.1B). Indeed, as for the reference network, all the 16 zones are connected to each other, but with difference in the weight values of the different edges (Figure 4.1A). For a given connectivity approach, changing the inverse method modifies the network topology. When using h^2 or R^2, MNE gives the closest graph in contrast with sLORETA. When using *Icoh*, the graph topology does not drastically change when changing the inverse method. On the same way, for a given source localization approach, changing the functional connectivity measure changed, qualitatively, the network.

The quantification of these differences is provided in Figure 4.1C. Overall, values of network similarity were relatively high and ranged from 66 to 78%. For a given connectivity approach, changing only the localization algorithm slightly modified SI values for h^2 and R^2 (5%). For a given source localization approach, the SIs changed when changing the connectivity method, by 7% for wMNE, 10% for sLORETA and 12% (the highest change) for MNE. Results obtained by using h^2 were on average better than with R^2 and *Icoh*. The combination providing the highest

similarity values between the estimated and the reference network was MNE/h^2 (78.2%) followed by sLORETA/h^2 (76.3%) and sLORETA/R^2 (76.2%). Icoh gives the lowest similarity whatever the localization algorithm. Results obtained with MNE/h^2 were significantly closer to the reference network than the other ones (Wilcoxon rank-sum test, p<0.01, corrected using Bonferroni).

2) Scenario 2

The results obtained in the case of a single intra-connected network scenario are illustrated Figure 4.2, for the 9 different combinations of the source reconstruction and functional connectivity methods. The visual investigation of these results revealed that networks identified by using the different combinations of methods present important differences from the reference network (Figure 4.1B).

The qualitative analysis showed also that the number of connections between the different zones varied according to the combination of methods used. For a given connectivity approach, changing the localization method modify more or less the network, depending on the connectivity method. On the other hand, for a given source localization approach, the functional connectivity measure changes qualitatively the network only for *Icoh*. h^2 or R^2 combined with sLORETA give the network that best matched the reference network.

The quantification of these differences is provided Figure 4.2C. Overall, values of the Similarity Index are low and range from 16% to 27%. For a given connectivity approach, a change in the localization algorithm modifies the SI values for h^2 (4%) and R^2 (8%), not for Icoh. For a given source localization approach, the change in SI values is smaller for wMNE (7%) than for MNE (10%), and sLORETA (10%). Results obtained by using h^2 were on average better than by using R^2 and *Icoh*. The combination providing the highest similarity values between the estimated and the reference network was sLORETA/h^2 (27.8%), followed by sLORETA/R^2 (27.7%) and. wMNE /h^2 (27%). *Icoh* gives the lowest similarity whatever was the localization algorithm.

Similarly, for scenario 2, the results obtained with sLORETA/h^2 and sLORETA/R^2 were significantly closer to the reference network than the other ones (Wilcoxon rank-sum test, p<0.01, corrected using Bonferroni).

3) Scenario 3

In this scenario we have simulated two interconnected networks. As for the previously scenario, this scenario presents connections between distant nodes. The results obtained in this case (Figure 4.3A) indicate that the networks identified by all the combinations present important difference from the reference network (Figure 4.3B).

The networks slightly change for a given connectivity measure. The results of h^2 (whatever the inverse solution algorithm) provide the closest result to the reference network, while *Icoh* showed, visually, the farthest result from this reference network whatever the inverse problem method.

Values of network similarity are reported in Figure 4.3C. These values were a little bit higher than those obtained for the single network of scenario 2, but staying low, with a range from 20 to 30%. For a particular connectivity measure, changing the inverse algorithm modified the SIs by 3% (R^2) to 4% (h^2). While for a given source reconstruction algorithm, the SI variation remains low around 9% for wMNE, 8% for MNE and 5% for sLORETA. The combination providing the highest similarity values between the estimated and the reference networks is wMNE/h^2 (30%). Closer values were also obtained with MNE/h^2 (29%). The Icoh combination shows the lowest SI value (20%).

Similarly, for scenario 3, the results obtained with wMNE/h^2 were significantly closer to the reference network than the other ones (Wilcoxon rank-sum test, $p<0.01$, corrected using Bonferroni).

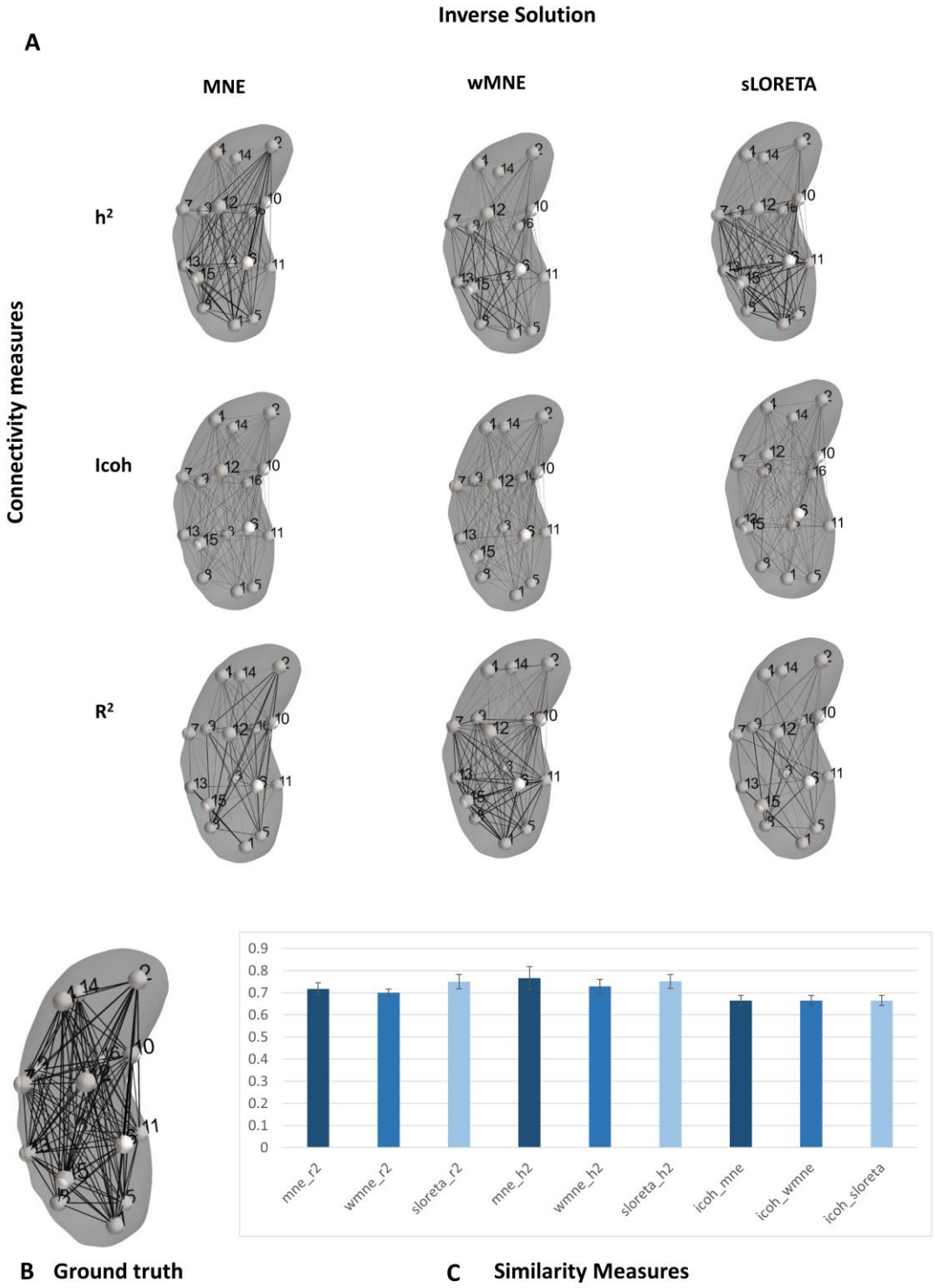


Figure 4.1 Complete network scenario. A) Uterine networks obtained by using the different inverse and connectivity methods, B) The original network (ground truth) and C) Values (mean ± standard deviation) of the similarity indices computed between the network identified by each combination and the model network.

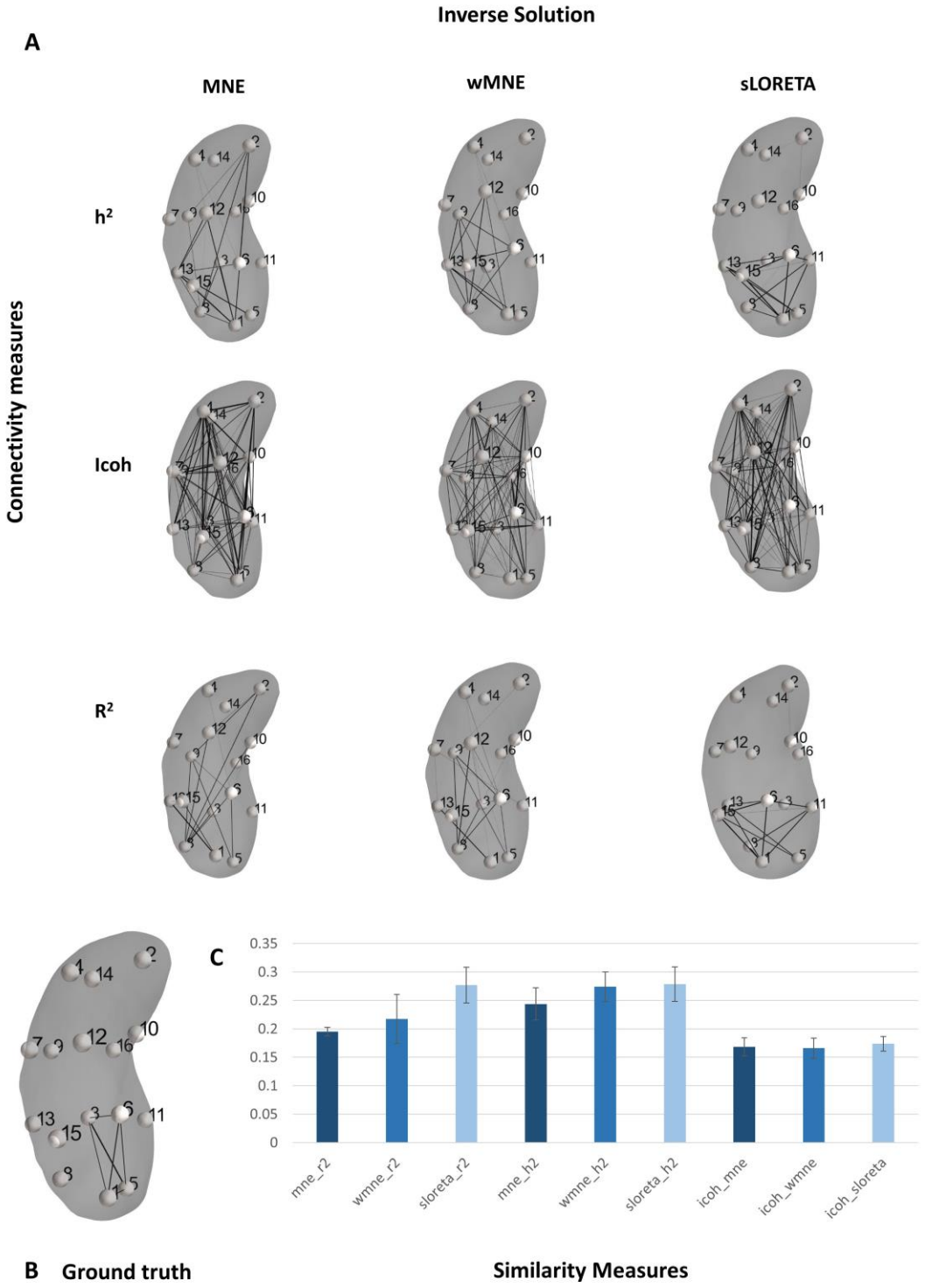


Figure 4.2 One network scenario. A) Uterine networks obtained by using the different inverse and connectivity methods, B) The original network (ground truth) and C) Values (mean ± standard deviation) of the similarity indices computed between the network identified by each combination and the model network.

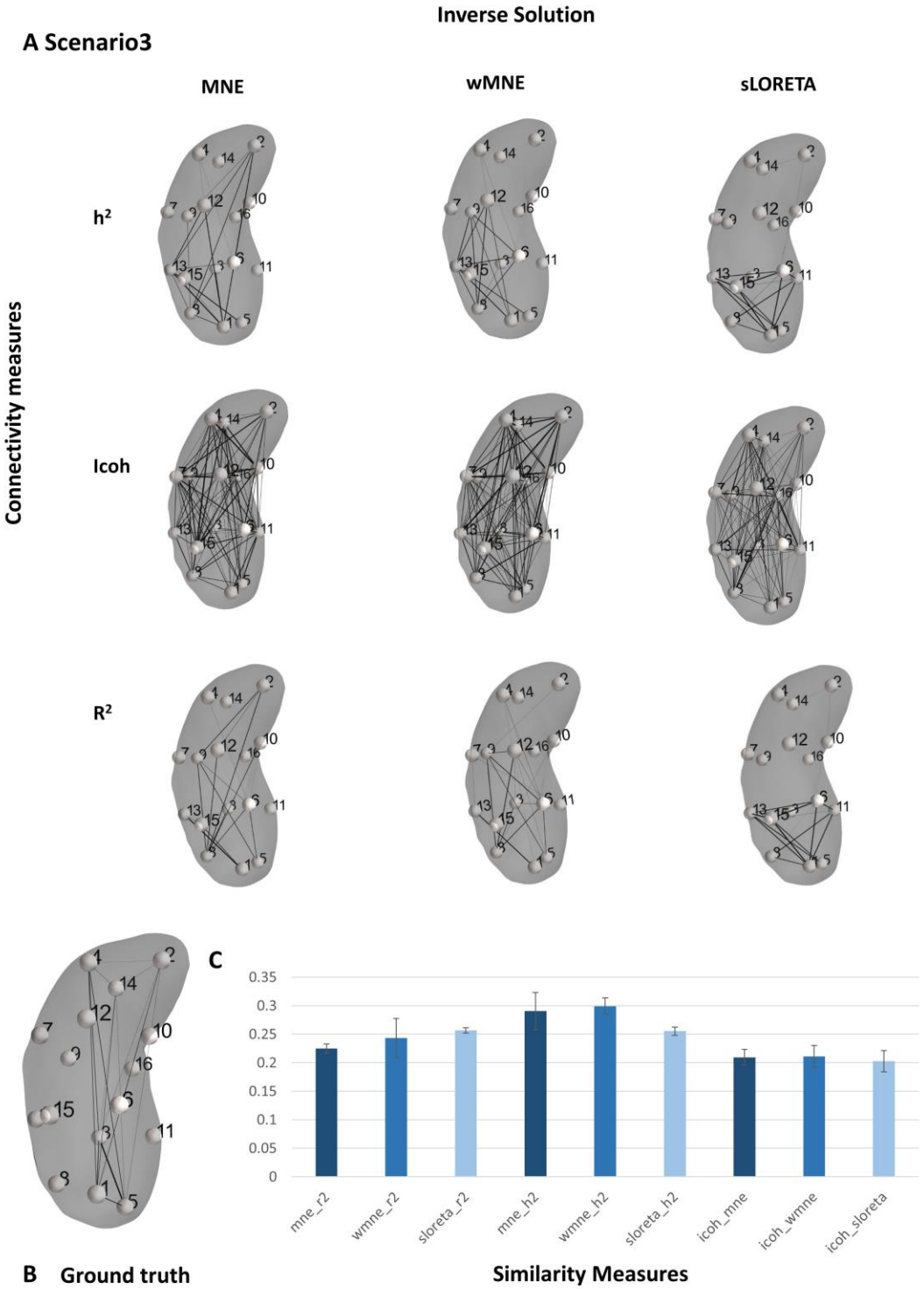


Figure 4.3 Two interconnected networks scenario. A) Uterine networks obtained by using the different inverse and connectivity methods, B) The original network (ground truth) and C) Values (mean ± standard deviation) of the similarity indices computed between the network identified by each combination and the model network.

4.3 RESULTS ON REAL DATA

We there apply the EHG source connectivity methods to real EHG data. The main motivation is to find a possible significant difference (with the graph parameters, at node or edge level) between networks obtained for pregnancy and labor contractions.

As no combination of inverse/connectivity methods arose from the previous study (simulated signals) as being the most pertinent one, we applied on real EHG (segmented and denoised bursts), all the combinations between inverse problem methods and connectivity measures methods (For more information see Chapter 2 section 2.3.1).

4.3.1 Node Wise Analysis

In this analysis we compute three graph measures: Str, Eff and CC for each zone. We then perform a statistical test at the level of each node (each zone) between pregnancy and labor networks. We plot for each inverse/connectivity combination method only the zones that present a difference between labor and pregnancy.

Figure 4.4 shows the different zones that present a significant difference between labor and pregnancy when using Str as a graph measure. All the nodes presented in this figure have *p*-value < 0.01 using Wilcoxon test, corrected for multiple comparison using Bonferroni method.

Results showed that, when using h^2 as a connectivity method, the number of the significant zones (6/16) is the same whatever the inverse problem method used. The lowest *p*_value is obtained when using the wMNE for zone 8 ($p=1.27\ 10^{-30}$), and for zone 9 with MNE or sLORETA ($p=4.44\ 10^{-27}$). R^2 gave the highest number of zones combined with sLORETA (10 zones) and with wMNE (9 zones). The lowest *p*_value is given for zone 8 with wMNE ($p=6.69\ 10^{-27}$) then for zone 9 with MNE ($p=3.77\ 10^{-20}$). Only one zone (zone 16) provided a significant difference when using MNE/Icoh ($p=4.4\ 10^{-4}$), while no efficient zones are given with wMNE/Icoh and sLORETA/Icoh.

The results of significant zones when using CC as a graph parameter are presented in Figure 4.5. All the nodes presented in this figure have a p_value under 0.01 using Wilcoxon test, corrected for multiple comparison using Bonferroni method.

The results obtained when using h^2 were similar whatever the inverse method. We obtained five zones when using MNE and sLORETA and six zones when using wMNE. Zones 8 and 16 were significant when using any inverse method. Zone 8 was the most efficient when using wMNE ($p=7.90\ 10^{-20}$), then zone 9 when using MNE ($p=1.39\ 10^{-13}$) and sLORETA ($p=4.67\ 10^{-13}$). *Icoh* gives the worst results. There was not any significant zone when using this method.

The results obtained when using Eff as a graph parameter are the same than when using CC.

4.3.2 Edge Wise Analysis

In this part, we performed the significant test at the level of each edge ($p<0.01$, corrected for multiple comparison using Bonferroni method) between labor and pregnancy. Edges with significant differences between pregnancy and labor are showed in figure 4.6.

Figure 4.6 presents the significant set of edges for each inverse/connectivity combination. For a given inverse method, the number of significant edges changes when changing the connectivity method. For instance, the number of significant edges is 23 for wMNE/h^2 and 27 for wMNE/R^2. Similar results were obtained for sLORETA and MNE.

For a given connectivity method, sLORETA gives always the lowest number of edges. The number of significant edges was 9 and 18, for h^2 and R^2 respectively. These results slightly increase when using MNE (20 edges with h^2 and 23 with R^2). The best results were obtained for wMNE as an inverse method. There were again no significant edges for Icoh.

The significant edges for all the combinations are listed in Table E.1, Appendix E.

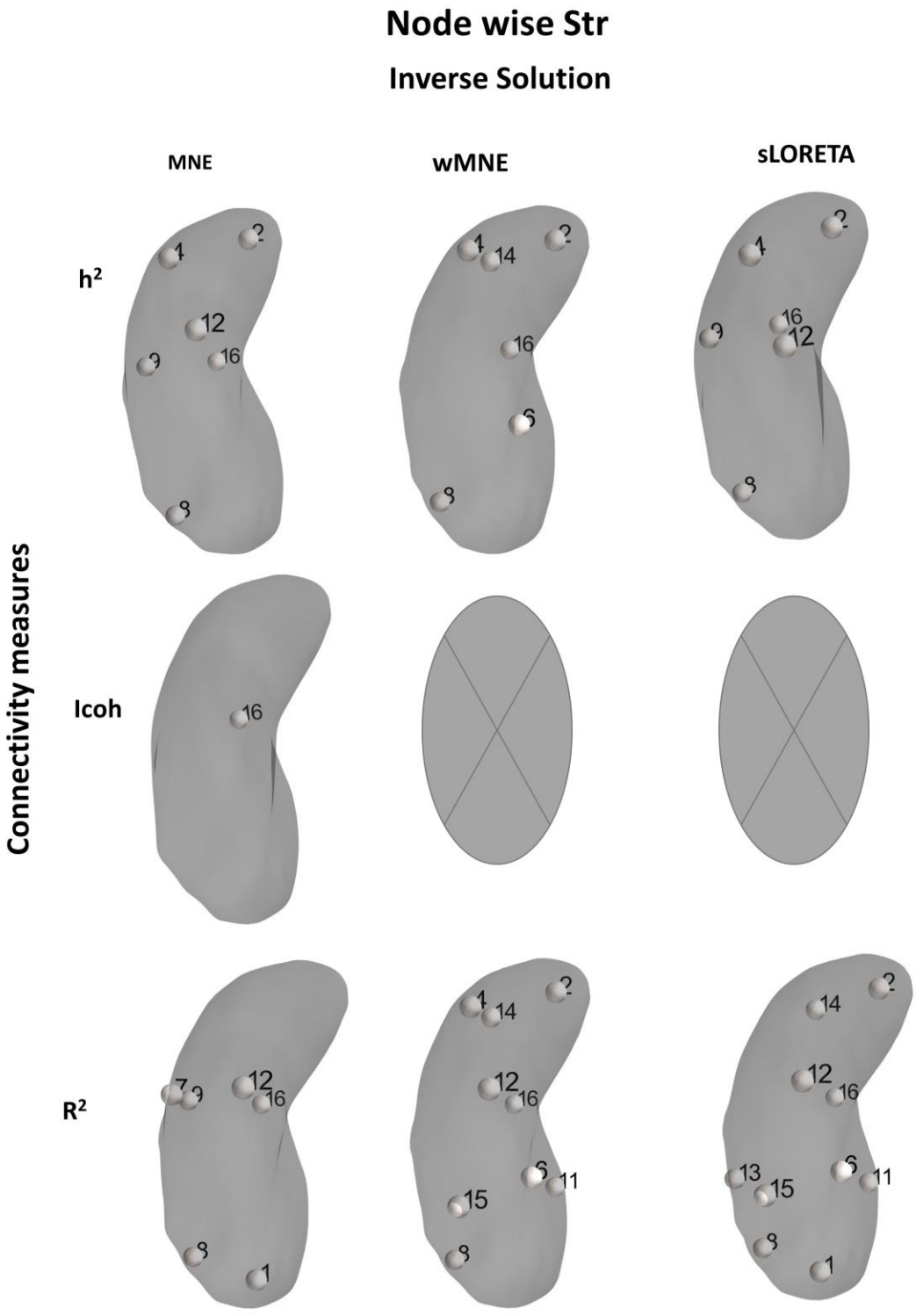


Figure 4.4 Node-wise analysis for Strength metric. Only nodes showing significant differences between pregnancy/labor were visualized

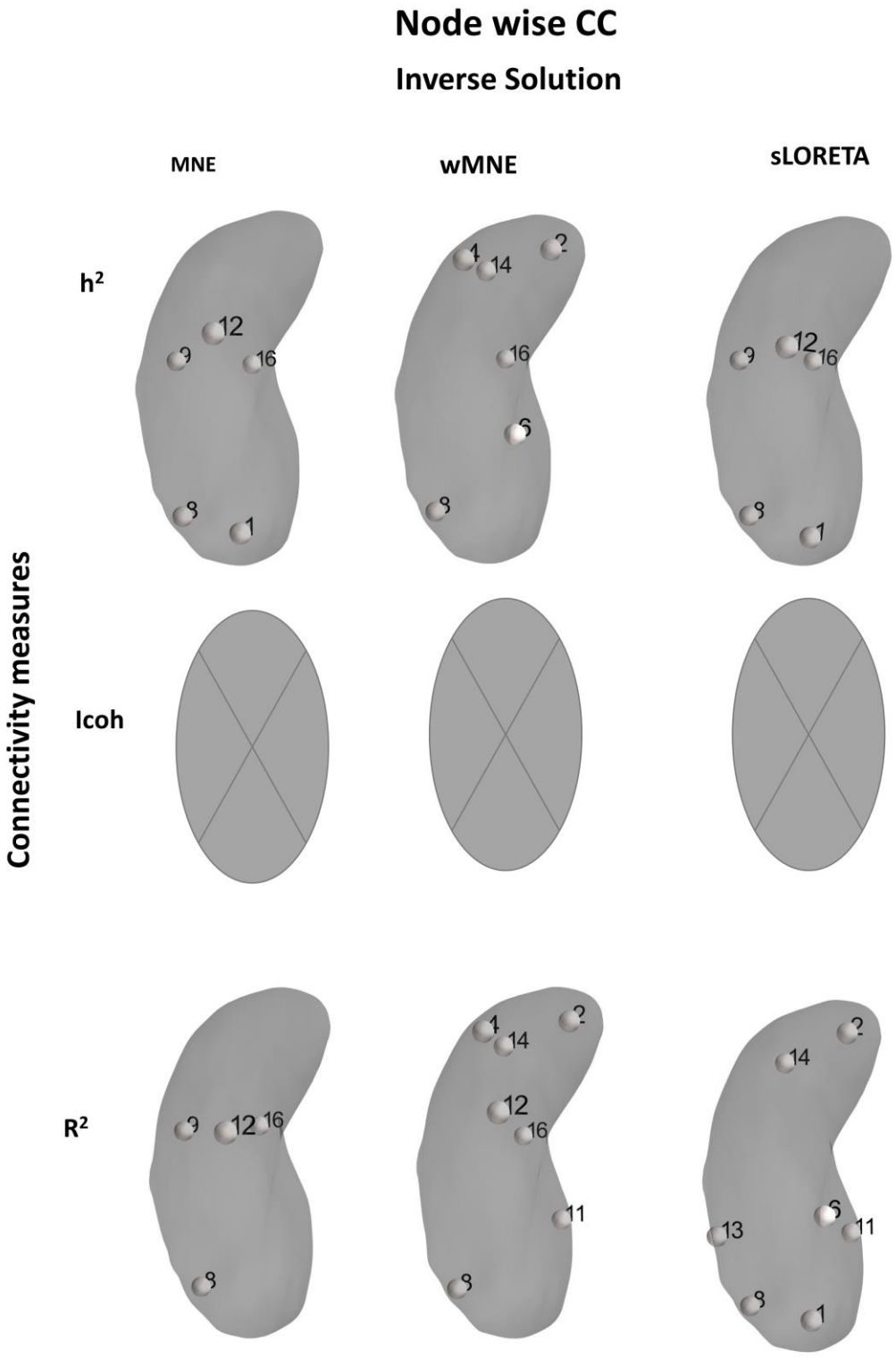


Figure 4.5 Node-wise analysis for clustering coefficient metric. Only nodes showing significant differences between pregnancy/labor were visualized

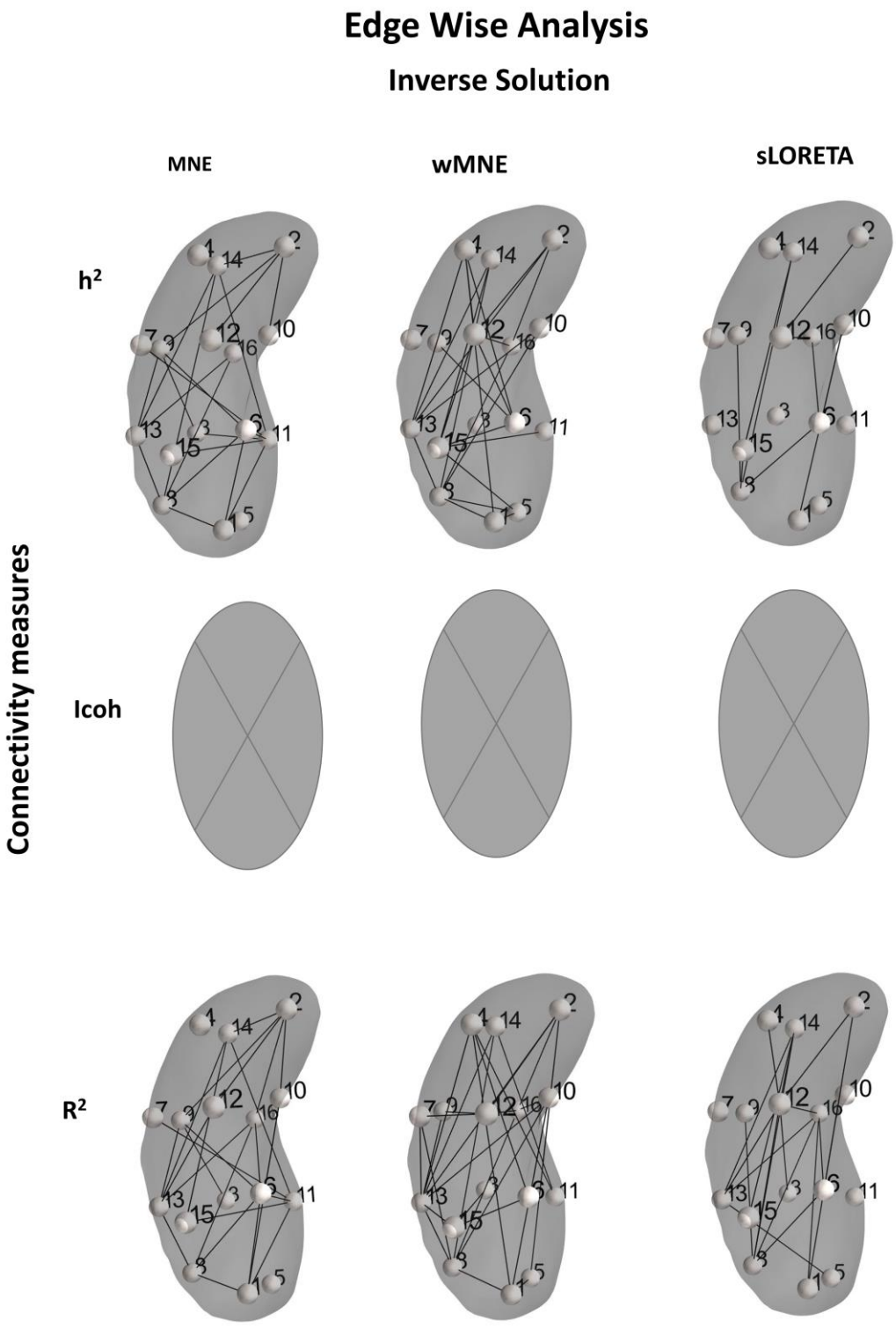


Figure 4.6 Edge-wise analysis. Only edges showing significant differences between pregnancy/labor were visualized

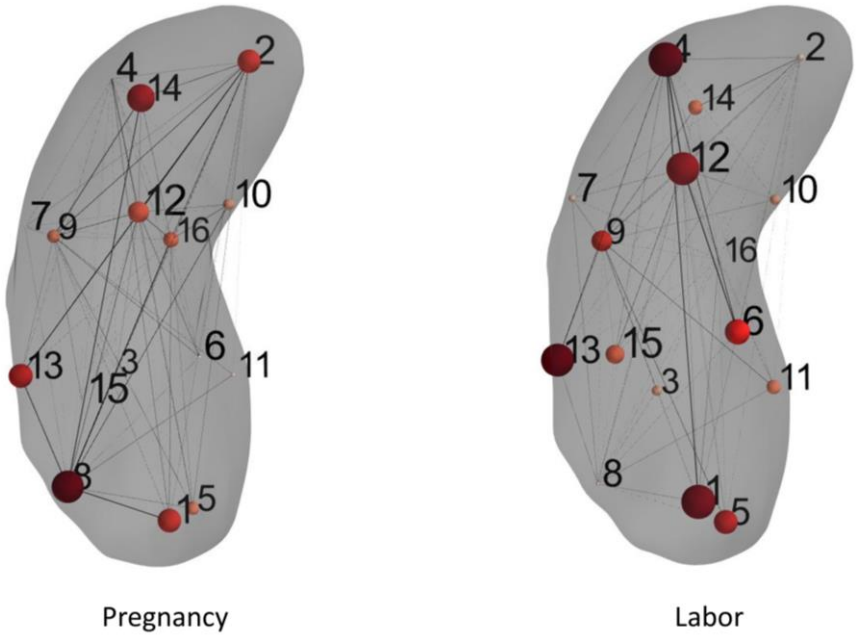


Figure 4.7 Mean graph for pregnancy and labor by using wMNE/h^2

Figure 4.7 presents a typical example of the mean graph of pregnancy and labor obtained by using wMNE/h^2 combination. The graphs of the other combinations are presented Appendix F.

The color and the size of the nodes reflect their strength; the thickness of the edges reflects their weights. An increase in connectivity is noticed in zones 4 and 6 from pregnancy to labor. A decrease in connectivity appears in the other zones (14, 2, 16, and 8).

4.4 DISCUSSION AND CONCLUSION

In this chapter, we presented the preliminary results of a novel approach aiming at characterizing the EHG functional connectivity at the source level.

Source localization combined with functional connectivity analysis has been widely used in the estimation of functional cortical brain networks from scalp M/EEG recordings (Coito et al., 2015; Hassan et al., 2016; Jiruska et al., 2013). The originality in this work is that it is the first time that we use this analysis in order to study the propagation on the uterine source level from noninvasive EHG data. Nevertheless, the joint use of these two approaches raises a number of methodological issues that should be controlled in order to get appropriate and interpretable results. Here we reported a comparative study of the networks obtained from all possible

combinations between three algorithms to solve the EHG inverse problem and three methods to estimate the functional connectivity. A second originality of this study is related to the use of simulated EHG signals from a realistic uterine model, as a ground truth to compare the performance of the studied methods.

Results obtained on different simulated data indicated that more than one combination give the most relevant networks when compared with the ground-truth (simulations), depending on the defined scenario. Indeed, the combination of MNE and h^2 methods gives the higher similarity index in the first scenario, sLORETA combined with h^2 in the second scenario and wMNE combined with h^2 in the third scenario. We should also notice that in these two last scenarios the similarity indexes were low. We thus applied on real EHGs all the possible combinations. The obtained results indicate that wMNE combined with R^2 or h^2 gives better results than the other combinations. Results are more specifically discussed hereafter.

Methodological consideration

The connectivity matrices were thresholded by keeping the edges with the highest weight values (stronger than 10%). This procedure was used to standardize the comparison between all the combinations. We were aware of a possible effect of this threshold. We thus previously realized, on the simulated data, a comparative study by using different threshold values, going from the 50% to the 5% strongest weights. The highest similarity indexes were obtained when we kept the highest 10%. We thus used this thresholding procedure on real data.

In this study, we have grouped the reconstructed sources into sixteen zones. Indeed, in our work we are interested in the analysis of the global propagation between the different parts of the uterus. We thus chose to study the propagation between different zones that cover the uterus. As a preliminary study, we have started with an arbitrary number of sixteen. Recent data indicate that the uterus may be parted in different zones of size estimated, to 64 cm^2 (Young, 2015). Thus, when computed in our meshed uterus, the number of region should be about 27-30. Then a higher number of zones could be used in future work.

Three classical inverse and connectivity algorithms were evaluated in this chapter. Indeed, we focused this study on evaluating different families of ‘functional’ connectivity methods

regardless the directionality of these connections. Nevertheless, we consider that the analyses of the 'effective' connectivity methods that investigate the directions between the different active zones may be of interest in order to study the propagation direction in labor and pregnancy. In addition, using other inverse methods more suited to the uterine activity (under study in the team) will be of great interest to improve the present results.

The uterus model used in this study was computed by using the Boundary Element Method (BEM) with four tissue layers. This model was widely used in the context of M/EEG source estimation (Fuchs et al., 2007; Hassan et al., 2016) as a compromise between computational cost and accuracy. Nevertheless, other methods exist to solve the forward model such as the Finite Element Method (FEM). Future work will be done in our team to improve this model.

Node and Edge wise analysis

Three graph parameters were extracted from all the computed graphs. We then evidenced only the zones that present significant difference between labor and pregnancy contractions. Indeed, the results obtained with all the parameters were interesting. We got higher performance for Str in this preliminary study. In fact, two zones (8 and 16) were always significant, whatever the inverse/connectivity combination. However, other zones in different parts of the uterus were also frequently significant.

Edge analysis has been also performed by keeping only the significant edges. These edges or links presented significant differences between labor and pregnancy. These edges are present between most of the zones, located in the whole uterus (upper, middle and lower parts).

All these observations have been made by using two averaged graphs (Pregnancy and Labor), obtained from all the graphs computed from all the women contained in the pregnancy and labor groups. This averaging does not take into account the possible anatomical differences between women. It should be interesting also to test the graph evolution for a given woman, in a longitudinal approach.

However, these findings were obtained by using only 16 surface EHG. In fact, a higher number of electrodes that could cover the whole uterus could improve these results, by improving the inverse problem step (work under study).

DISCUSSION AND PERSPECTIVES

We have presented in this thesis novel approaches aiming at characterizing the functional connectivity of the uterine electrical activity for clinical purpose. Our approaches were based on the analysis of the synchronization of the uterine electrical activity by using the graph theory analysis. We have also investigated the usefulness of the network-based analysis to characterize the evolution of uterine contractions from pregnancy to labor and to discriminate pregnancy and labor contractions, at the abdominal as well at the source levels.

The electrohysterography (EHG), a noninvasive abdominal measurement of the uterine electrical activity (Devedeux et al., 1993), has been already used to predict preterm labor in many previous studies. (Euliano et al., 2009, 2009; Laforet et al., 2013; Marque and Duchene, 1989; Planes et al., 1984). Moreover, labor and delivery are preceded by changes in two physiological phenomena known to control the efficiency of uterine contractions: i) increased excitability and ii) increased synchronization of the uterus. This synchronization could be the result of two phenomena: increased connectivity between the myometrial cells, due to the appearance of Gap Junctions, which results in an increase in the local diffusion of the action potentials (Devedeux et al., 1993).; increased sensitivity to mechanotransduction, at the cell level, that permit a longer distance activation of the uterine muscle due to its stretching (Young, 2007).

Concerning the global analysis of the uterine synchronization (whole burst), in most previous studies, the EHG correlation matrices were reduced by keeping only their mean and standard deviations. The innovative approach proposed in this work is to extract from these correlation matrices, a much more complete picture of the organization of the uterus, as pregnancy evolves to delivery. The graph theory based analysis used in this thesis seems indeed a better way to characterize the EHG connectivity matrices than a simple averaging.

Connectivity at the abdominal surface level

First, we have proved in this work that the graph theory based analysis is more efficient to quantify the connectivity matrices of normal pregnancy and labor EHGs, when compared to the previous studies based on averaging the connectivity matrices. However, the method showed

lower performance for the monitoring of pregnancy, as no significant change was observed between the different pregnancy weeks before labor. An increase in synchronization from pregnancy to labor has been obtained from this work based on graph theory using whole burst analysis. This obtained result agrees with the previously reported results using EHG (Hassan et al., 2013) or MMG-based studies where authors showed an increase in synchrony as the women approach active labor (Govindan et al., 2015).

We showed also a clear increased connectivity during labor. A classification rate of 80% has been reached with the combination of the *Icoh* as connectivity measure and the strength as graph measure. This increase from pregnancy to labor was observed for all the electrodes. Once again, these findings agree with the results obtained previously by Hassan et al. when using the nonlinear correlation coefficient on a smaller dataset (Hassan et al., 2013). A possible explanation of this increase in connectivity during labor is the electrical diffusion phenomenon, associated with the appearance of a large number of gap junctions prior to labor (Garfield and Hayashi, 1981), as well as the electromechanical coupling proposed by Young as one of the synchronization process appearing during labor (Young, 2007).

The above mentioned results can be improved as following:

- To validate the clinical impact of the proposed approach, it should be applied to a larger database, including signals recorded on women with premature labor, kind of data still missing in our database. A classification between normal labor and premature labor will be of great interest to test the clinical performance of the proposed approach, as well as to understand the process of premature labor, still poorly understood.
- Different steps in the pipeline should be automatized when using this approach for clinical perspective, such as the manual segmentation of the uterine burst. Manual segmentation is time consuming and depends on the ability of the person who segments the signals. This point is under development in our team.
- So far, we have used only one parameter for the classification. The combination of several graph parameters could improve the classification rate based on the uterine synchronization analysis. Furthermore, as shown in a study recently done in our lab (Alamedine et al., 2014), different parameters representing either the excitability

(frequency content, non-linearity) or the synchronization of the uterus should be used simultaneously to get the best classification rate between pregnancy and labor EHGs. The selected graph parameters should be tested together with the excitability ones already selected, in order to improve this classification.

- In our work we were interested in the analysis of the global synchronization of the uterus. We have thus applied the approach on whole EHG bursts. We think that analyzing the EHG local propagation (by applying the approach on single spikes) could be of interest.
- In this thesis, we focused on the functional connectivity methods regardless directionality of the connectivity. Another type of connectivity called effective connectivity, that investigate the causality of the relationships, may provide new information about the possible directionality of the synchronization.
- All the analysis presented in the thesis were computed on the whole burst duration (static analysis). As EHG signals present nonstationary behaviors, a dynamic analysis (by using sliding window) would permit to better respect the intrinsic characteristics of the signals.

Connectivity at the source level

Then, we tackled in this work the connectivity of the EHG at the source level. This work represents, the first use of this source analysis in order to study the synchronization of the uterine muscle level, from noninvasive abdominal EHGs. We have presented in this work the preliminary results obtained by using this approach. The originality of this work is the combination between source localization and functional connectivity. Indeed, this type of analysis has been widely used on EEG (Coito et al., 2015; Hassan et al., 2016; Jiruska et al., 2013) but it is the first time that it is used on EHG. First, the uterus mesh was parted into sixteen zones, in order to simplify the global uterine level analysis. The approach was first validated on simulated networks by using a realistic uterine model. The EHGs were simulated to produce a reference networks (ground truth) in order to compare the performance of the considered methods.

Three classical inverse methods were first used (wMNE, MNE and sLORETA) and three connectivity methods (h^2, R^2 *and Icoh*). The main objective of this part was to find the best combination of inverse/connectivity methods that gives the network closest to the reference network. Results obtained on simulated data indicated that more than one combination could

leads to the most relevant networks when compared to the reference network. However, h^2 appeared more frequently in the most efficient methods. Therefore, all the possible combinations were applied on real data in order to differentiate between labor and pregnancy contractions. The obtained results indicate that wMNE combined with R^2 or h^2 provided better results than the other combinations. The significant zones, different in labor and pregnancy, were mainly located in the middle and the lower part of the uterus. A network pattern (a set of edges) showed also significant difference between pregnancy and labor, but not always associated to an increase in connectivity from pregnancy to labor. These edges were identified between almost all the zones.

This analysis was performed based on a recording grid of only sixteen surfaces EHG channels, covering a small part of the abdominal wall (6 cm x 6 cm). A higher number of electrodes, covering a larger part of the mother's abdomen, could improve the inverse problem results and specify more the synchronization pattern as reported in other applications (Hassan et al., 2014; Song et al., 2015).

These findings were the preliminary results on the EHG source connectivity. Possible improvements of the methods in order to improve these results can be summarized as following:

- The uterus mesh was segmented into sixteen zones, a higher (more realistic) number of zones would give more precise results and improve the classification rate.
- We used here as a first attempt, only classical inverse methods. Testing new algorithms more suited to the uterine activity, will be of great interest to improve the present results.
- The mesh used in our uterine model was obtained from a MRI of a woman during pregnancy (34,5 weeks of pregnancy). Another mesh obtained for woman in labor (or from the same woman at different weeks of pregnancy) may improve the specificity of the results.
- The uterus forward model used in the thesis was solved using a BEM model. A Finite Element Method (FEM) was shown to improve the solution of the EEG forward problem (Hallez et al., 2007). This approach may also be used and lead to improvements of the EHG source connectivity results.
- In this preliminary study, we have investigated the classification of normal pregnancy and term labor contractions, in relation to the EHG signals available in our database.

Testing the capacity of the EHG source connectivity method to monitor pregnancy evolution is one of the main interesting application, for the ealy detection of preterm labor. We will thus need to include in this analysis EHGs recorded on risk pregnancies, as well as on preterm labors.

To sum up, we have presented in this thesis a new approach based on connectivity analysis of the EHG signals combined with a graph theory based analysis. Our results showed that this network-based approach is a very promising tool to quantify uterine synchronization, when applied at the abdominal level, for a better pregnancy monitoring. We expect this approach to be further used for the monitoring of pregnancy and would thus help for the early prediction of preterm labor.

APPENDIX A: DATABASE OF THE RECORDED WOMEN

Table A. 1: Information of women used in our database.

Woman	Weight (Kg)	Height (m)	Week of pregnancy (WP)	Week of Delivery (WD)	Group	Number of contractions
W1	89	1.7	42	42	Labor	22
W2	92.4	1.78	35	40	5 WBL	5
			37		3 WBL	5
			38		2 WBL	6
			39		1 WBL	2
W3	105	1.72	33	38	5 WBL	1
			36		2 WBL	5
			37		1 WBL	3
			38		Labor	10
W4	67	1.64	34	38	4 WBL	6
			36		2 WBL	7
			37		1 WBL	9
W5	76.2	1.7	37	37	Labor	5
W6	71	1.75	33	41	9 WBL	7
			37		4 WBL	3
W7	61	1.75	35	40	5 WBL	7
			38		2 WBL	5
			39		1 WBL	6
W8	62	1.65	33	39	6 WBL	4
W9	48 - 50	1.6	29	41	12 WBL	2
			31		10 WBL	2
			34		7 WBL	1
W10	75	1.72	36	40	4 WBL	2
			38		2 WBL	3
			40		Labor	1
W11	70 - 75	1.76	33	41	8 WBL	4
			35		6 WBL	2
			38		3 WBL	4
W12	63.4	1.63	39	39	Labor	7

W13	56	1.63	40	41	1 WBL	8
W14	100	1.78	33	41	8 WBL	7
W15	62	1.63	39	39	Labor	4
W16	109	xxx	40	40	Labor	3
W17	xxx	xxx	40	40	Labor	26
W18	xxx	xxx	40	40	Labor	33
W19	xxx	xxx	39	39	Labor	23
W20	xxx	xxx	42	42	Labor	11
W21	xxx	xxx	xxx	xxx	Labor	18
W22	95	1.63	39	39	Labor	1
W23	83	1.7	34	40	6 WBL	1
			36		4 WBL	2
			37		3 WBL	4
			39		1 WBL	4
W24	68	1.68	33	39	6 WBL	7
W25	69.5	1.67	31	39	8 WBL	3
			36		6 WBL	4
			39		Labor	4
W26	95.3	1.62	34	39	5 WBL	1
W27	110	1.76	37	41	4 WBL	1
			38		3 WBL	1
			39		2 WBL	2
			40		1 WBL	9
W28	90	1.68	37	39	2 WBL	1
W29	85.5	1.68	32	40	8 WBL	10
			37		3 WBL	9
			38		2 WBL	2
W30	78	1.63	39	42	3 WBL	1
W31	113.3	1.73	36	39	3 WBL	3
W32	65.5	1.69	38	40	2 WBL	6
W33	74	1.68	37	41	4 WBL	4
W34	88	1.76	36	40	4 WBL	1
	89		39		1 WBL	1
W35	82	1.67	33	40	7 WBL	11
	83		36		4 WBL	7
	84		37		3 WBL	9
	85		39		1 WBL	9

APPENDIX B: PREGNANCY MONITORING FOR EACH WOMAN

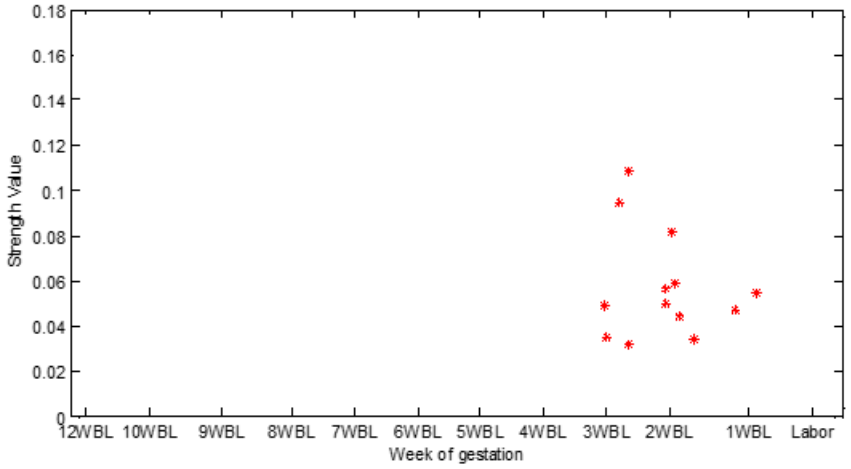


Figure B. 1 Evolution of Str for woman W2

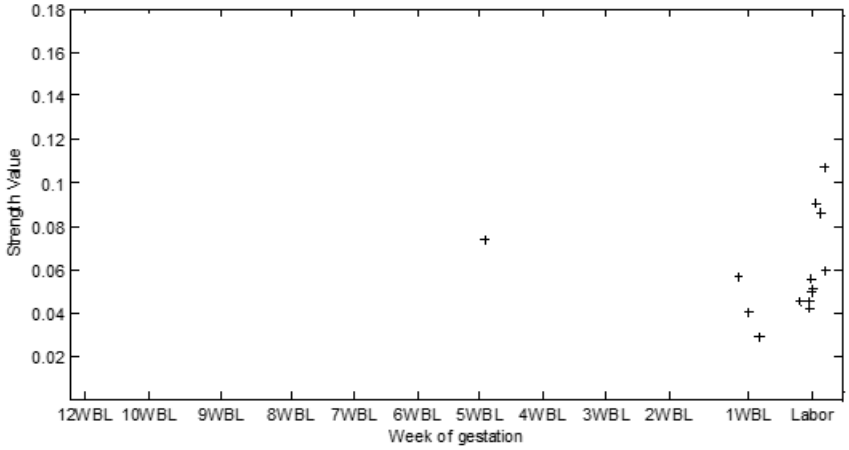


Figure B. 2 Evolution of Str for woman W3

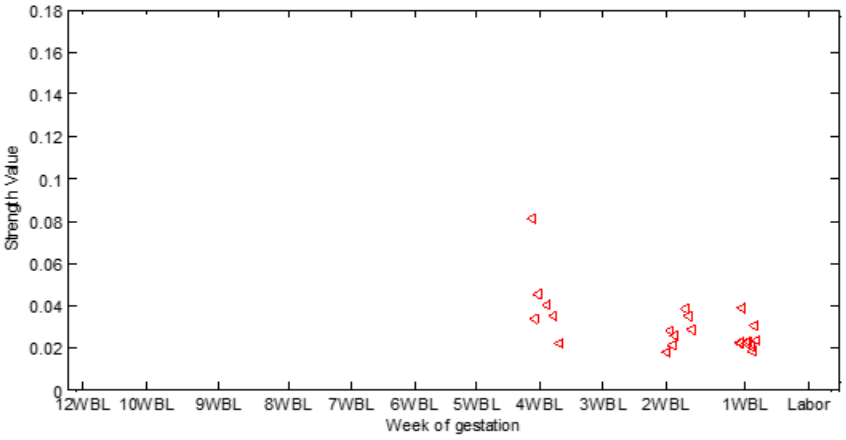


Figure B. 3 Evolution of Str for woman W4

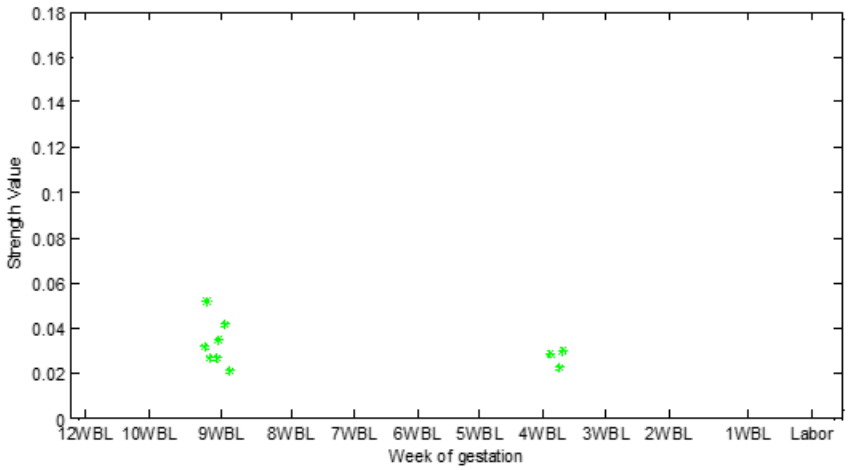


Figure B. 4 Evolution of Str for woman W5

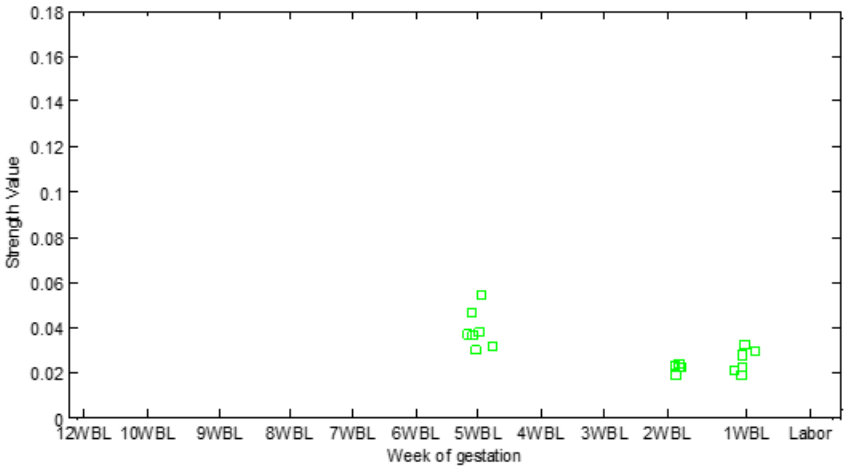


Figure B. 5 evolution of Str for woman W6

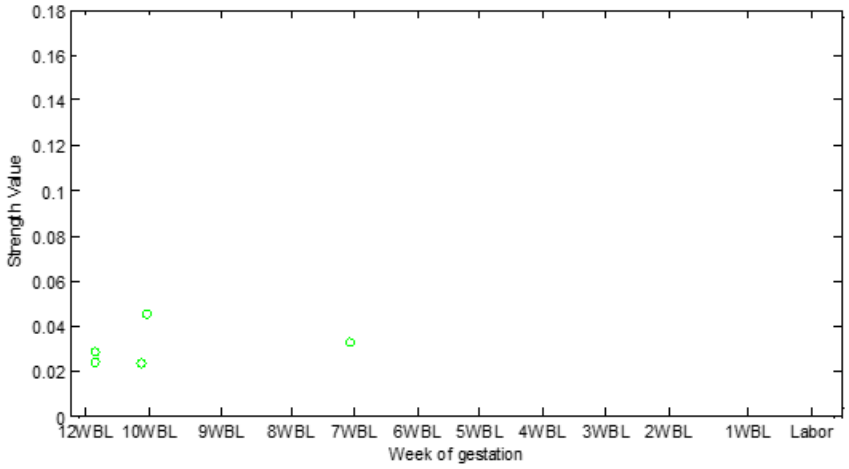


Figure B. 6 Evolution of Str for woman W9

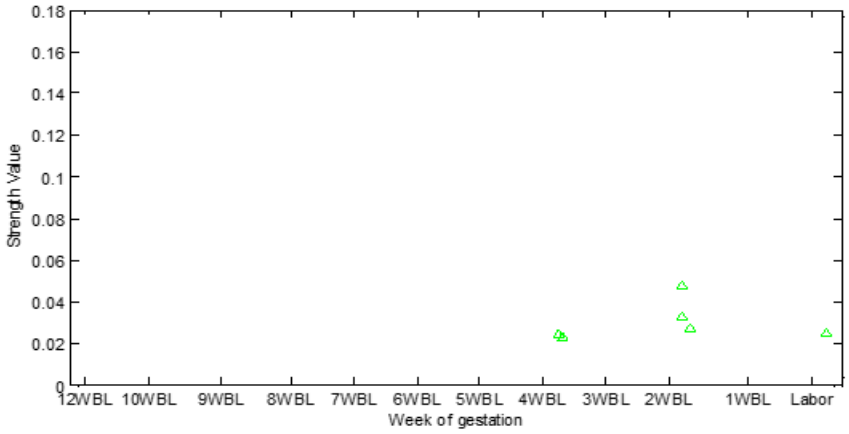


Figure B. 7 Evolution of Str for woman W10

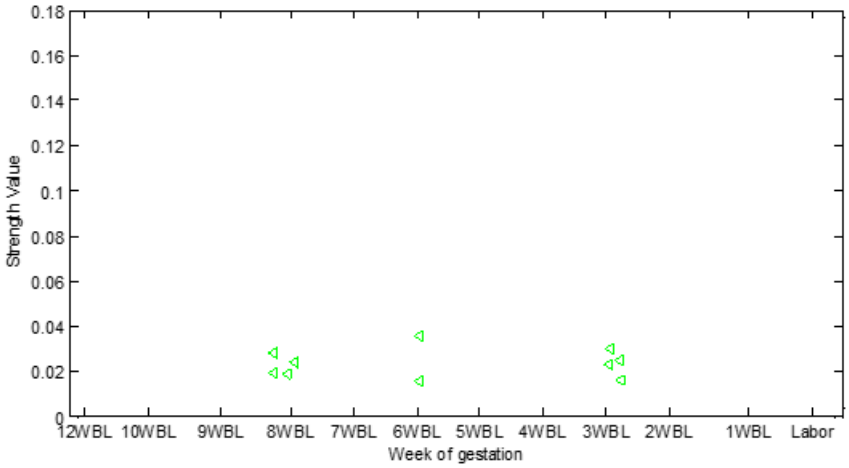


Figure B. 8 Evolution of Str for woman W11

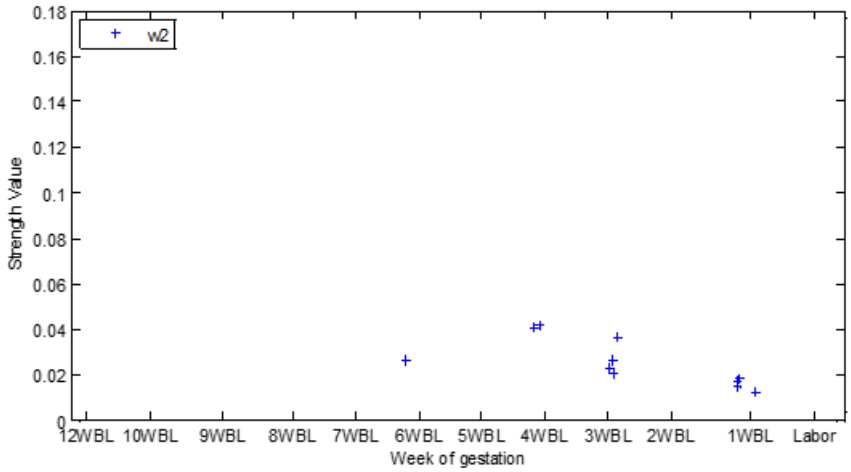


Figure B. 9 Evolution of Str for woman W23

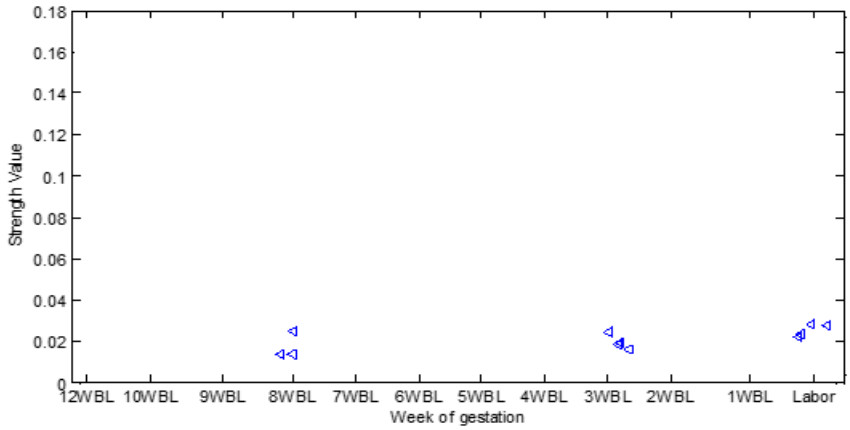


Figure B. 10 Evolution of Str for woman W25

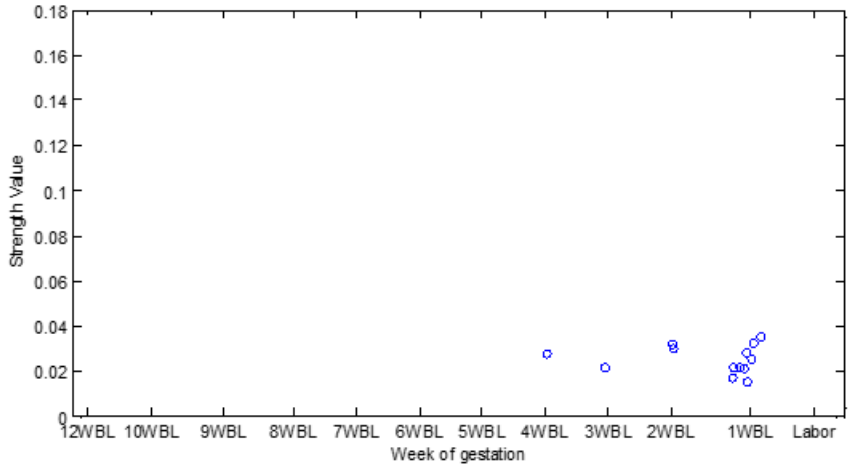


Figure B. 11 Evolution of Str for woman W27

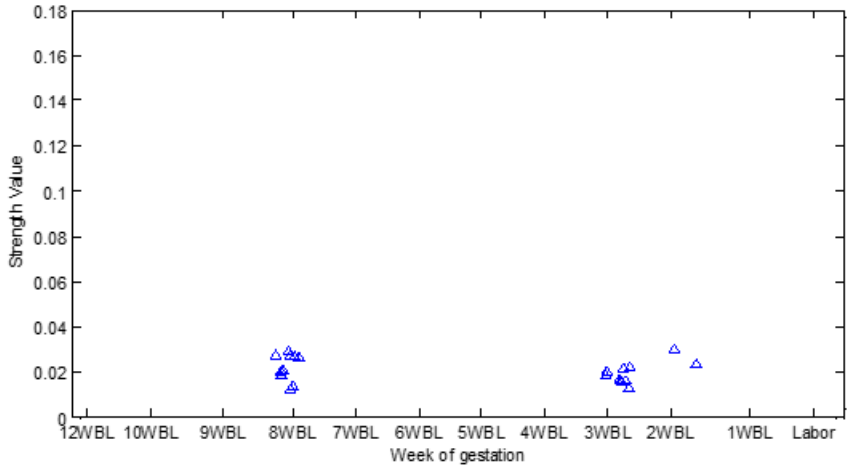


Figure B. 12 Evolution of Str for woman W29

APPENDIX C: PREGNANCY AND LABOR GRAPHS AT SAME WEEK OF GESTATION

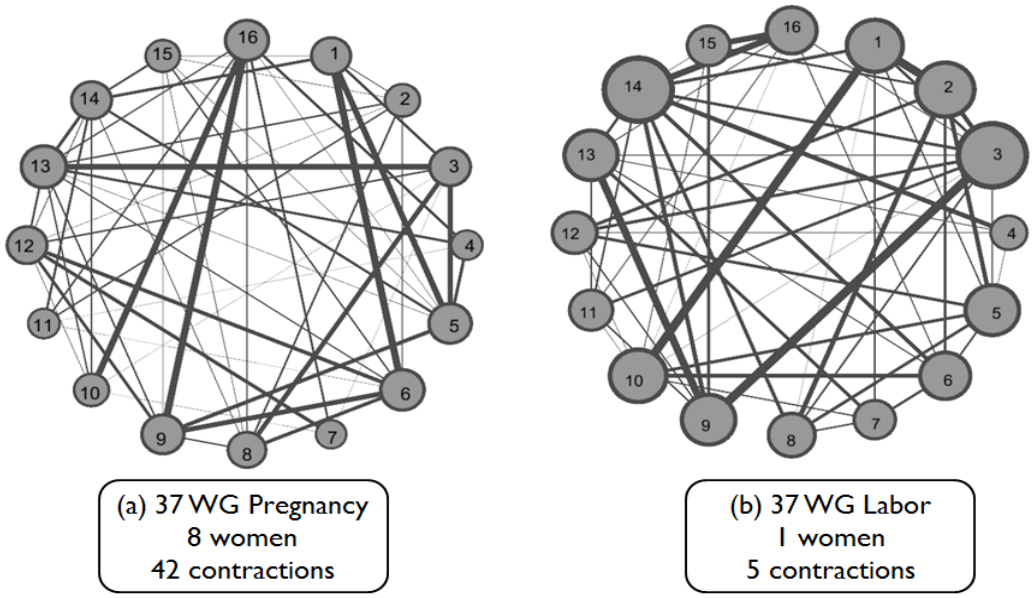


Figure C. 1 Mean graphs for EHGs recorded at 37WG: (a) Pregnancy, (b) Labor.

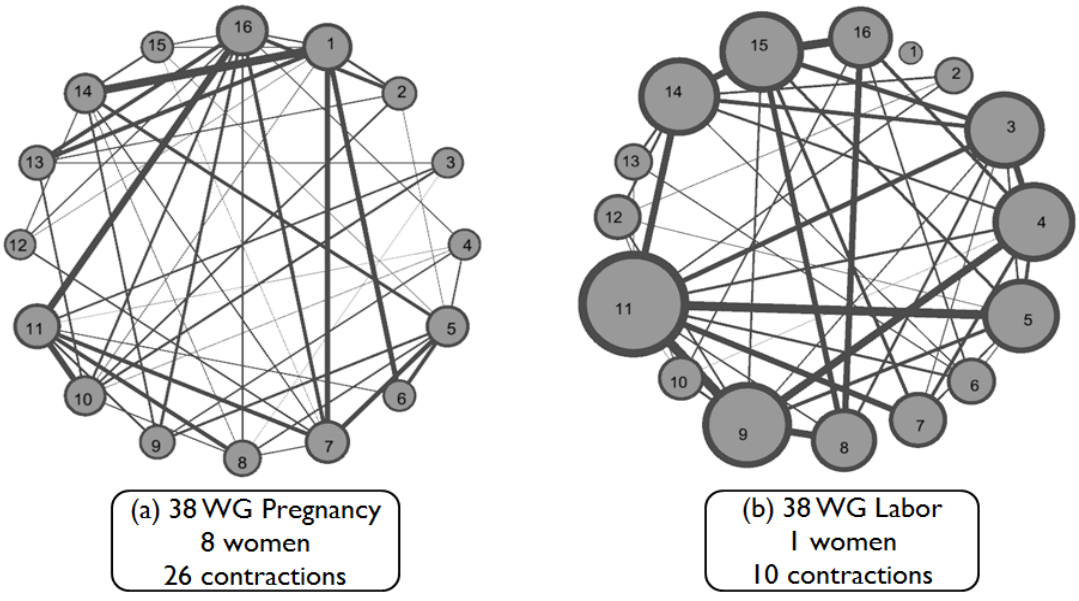


Figure C. 2 Mean graphs for EHGs recorded at 38WG: (a) Pregnancy, (b) Labor.

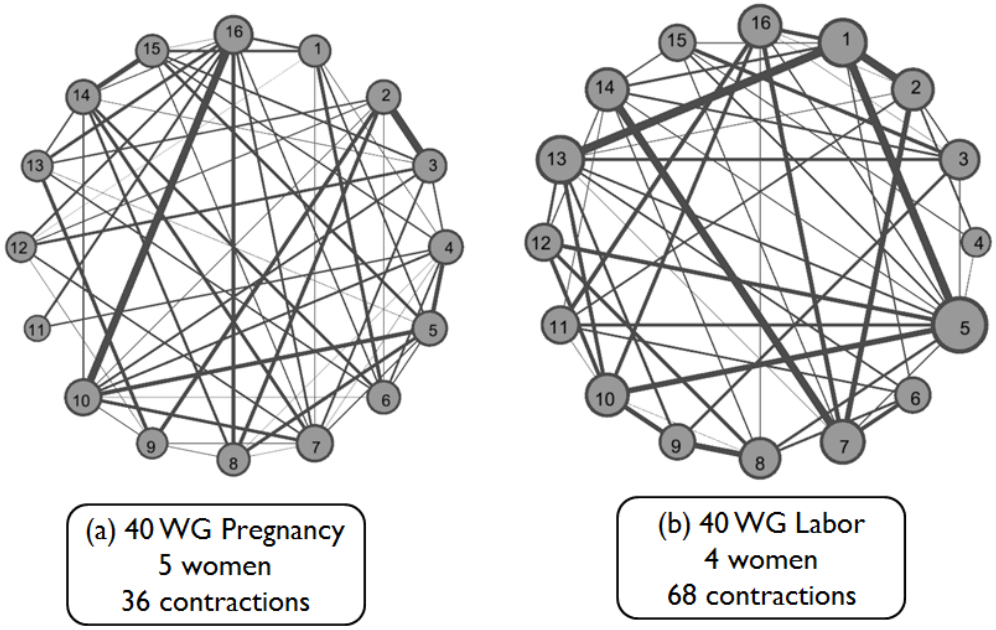
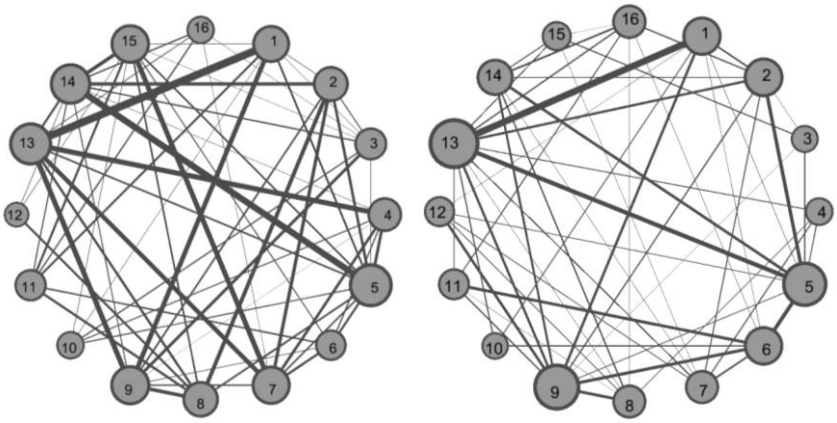


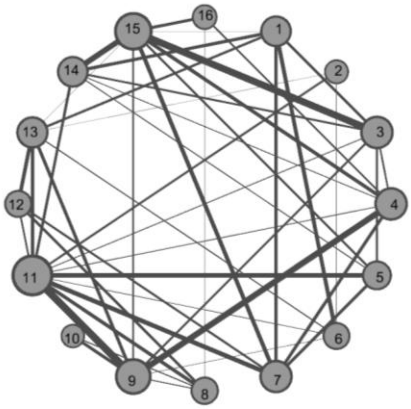
Figure C. 3 Mean graphs for EHGs recorded at 40WG: (a) Pregnancy, (b) Labor.

APPENDIX D: WEEKS OF GESTATION GRAPHS

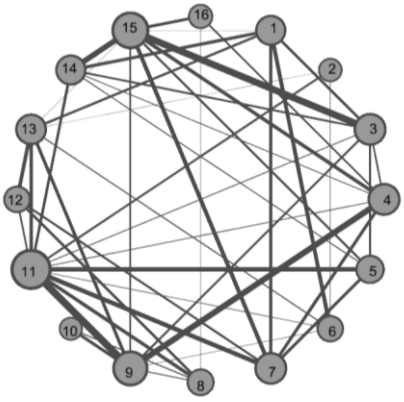


30

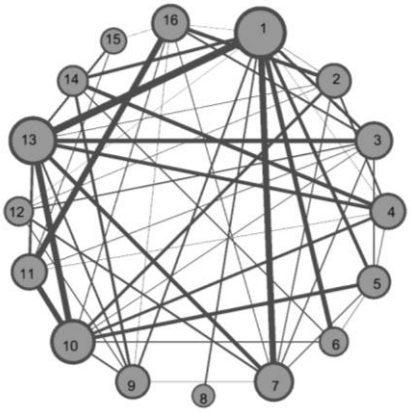
32



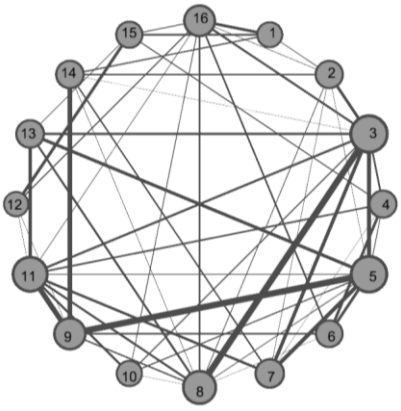
33



34

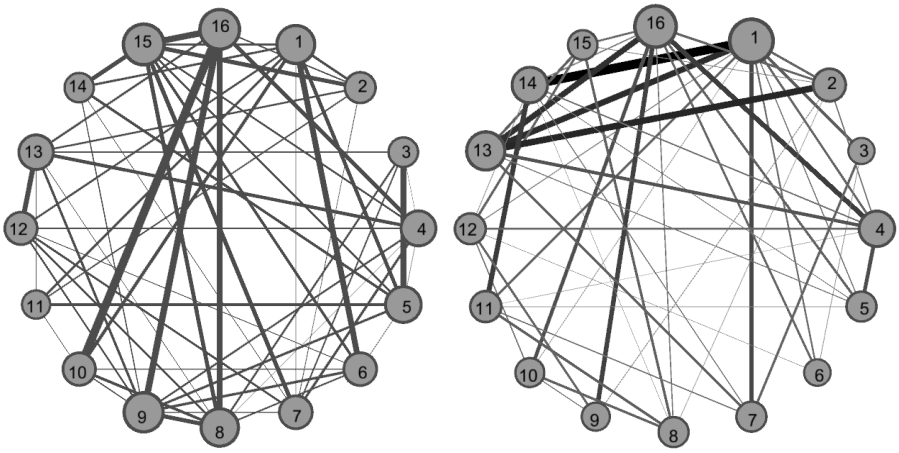


35



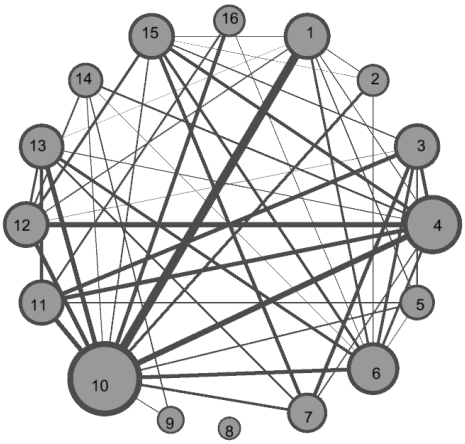
36

Figure D. 1 Mean graph for weeks of gestation (30WG---36WG)

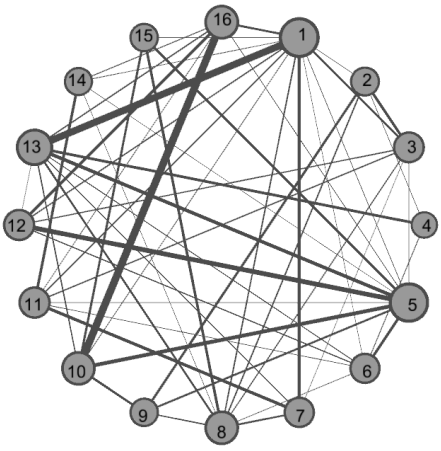


37

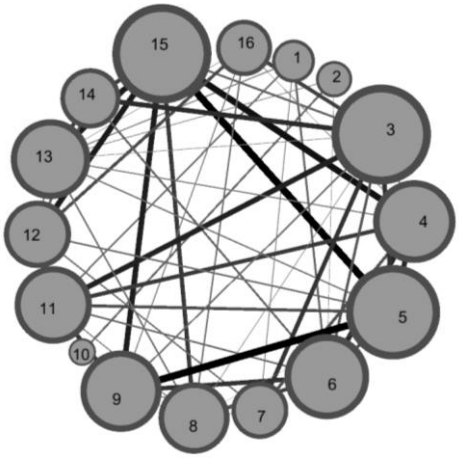
38



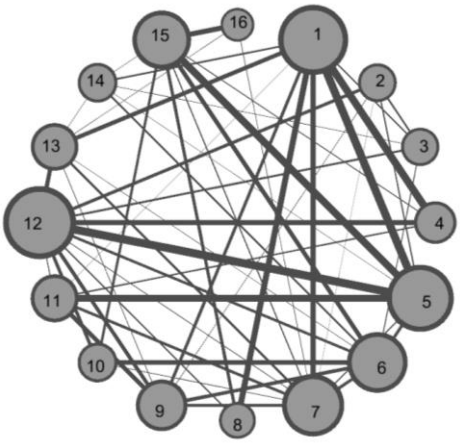
39



40



41



42

Figure D. 2 Mean graph for weeks of gestation (37WG---42WG)

APPENDIX E: TABLE OF SIGNIFICANT EDGES

Table E.1 Significant edges in all the combinations

h2			R2		
MNE	wMNE	sLORETA	MNE	wMNE	sLORETA
'Edge1_6'	Edge1_4'	'Edge1_10'	'Edge1_6'	'Edge1_4'	'Edge1_2'
'Edge1_8'	'Edge1_5'	'Edge2_12'	'Edge1_8'	'Edge1_5'	'Edge1_16'
'Edge1_11'	'Edge1_8'	'Edge6_8'	'Edge1_10'	'Edge1_8'	'Edge2_12'
'Edge2_9'	'Edge2_12'	'Edge6_16'	'Edge1_11'	'Edge1_10'	'Edge3_12'
'Edge2_10'	'Edge2_13'	'Edge8_9'	'Edge2_9'	'Edge2_5'	'Edge4_12'
'Edge2_12'	'Edge2_16'	'Edge8_14'	'Edge2_10'	'Edge2_12'	'Edge5_13'
'Edge2_14'	'Edge4_6'	'Edge8_15'	'Edge2_12'	'Edge2_13'	'Edge6_8'
'Edge3_9'	'Edge4_12'	'Edge12_16'	'Edge2_14'	'Edge2_16'	'Edge6_16'
'Edge3_11'	'Edge4_13'	'Edge14_15'	'Edge2_16'	'Edge3_15'	'Edge8_9'
'Edge6_8'	'Edge5_8'		'Edge3_9'	'Edge4_6'	'Edge8_12'
'Edge6_9'	'Edge5_15'		'Edge6_8'	'Edge4_11'	'Edge8_14'
'Edge6_11'	'Edge6_9'		'Edge6_9'	'Edge4_13'	'Edge8_16'
'Edge7_11'	'Edge6_12'		'Edge6_11'	'Edge6_15'	'Edge12_13'
'Edge8_13'	'Edge6_15'		'Edge6_16'	'Edge7_8'	'Edge12_14'
'Edge8_14'	'Edge8_10'		'Edge7_11'	'Edge7_12'	'Edge12_16'
'Edge8_16'	'Edge8_13'		'Edge8_13'	'Edge7_13'	'Edge13_14'
'Edge9_13'	'Edge8_14'		'Edge8_16'	'Edge8_10'	'Edge13_16'
'Edge11_14'	'Edge8_16'		'Edge9_13'	'Edge8_13'	'Edge14_15'
'Edge11_15'	'Edge10_13'		'Edge11_14'	'Edge8_14'	
'Edge13_14'	'Edge11_15'		'Edge11_15'	'Edge8_16'	
'Edge13_16'	'Edge12_15'		'Edge12_13'	'Edge9_12'	
	'Edge12_16'		'Edge13_14'	'Edge9_13'	
	'Edge13_14'		'Edge13_16'	'Edge10_13'	
	Edge14_15'		'Edge14_15'	'Edge10_16'	
				'Edge11_14'	
				'Edge12_16'	
				'Edge13_14'	
				'Edge13_15'	

APPENDIX F: PREGNANCY AND LABOR GRAPHS BY USING ALL THE INVERSE/CONNECTIVITY COMBINATIONS

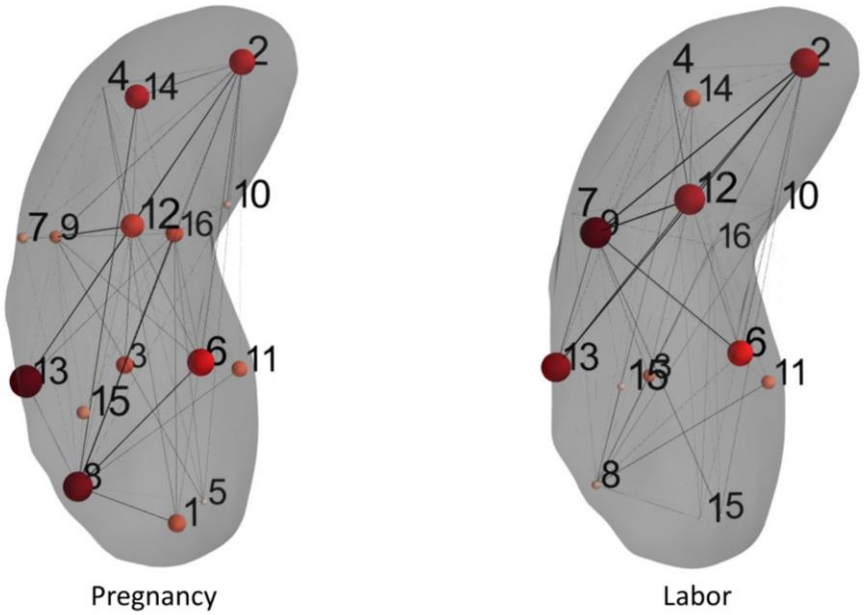


Figure F. 1 Mean graph for pregnancy and labor by using MNE/h^2

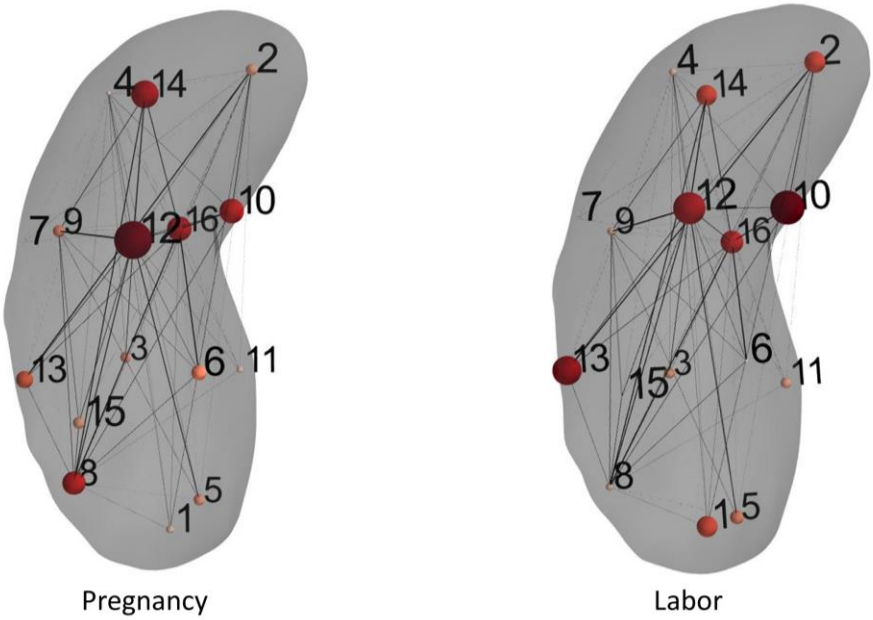


Figure F. 2 Mean graph for pregnancy and labor by using sLORETA/h^2

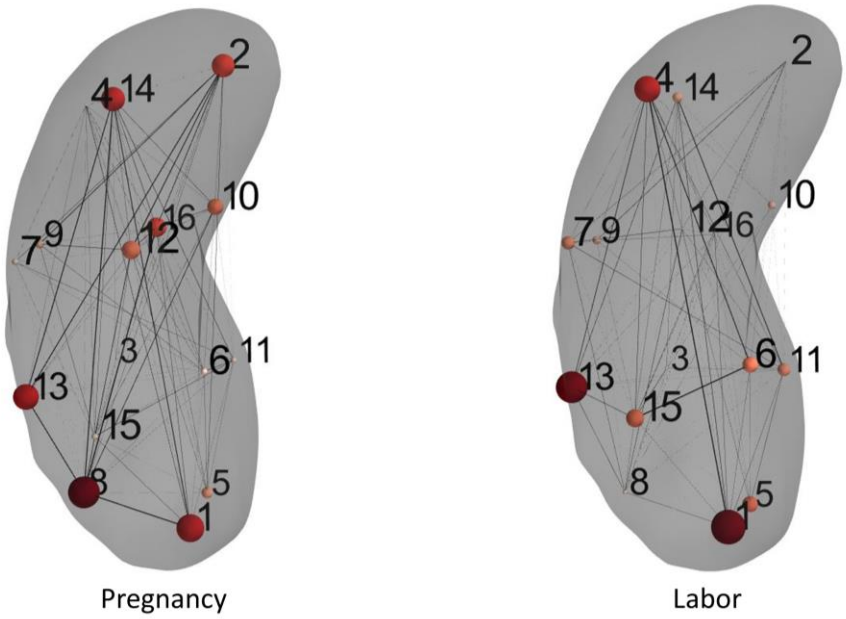


Figure F. 3 Mean graph for pregnancy and labor by using wMNE/R^2

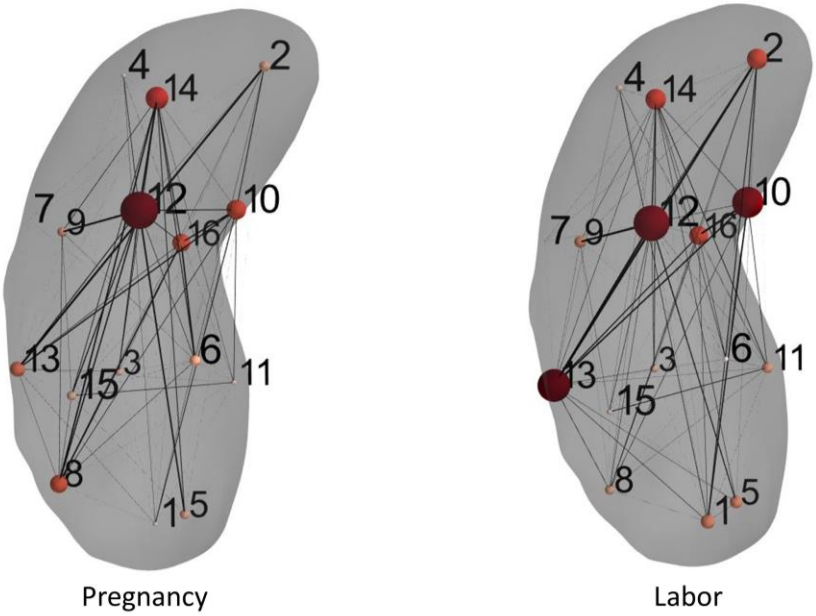


Figure F. 4 Mean graph for pregnancy and labor by using sLORETA/R^2

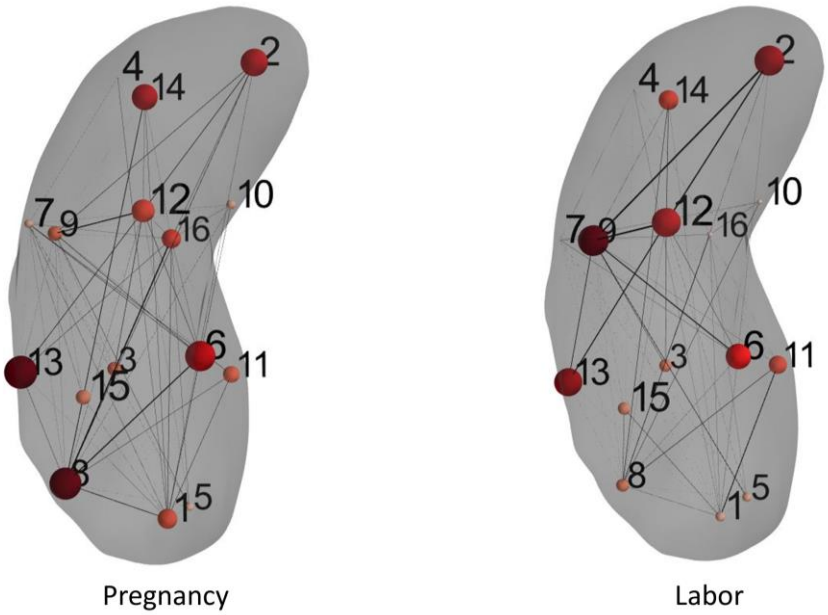


Figure F. 5 Mean graph for pregnancy and labor by using MNE/R^2

ABSTRACT

Preterm birth remains a major problem in obstetrics. Therefore**,** it has been a topic of interest for many researchers. Among the many methods used to record the uterine contractility, the most used is the abdominal EHG, as being an easy to use and a non-invasive tool. Many studies have reported that the use of this signal could be a very powerful tool to monitor pregnancy and to detect labor. It indeed permits to access the uterine as well as the synchronization of the uterine activity, by using multiple signals. It has been shown that the connectivity analysis gave promising results when using EHG recordings in clinical application, such as the classification labor/pregnancy contractions. However, in almost all previous studies EHG correlation matrices were often reduced keeping only their mean and standard deviations thus relevant information may have been missed due to this averaging, which may induce the relatively low classification rate reported so far. To characterize precisely the correlation matrix and quantify the associated connectivity, we proposed in this thesis to use a network measure technique based on graph theory. According to this approach, the obtained correlation matrix can be represented as graphs consisting of a set of nodes (electrodes) interconnected by edges (connectivity/correlation values between electrodes). The new framework, to analyze the EHG signals recorded during pregnancy and labor, is based on the characterization of the correlation between the uterine electrical activities and on its precise quantification by using graph theory approach. The processing pipeline includes i) the estimation of the statistical dependencies between the different recorded EHG signals, ii) the quantification of the obtained connectivity matrices using graph theory-based analysis and iii) the clinical use of network measures for pregnancy monitoring as well as for the classification between pregnancy and labor EHG bursts. A comparison with the already existing parameters used in the state of the art for labor detection and preterm labor prediction will also be performed. We also investigate a new method to study the EHG source connectivity, to overcome the problem of computing the connectivity at the abdominal surface level.

The results of this thesis showed that this network-based approach is a very promising tool to quantify uterine synchronization, when applied at the abdominal level, for a better pregnancy monitoring. We expect this approach to be further used for the monitoring of pregnancy and would thus help for the early prediction of preterm labor.

Keywords: Uterine electrical activity, Graph theory, pregnancy and labor contractions.

RESUME

L’accouchement prématurée est l’un des problèmes majeurs en obstétrique. Par suite, il a été un sujet d'intérêt pour de nombreux chercheurs. Parmi les nombreuses méthodes utilisées pour enregistrer la contractilité utérine, le plus utilisé est l'EHG abdominal, comme étant un outil facile à utiliser et non invasif. De nombreuses études ont indiqué que l'utilisation de ce signal pourrait être un outil très puissant pour surveiller la grossesse et pour détecter le travail. Il permet en effet d'accéder à l'utérus ainsi que la synchronisation de l'activité utérine, en utilisant des signaux multiples. Il a été démontré que l'analyse de connectivité des signaux EHG a donné des résultats prometteurs lors de en application clinique, comme la classification des contractions de travail et de grossesse. Cependant, dans presque toutes les études antérieures, les matrices de corrélation EHG étaient souvent réduites en ne gardant que leur moyenne et les écarts-types, ce qui a peut aboutir à perdre des informations pertinentes en raison de ce moyennage, ce qui peut induire le taux de classification relativement faible jusqu'à présent. Pour caractériser précisément la matrice de corrélation et quantifier la connectivité associée, nous avons proposé dans cette thèse d'utiliser une technique de mesure de réseau basée sur la théorie des graphes. Selon cette approche, la matrice de corrélation obtenue peut être représentée sous forme de graphiques constitués d'un ensemble de noeuds (électrodes) interconnectés par des arêtes (valeurs de connectivité / corrélation entre électrodes). La nouvelle procédure de l'analyse des signaux EHG enregistrés pendant la grossesse et le travail se base sur la caractérisation de la corrélation entre les activités électriques utérines et sur sa quantification précise en utilisant l'approche de la théorie des graphes. Le pipeline de traitement inclut i) l'estimation des dépendances statistiques entre les différents signaux EHG enregistrés, ii) la quantification des matrices de connectivité obtenues à l'aide de l'analyse théorique des graphes et iii) l'utilisation clinique des mesures de réseau pour la surveillance de la grossesse ainsi que la classification entre les éclosions d'EHG de grossesse et de travail. Une comparaison avec les paramètres déjà existants utilisés pour la détection du travail et la détection d’accouchement prématuré sera également effectuée. Nous étudions également une nouvelle méthode pour étudier la connectivité source EHG, afin de surmonter le problème du calcul de la connectivité au niveau de la surface abdominale.

Les résultats de cette thèse montrent que cette approche basée sur la théorie de graphe est un outil très prometteur pour quantifier la synchronisation utérine, lorsqu'elle est appliquée à l'abdomen, pour une meilleure surveillance de la grossesse. Nous espérons que cette approche soit utilisée pour le suivi de la grossesse et contribuerait ainsi à la prédiction précoce de l’accouchement prématuré.

Mots-clés: Activité électrique utérine, théorie des graphes, contractions de la grossesse et du travail.

REFERENCES

Alamedine, D., Diab, A., Muszynski, C., Karlsson, B., Khalil, M., Marque, C., 2014. Selection algorithm for parameters to characterize uterine EHG signals for the detection of preterm labor. Signal Image Video Process. 8, 1169–1178. doi:10.1007/s11760-014-0655-2

Alexandersson, A., Steingrimsdottir, T., Terrien, J., Marque, C., Karlsson, B., 2015. The Icelandic 16-electrode electrohysterogram database. Sci. Data 2, 150017. doi:10.1038/sdata.2015.17

Al-Omar, S., Diab, A., Nader, N., Khalil, M., Karlsson, B., Marque, C., 2015. Detecting labor using graph theory on connectivity matrices of uterine EMG. Conf. Proc. Annu. Int. Conf. IEEE Eng. Med. Biol. Soc. IEEE Eng. Med. Biol. Soc. Annu. Conf. 2015, 2195–2198. doi:10.1109/EMBC.2015.7318826

Ansari-Asl, K., Wendling, F., Bellanger, J.J., Senhadji, L., 2004. Comparison of two estimators of time-frequency interdependencies between nonstationary signals: application to epileptic EEG, in: 26th Annual International Conference of the IEEE Engineering in Medicine and Biology Society, 2004. IEMBS '04. Presented at the 26th Annual International Conference of the IEEE Engineering in Medicine and Biology Society, 2004. IEMBS '04, pp. 263–266. doi:10.1109/IEMBS.2004.1403142

Baghamoradi, S.M.S., Naji, M., Aryadoost, H., 2011. Evaluation of cepstral analysis of EHG signals to prediction of preterm labor, in: 2011 18th Iranian Conference of Biomedical Engineering (ICBME). Presented at the 2011 18th Iranian Conference of Biomedical Engineering (ICBME), pp. 81–83. doi:10.1109/ICBME.2011.6168591

Bastian, M., Heymann, S., Jacomy, M., 2009. Gephi: an open source software for exploring and manipulating networks. ICWSM 8, 361–362.

Becker, H., Albera, L., Comon, P., Haardt, M., Birot, G., Wendling, F., Gavaret, M., Bénar, C.G., Merlet, I., 2014. EEG extended source localization: Tensor-based vs. conventional methods. NeuroImage 96, 143–157. doi:10.1016/j.neuroimage.2014.03.043

Behrman, R.E., Butler, A.S., Outcomes, I. of M. (US) C. on U.P.B. and A.H., 2007. Consequences of Preterm Birth. National Academies Press (US).

Bibin, L., Anquez, J., de la Plata Alcalde, J.P., Boubekeur, T., Angelini, E.D., Bloch, I., 2010. Whole-body pregnant woman modeling by digital geometry processing with detailed

uterofetal unit based on medical images. IEEE Trans. Biomed. Eng. 57, 2346–2358. doi:10.1109/TBME.2010.2053367

Blencowe, H., Cousens, S., Chou, D., Oestergaard, M., Say, L., Moller, A.-B., Kinney, M., Lawn, J., 2013. Born Too Soon: The global epidemiology of 15 million preterm births. Reprod. Health 10, S2. doi:10.1186/1742-4755-10-S1-S2

Boccaletti, S., Latora, V., Moreno, Y., Chavez, M., Hwang, D.-U., 2006. Complex networks: Structure and dynamics. Phys. Rep. 424, 175–308. doi:10.1016/j.physrep.2005.10.009

Bozler, E., 1970. Action potentials of visceral smooth muscles and their relation to mechanical activity. Nihon Heikatsukin Gakkai Zasshi 6, 63–65.

Buhimschi, C.S., 2009. Spatiotemporal electromyography during human labor to monitor propagation of the uterine contraction wave and diagnose dystocia. Am. J. Obstet. Gynecol. 200, 1–3. doi:10.1016/j.ajog.2008.09.007

Bullmore, E., Sporns, O., 2009. Complex brain networks: graph theoretical analysis of structural and functional systems. Nat. Rev. Neurosci. 10, 186–198. doi:10.1038/nrn2575

Chard, T., 1994. The Uterus. Cambridge University Press.

Coito, A., Plomp, G., Genetti, M., Abela, E., Wiest, R., Seeck, M., Michel, C.M., Vulliemoz, S., 2015. Dynamic directed interictal connectivity in left and right temporal lobe epilepsy. Epilepsia 56, 207–217. doi:10.1111/epi.12904

Creasy, R.K., 1993. Preterm birth prevention: where are we? Am. J. Obstet. Gynecol. 168, 1223–1230.

Csapo, A.I., 1962. Smooth muscle as a contractile unit. Physiol. Rev. Suppl. 5, 7–33.

Daniel, E.E., 1960. Effect of the placenta on the electrical activity of the cat uterus in vivo and in vitro. Am. J. Obstet. Gynecol. 80, 229–244. doi:10.1016/0002-9378(60)90118-6

de Lau, H., Rabotti, C., Bijloo, R., Rooijakkers, M.J., Mischi, M., Oei, S.G., 2013. Automated Conduction Velocity Analysis in the Electrohysterogram for Prediction of Imminent Delivery: A Preliminary Study. Comput. Math. Methods Med. 2013, e627976. doi:10.1155/2013/627976

Devedeux, D., Marque, C., Mansour, S., Germain, G., Duchêne, J., 1993. Uterine electromyography: a critical review. Am. J. Obstet. Gynecol. 169, 1636–1653.

Diab, A., 2014. Study of The Nonlinear Properties And Propagation Characteristics Of The Uterine Electrical Activity During Pregnancy And Labor. Université de Technologie de Compiègne, Compiegne.

Diab, A., Hassan, M., Laforêt, J., Karlsson, B., Marque, C., 2014. Estimation of Coupling and Directionality between Signals Applied to Physiological Uterine EMG Model and Real EHG Signals, in: Romero, L.M.R. (Ed.), XIII Mediterranean Conference on Medical and Biological Engineering and Computing 2013, IFMBE Proceedings. Springer International Publishing, pp. 718–721.

Duchene, J., Marque, C., Planque, S., 1990. Uterine EMG Signal : Propagation Analysis, in: , Proceedings of the Twelfth Annual International Conference of the IEEE Engineering in Medicine and Biology Society, 1990. Presented at the , Proceedings of the Twelfth Annual International Conference of the IEEE Engineering in Medicine and Biology Society, 1990, pp. 831–832. doi:10.1109/IEMBS.1990.691421

Ellis, H., 2005. Anatomy of the uterus. Anaesth. Intensive Care Med., Neonatal / Obstetrics 6, 74–75. doi:10.1383/anes.6.3.74.62222

Escalona-Vargas, D., Govindan, R.B., Furdea, A., Murphy, P., Lowery, C.L., Eswaran, H., 2015. Characterizing the Propagation of Uterine Electrophysiological Signals Recorded with a Multi-Sensor Abdominal Array in Term Pregnancies. PloS One 10, e0140894. doi:10.1371/journal.pone.0140894

Eswaran, H., Preissl, H., Wilson, J.D., Murphy, P., Lowery, C.L., 2004. Prediction of labor in term and preterm pregnancies using non-invasive magnetomyographic recordings of uterine contractions. Am. J. Obstet. Gynecol. 190, 1598-1602-1603. doi:10.1016/j.ajog.2004.03.063

Euliano, T.Y., Marossero, D., Nguyen, M.T., Euliano, N.R., Principe, J., Edwards, R.K., 2009. Spatiotemporal electrohysterography patterns in normal and arrested labor. Am. J. Obstet. Gynecol. 200, 54.e1-7. doi:10.1016/j.ajog.2008.09.008

Fele-Zorz, G., Kavsek, G., Novak-Antolic, Z., Jager, F., 2008. A comparison of various linear and non-linear signal processing techniques to separate uterine EMG records of term and pre-term delivery groups. Med. Biol. Eng. Comput. 46, 911–922. doi:10.1007/s11517-008-0350-y

Fergus, P., Cheung, P., Hussain, A., Al-Jumeily, D., Dobbins, C., Iram, S., 2013. Prediction of Preterm Deliveries from EHG Signals Using Machine Learning. PLoS ONE 8. doi:10.1371/journal.pone.0077154

Freeman, L.C., 1978. Centrality in social networks conceptual clarification. Soc. Netw. 1, 215–239. doi:10.1016/0378-8733(78)90021-7

Friston, K.J., 1994. Functional and Effective Connectivity in Neuroimaging: A Synthesis.

Fuchs, M., Wagner, M., Kastner, J., 2007. Development of volume conductor and source models to localize epileptic foci. J. Clin. Neurophysiol. Off. Publ. Am. Electroencephalogr. Soc. 24, 101–119. doi:10.1097/WNP.0b013e318038fb3e

Fuchs, M., Wagner, M., Köhler, T., Wischmann, H.A., 1999. Linear and nonlinear current density reconstructions. J. Clin. Neurophysiol. Off. Publ. Am. Electroencephalogr. Soc. 16, 267–295.

Garfield, R.E., Chwalisz, K., Shi, L., Olson, G., Saade, G.R., 1998a. Instrumentation for the diagnosis of term and preterm labour. J. Perinat. Med. 26, 413–436.

Garfield, R.E., Hayashi, R.H., 1981. Appearance of gap junctions in the myometrium of women during labor. Am. J. Obstet. Gynecol. 140, 254–260. doi:10.5555/uri:pii:0002937881902702

Garfield, R.E., Maner, W.L., 2007. Physiology and electrical activity of uterine contractions. Semin. Cell Dev. Biol. 18, 289–295. doi:10.1016/j.semcdb.2007.05.004

Garfield, R.E., Maul, H., Shi, L., Maner, W., Fittkow, C., Olsen, G., Saade, G.R., 2001. Methods and Devices for the Management of Term and Preterm Labor. Ann. N. Y. Acad. Sci. 943, 203–224. doi:10.1111/j.1749-6632.2001.tb03803.x

Garfield, R.E., Saade, G., Buhimschi, C., Buhimschi, I., Shi, L., Shi, S.Q., Chwalisz, K., 1998b. Control and assessment of the uterus and cervix during pregnancy and labour. Hum. Reprod. Update 4, 673–695.

Garfield, R.E., Sims, S., Daniel, E.E., 1977. Gap junctions: their presence and necessity in myometrium during parturition. Science 198, 958–960.

Gondry, J., Marque, C., Duchene, J., Cabrol, D., 1993. Electrohysterography during pregnancy: preliminary report. Biomed. Instrum. Technol. Assoc. Adv. Med. Instrum. 27, 318–324.

Govindan, R.B., Siegel, E., Mckelvey, S., Murphy, P., Lowery, C.L., Eswaran, H., 2015. Tracking the changes in synchrony of the electrophysiological activity as the uterus

approaches labor using magnetomyographic technique. Reprod. Sci. Thousand Oaks Calif 22, 595–601. doi:10.1177/1933719114556484

Graczyk, S., Jezewski, J., Wrobel, J., Gacek, A., 1995. Abdominal electrohysterogram data acquisition problems and their source of origin, in: , IEEE Engineering in Medicine and Biology Society, 1995 and 14th Conference of the Biomedical Engineering Society of India. An International Meeting, Proceedings of the First Regional Conference. Presented at the , IEEE Engineering in Medicine and Biology Society, 1995 and 14th Conference of the Biomedical Engineering Society of India. An International Meeting, Proceedings of the First Regional Conference, pp. PS13-PS14. doi:10.1109/RCEMBS.1995.511701

Gramfort, A., Papadopoulo, T., Olivi, E., Clerc, M., 2010. OpenMEEG: opensource software for quasistatic bioelectromagnetics. Biomed. Eng. Online 9, 45. doi:10.1186/1475-925X-9-45

Grech, R., Cassar, T., Muscat, J., Camilleri, K.P., Fabri, S.G., Zervakis, M., Xanthopoulos, P., Sakkalis, V., Vanrumste, B., 2008. Review on solving the inverse problem in EEG source analysis. J. NeuroEngineering Rehabil. 5, 25. doi:10.1186/1743-0003-5-25

Groetsch, C.W., 1993. Inverse Problems in the Mathematical Sciences. Vieweg+Teubner Verlag, Wiesbaden.

Hall, W.S., 1994. The Boundary Element Method, Solid Mechanics and Its Applications. Springer Netherlands, Dordrecht.

Hallez, H., Vanrumste, B., Grech, R., Muscat, J., Clercq, W.D., Vergult, A., D'Asseler, Y., Camilleri, K.P., Fabri, S.G., Huffel, S.V., Lemahieu, I., 2007. Review on solving the forward problem in EEG source analysis. J. NeuroEngineering Rehabil. 4, 46. doi:10.1186/1743-0003-4-46

Hämäläinen, M.S., Ilmoniemi, R.J., 1994. Interpreting magnetic fields of the brain: minimum norm estimates. Med. Biol. Eng. Comput. 32, 35–42.

Hassan, M., Benquet, P., Biraben, A., Berrou, C., Dufor, O., Wendling, F., 2015. Dynamic reorganization of functional brain networks during picture naming. Cortex J. Devoted Study Nerv. Syst. Behav. 73, 276–288. doi:10.1016/j.cortex.2015.08.019

Hassan, M., Boudaoud, S., Terrien, J., Karlsson, B., Marque, C., 2011. Combination of Canonical Correlation Analysis and Empirical Mode Decomposition Applied to

Denoising the Labor Electrohysterogram. IEEE Trans. Biomed. Eng. 58, 2441–2447. doi:10.1109/TBME.2011.2151861

Hassan, M., Dufor, O., Merlet, I., Berrou, C., Wendling, F., 2014. EEG Source Connectivity Analysis: From Dense Array Recordings to Brain Networks. PLoS ONE 9, e105041. doi:10.1371/journal.pone.0105041

Hassan, M., Merlet, I., Mheich, A., Kabbara, A., Biraben, A., Nica, A., Wendling, F., 2016. Identification of interictal epileptic networks from dense-EEG. Brain Topography, pp. pp 1–17, 2017.

Hassan, M., Terrien, J., Alexandersson, A., Marque, C., Karlsson, B., 2010. Nonlinearity of EHG signals used to distinguish active labor from normal pregnancy contractions. Conf. Proc. Annu. Int. Conf. IEEE Eng. Med. Biol. Soc. IEEE Eng. Med. Biol. Soc. Annu. Conf. 2010, 2387–2390. doi:10.1109/IEMBS.2010.5627413

Hassan, M., Terrien, J., Karlsson, B., Marque, C., 2010. Interactions between Uterine EMG at Different Sites Investigated Using Wavelet Analysis: Comparison of Pregnancy and Labor Contractions. EURASIP J. Adv. Signal Process. 2010, 918012. doi:10.1155/2010/918012

Hassan, M.M., Terrien, J., Muszynski, C., Alexandersson, A., Marque, C., Karlsson, B., 2013. Better Pregnancy Monitoring Using Nonlinear Correlation Analysis of External Uterine Electromyography. IEEE Trans. Biomed. Eng. 60, 1160–1166. doi:10.1109/TBME.2012.2229279

Hauk, O., 2004. Keep it simple: a case for using classical minimum norm estimation in the analysis of EEG and MEG data. NeuroImage 21, 1612–1621. doi:10.1016/j.neuroimage.2003.12.018

Hauk, O., Wakeman, D.G., Henson, R., 2011. Comparison of noise-normalized minimum norm estimates for MEG analysis using multiple resolution metrics. NeuroImage 54, 1966–1974. doi:10.1016/j.neuroimage.2010.09.053

Holsheimer, J., Feenstra, B.W., 1977. Volume conduction and EEG measurements within the brain: a quantitative approach to the influence of electrical spread on the linear relationship of activity measured at different locations. Electroencephalogr. Clin. Neurophysiol. 43, 52–58.

Iams, J.D., 2003. Prediction and early detection of preterm labor. Obstet. Gynecol. 101, 402–412.

Jacob, F., 1976. The logic of life: a history of heredity. Vintage Books.

Jeong, H., Tombor, B., Albert, R., Oltvai, Z.N., Barabási, A.L., 2000. The large-scale organization of metabolic networks. Nature 407, 651–654. doi:10.1038/35036627

Jiruska, P., de Curtis, M., Jefferys, J.G.R., Schevon, C.A., Schiff, S.J., Schindler, K., 2013. Synchronization and desynchronization in epilepsy: controversies and hypotheses. J. Physiol. 591, 787–797. doi:10.1113/jphysiol.2012.239590

Kanda, S., Kuriyama, H., 1980. Specific features of smooth muscle cells recorded from the placental region of the myometrium of pregnant rats. J. Physiol. 299, 127–144.

Karlsson, B., Terrien, J., Gudmundsson, V., Steingrimsdottir, T., Marque, C., 2007. Abdominal EHG on a 4 by 4 grid: mapping and presenting the propagation of uterine contractions, in: Jarm, T., Kramar, P., Zupanic, A. (Eds.), 11th Mediterranean Conference on Medical and Biomedical Engineering and Computing 2007, IFMBE Proceedings. Springer Berlin Heidelberg, pp. 139–143.

Khalil, M., Duchene, J., Marque, C., 1997. Detection and isolation of multiple events in non stationary signal by multiscale decomposition. Application to uterine EMG. Intell. Eng. Syst. Artif. Neural Netw.

Kuriyama, H., Suzuki, H., 1976. Changes in electrical properties of rat myometrium during gestation and following hormonal treatments. J. Physiol. 260, 315–333.

Kybic, J., Clerc, M., Abboud, T., Faugeras, O., Keriven, R., Papadopoulo, T., 2005. A common formalism for the integral formulations of the forward EEG problem. IEEE Trans. Med. Imaging 24, 12–28.

Laforet, J., Rabotti, C., Mischi, M., Marque, C., 2013. Improved multi-scale modeling of uterine electrical activity. IRBM, Digital Technologies for Healthcare 34, 38–42. doi:10.1016/j.irbm.2012.12.004

Lammers, W.J., 1997. Circulating excitations and re-entry in the pregnant uterus. Pflüg. Arch. Eur. J. Physiol. 433, 287–293.

Lammers, W.J., Arafat, K., el-Kays, A., el-Sharkawy, T.Y., 1994. Spatial and temporal variations in local spike propagation in the myometrium of the 17-day pregnant rat. Am. J. Physiol. 267, C1210-1223.

Lammers, W.J.E.P., 2013. The electrical activities of the uterus during pregnancy. Reprod. Sci. Thousand Oaks Calif 20, 182–189. doi:10.1177/1933719112446082

Lammers, W.J.E.P., Mirghani, H., Stephen, B., Dhanasekaran, S., Wahab, A., Sultan, M.A.H.A., Abazer, F., 2008. Patterns of electrical propagation in the intact pregnant guinea pig uterus. Am. J. Physiol. - Regul. Integr. Comp. Physiol. 294, R919–R928. doi:10.1152/ajpregu.00704.2007

Lange, L., Vaeggemose, A., Kidmose, P., Mikkelsen, E., Uldbjerg, N., Johansen, P., 2014. Velocity and Directionality of the Electrohysterographic Signal Propagation. PLoS ONE 9, e86775. doi:10.1371/journal.pone.0086775

Lau, H. de, Rabotti, C., Oosterbaan, H.P., Mischi, M., Oei, G.S., 2014. Study protocol: PoPE-Prediction of Preterm delivery by Electrohysterography. BMC Pregnancy Childbirth 14, 192. doi:10.1186/1471-2393-14-192

Lehnertz, K., 2011. Assessing directed interactions from neurophysiological signals--an overview. Physiol. Meas. 32, 1715–1724. doi:10.1088/0967-3334/32/11/R01

López, J.D., Litvak, V., Espinosa, J.J., Friston, K., Barnes, G.R., 2014. Algorithmic procedures for Bayesian MEG/EEG source reconstruction in SPM. NeuroImage 84, 476–487. doi:10.1016/j.neuroimage.2013.09.002

Lucovnik, M., Maner, W., Chambliss, R., Blumrick, R., Balducci, J., Novak-Antolic, Z., Garfield, R., 2011. Noninvasive uterine electromyography for prediction of preterm delivery. Am. J. Obstet. Gynecol. 204, 228.e1-10. doi:10.1016/j.ajog.2010.09.024

Mansour, S., Devedeux, D., Germain, G., Marque, C., Duchene, P.J., 1996. Uterine EMG spectral analysis and relationship to mechanical activity in pregnant monkeys. Med. Biol. Eng. Comput. 34, 115–121. doi:10.1007/BF02520015

Marque, C., Diab, A., Laforêt, J., Hassan, M., Karlsson, B., 2015. Dynamic Behavior of Uterine Contractions: An Approach Based on Source Localization and Multiscale Modeling, in: Nguyen, V.-H., Le, A.-C., Huynh, V.-N. (Eds.), Knowledge and Systems Engineering, Advances in Intelligent Systems and Computing. Springer International Publishing, pp. 527–540. doi:10.1007/978-3-319-11680-8_42

Marque, C., Duchene, J., 1989. Human abdominal EHG processing for uterine contraction monitoring. Biotechnol. Read. Mass 11, 187–226.

Marque, C., Duchêne, J., Université de Technologie de Compiègne, 1987. Analyse de la dynamique des contractions utérines par électromyographie abdominale. [s.n.], S.l.

Marque, C.K., Terrien, J., Rihana, S., Germain, G., 2007. Preterm labour detection by use of a biophysical marker: the uterine electrical activity. BMC Pregnancy Childbirth 7, S5. doi:10.1186/1471-2393-7-S1-S5

Marshall, J.M., 1959. Effects of estrogen and progesterone on single uterine muscle fibers in the rat. Am. J. Physiol. -- Leg. Content 197, 935–942.

Mattout, J., Phillips, C., Penny, W.D., Rugg, M.D., Friston, K.J., 2006. MEG source localization under multiple constraints: an extended Bayesian framework. NeuroImage 30, 753–767. doi:10.1016/j.neuroimage.2005.10.037

Melton, C.E., Saldivar, J.T., 1964. Impulse velocity and conduction pathways in rat myometrium. Am. J. Physiol. -- Leg. Content 207, 279–285.

Metz, C.E., 1978. Basic principles of ROC analysis. Semin. Nucl. Med. 8, 283–298.

Mheich, A., Hassan, M., Gripon, V., Khalil, M., Berrou, C., Dufor, O., Wendling, F., 2015. A novel algorithm for measuring graph similarity: Application to brain networks, in: 2015 7th International IEEE/EMBS Conference on Neural Engineering (NER). Presented at the 2015 7th International IEEE/EMBS Conference on Neural Engineering (NER), pp. 1068–1071. doi:10.1109/NER.2015.7146812

Mideksa, K.G., Hellriegel, H., Hoogenboom, N., Krause, H., Schnitzler, A., Deuschl, G., Raethjen, J., Heute, U., Muthuraman, M., 2013. Dipole source analysis for readiness potential and field using simultaneously measured EEG and MEG signals. Conf. Proc. Annu. Int. Conf. IEEE Eng. Med. Biol. Soc. IEEE Eng. Med. Biol. Soc. Annu. Conf. 2013, 1362–1365. doi:10.1109/EMBC.2013.6609762

Miha Lucovnik, W.L.M., 2010. Noninvasive uterine electromyography for prediction of preterm delivery. Am. J. Obstet. Gynecol. 204, 228.e1-10. doi:10.1016/j.ajog.2010.09.024

Mikkelsen, E., Johansen, P., Fuglsang-Frederiksen, A., Uldbjerg, N., 2013. Electrohysterography of labor contractions: propagation velocity and direction. Acta Obstet. Gynecol. Scand. 92, 1070–1078. doi:10.1111/aogs.12190

Miller, S.M., Garfield, R.E., Daniel, E.E., 1989. Improved propagation in myometrium associated with gap junctions during parturition. Am. J. Physiol. - Cell Physiol. 256, C130–C141.

Montes-Restrepo, V., van Mierlo, P., Strobbe, G., Staelens, S., Vandenberghe, S., Hallez, H., 2014. Influence of skull modeling approaches on EEG source localization. Brain Topogr. 27, 95–111. doi:10.1007/s10548-013-0313-y

Muñoz-Martínez, E.J., 2000. Small Worlds: The Dynamics of Networks Between Order and Randomness, by Duncan J. Watts, (Princeton Studies in Complexity), Princeton University Press, 1999. $39.50 (hardcover), 262 pp. ISBN: 0-691-00541-9. (Book Reviews). Bull. Math. Biol. 62, 794–796. doi:10.1006/bulm.1999.0175

Muszynski, C., Terrien, J., Dréan, Y., Chkeir, A., Hassan, M., Marque, C., Gondry, J., 2012. [Evolution of electrohysterogram signals synchronization according to term of pregnancy: interest for preterm labor diagnosis]. Gynécologie Obstétrique Fertil. 40, 344–349. doi:10.1016/j.gyobfe.2012.02.022

Newman, M.E.J., 2002. Assortative mixing in networks. Phys. Rev. Lett. 89. doi:10.1103/PhysRevLett.89.208701

Nolte, G., Bai, O., Wheaton, L., Mari, Z., Vorbach, S., Hallett, M., 2004. Identifying true brain interaction from EEG data using the imaginary part of coherency. Clin. Neurophysiol. 115, 2292–2307. doi:10.1016/j.clinph.2004.04.029

Norwitz, E.R., Robinson, J.N., 2001. A systematic approach to the management of preterm labor. Semin. Perinatol. 25, 223–235.

Nunez, P.L., Srinivasan, R., Westdorp, A.F., Wijesinghe, R.S., Tucker, D.M., Silberstein, R.B., Cadusch, P.J., 1997. EEG coherency. I: Statistics, reference electrode, volume conduction, Laplacians, cortical imaging, and interpretation at multiple scales. Electroencephalogr. Clin. Neurophysiol. 103, 499–515.

Ohya, Y., Sperelakis, N., 1989. Fast Na+ and slow Ca2+ channels in single uterine muscle cells from pregnant rats. Am. J. Physiol. 257, C408-412.

Parkington, H.C., Harding, R., Sigger, J.N., 1988. Co-ordination of electrical activity in the myometrium of pregnant ewes. J. Reprod. Fertil. 82, 697–705. doi:10.1530/jrf.0.0820697

Pavlopoulos, G.A., Secrier, M., Moschopoulos, C.N., Soldatos, T.G., Kossida, S., Aerts, J., Schneider, R., Bagos, P.G., 2011. Using graph theory to analyze biological networks. BioData Min. 4, 10. doi:10.1186/1756-0381-4-10

Pellegrini, M., Haynor, D., Johnson, J.M., 2004. Protein interaction networks. Expert Rev. Proteomics 1, 239–249. doi:10.1586/14789450.1.2.239

Pereda, E., Quiroga, R.Q., Bhattacharya, J., 2005. Nonlinear multivariate analysis of neurophysiological signals. Prog. Neurobiol. 77, 1–37. doi:10.1016/j.pneurobio.2005.10.003

Planes, D.J.G., Morucci, J.P., Grandjean, H., Favretto, R., 1984. External recording and processing of fast electrical activity of the uterus in human parturition. Med. Biol. Eng. Comput. 22, 585–591. doi:10.1007/BF02443874

Rabotti, C., Mischi, M., 2015. Propagation of electrical activity in uterine muscle during pregnancy: a review. Acta Physiol. Oxf. Engl. 213, 406–416. doi:10.1111/apha.12424

Rabotti, C., Mischi, M., 2010. Two-dimensional estimation of the electrohysterographic conduction velocity. Conf. Proc. Annu. Int. Conf. IEEE Eng. Med. Biol. Soc. IEEE Eng. Med. Biol. Soc. Annu. Conf. 2010, 4262–4265. doi:10.1109/IEMBS.2010.5627172

Rabotti, C., Mischi, M., Beulen, L., Oei, G., Bergmans, J.W.M., 2010. Modeling and identification of the electrohysterographic volume conductor by high-density electrodes. IEEE Trans. Biomed. Eng. 57, 519–527. doi:10.1109/TBME.2009.2035440

Rabotti, C., Mischi, M., Laar, J.O.E.H. van, Oei, G.S., Bergmans, J.W.M., 2009. Inter-electrode delay estimators for electrohysterographic propagation analysis. Physiol. Meas. 30, 745. doi:10.1088/0967-3334/30/8/002

Rabotti, C., Mischi, M., Oei, S.G., Bergmans, J.W.M., 2010. Noninvasive Estimation of the Electrohysterographic Action-Potential Conduction Velocity. IEEE Trans. Biomed. Eng. 57, 2178–2187. doi:10.1109/TBME.2010.2049111

Rabotti, C., Mischi, M., van Laar, J.O.E.H., Oei, G.S., Bergmans, J.W.M., 2008. Estimation of internal uterine pressure by joint amplitude and frequency analysis of electrohysterographic signals. Physiol. Meas. 29, 829–841. doi:10.1088/0967-3334/29/7/011

Radomski, D., Grzanka, A., Graczyk, S., Przelaskowski, A., 2008. Assessment of Uterine Contractile Activity during a Pregnancy Based on a Nonlinear Analysis of the Uterine Electromyographic Signal, in: Pietka, E., Kawa, J. (Eds.), Information Technologies in Biomedicine, Advances in Soft Computing. Springer Berlin Heidelberg, pp. 325–331. doi:10.1007/978-3-540-68168-7_37

Romero, R., Gomez, R., Sepulveda, W., 1992. The uterine cervix, ultrasound and prematurity. Ultrasound Obstet. Gynecol. 2, 385–388. doi:10.1046/j.1469-0705.1992.02060384-2.x

Rubinov, M., Sporns, O., 2010. Complex network measures of brain connectivity: Uses and interpretations. NeuroImage, Computational Models of the Brain 52, 1059–1069. doi:10.1016/j.neuroimage.2009.10.003

Sanborn, B.M., 1995. Ion channels and the control of myometrial electrical activity. Semin. Perinatol. 19, 31–40.

Schlembach, D., Maner, W.L., Garfield, R.E., Maul, H., 2009. Monitoring the progress of pregnancy and labor using electromyography. Eur. J. Obstet. Gynecol. Reprod. Biol. 144 Suppl 1, S33-39. doi:10.1016/j.ejogrb.2009.02.016

Shmygol, A., Blanks, A.M., Bru-Mercier, G., Gullam, J.E., Thornton, S., 2007. Control of Uterine Ca2+ by Membrane Voltage. Ann. N. Y. Acad. Sci. 1101, 97–109. doi:10.1196/annals.1389.031

Song, J., Davey, C., Poulsen, C., Luu, P., Turovets, S., Anderson, E., Li, K., Tucker, D., 2015. EEG source localization: Sensor density and head surface coverage. J. Neurosci. Methods 256, 9–21. doi:10.1016/j.jneumeth.2015.08.015

Srinivasan, R., Winter, W.R., Ding, J., Nunez, P.L., 2007. EEG and MEG coherence: measures of functional connectivity at distinct spatial scales of neocortical dynamics. J. Neurosci. Methods 166, 41–52. doi:10.1016/j.jneumeth.2007.06.026

Terrien, J., 2005. Etude des répercussions de la position du placenta sur les caractéristiques des contractions utérines. Compiègne.

Terrien, J., Hassan, M., Marque, C., Karlsson, B., 2008. Use of piecewise stationary segmentation as a pre-treatment for synchronization measures, in: 30th Annual International Conference of the IEEE Engineering in Medicine and Biology Society, 2008. EMBS 2008. Presented at the 30th Annual International Conference of the IEEE Engineering in Medicine and Biology Society, 2008. EMBS 2008, pp. 2661–2664. doi:10.1109/IEMBS.2008.4649749

Terrien, J., Marque, C., Gondry, J., Steingrimsdottir, T., Karlsson, B., 2010. Uterine electromyogram database and processing function interface: An open standard analysis platform for electrohysterogram signals. Comput. Biol. Med. 40, 223–230. doi:10.1016/j.compbiomed.2009.11.019

Terrien, J., Rihana, S., Gondry, J., Marque, C., 2006. MODELING THE EFFECTS OF THE ELECTRODES POSITION ON THE SURFACE EMG CHARACTERISTICS. IFAC

Proc. Vol., 6th IFAC Symposium on Modeling and Control in Biomedical Systems 39, 171–176. doi:10.3182/20060920-3-FR-2912.00034

Uterus Anatomy: Overview, Gross Anatomy, Natural Variants, 2015.

van den Broek, S.P., Reinders, F., Donderwinkel, M., Peters, M.J., 1998. Volume conduction effects in EEG and MEG. Electroencephalogr. Clin. Neurophysiol. 106, 522–534. doi:10.1016/S0013-4694(97)00147-8

van den Heuvel, M.P., Sporns, O., 2013. Network hubs in the human brain. Trends Cogn. Sci. 17, 683–696. doi:10.1016/j.tics.2013.09.012

Vogel, C.R., 2002. Computational Methods for Inverse Problems. Society for Industrial and Applied Mathematics, Philadelphia, PA, USA.

Watts, D.J., Strogatz, S.H., 1998. Collective dynamics of "small-world" networks. Nature 393, 440–442. doi:10.1038/30918

Wendling, F., Bartolomei, F., Bellanger, J.J., Chauvel, P., 2001. Interpretation of interdependencies in epileptic signals using a macroscopic physiological model of the EEG. Clin. Neurophysiol. 112, 1201–1218. doi:10.1016/S1388-2457(01)00547-8

Westdrop, A.F., 1993. Volume conduction effects on correlation analysis of EEG data, in: Biomedical Engineering Conference, 1993., Proceedings of the Twelfth Southern. Presented at the Biomedical Engineering Conference, 1993., Proceedings of the Twelfth Southern, pp. 150–152. doi:10.1109/SBEC.1993.247393

WHO | Preterm birth [WWW Document], n.d. . WHO. URL http://www.who.int/mediacentre/factsheets/fs363/en/ (accessed 9.17.16).

Wikland, M., Lindblom, B., 1985. Relationship between electrical and mechanical activity of the isolated term-pregnant human myometrium. Eur. J. Obstet. Gynecol. Reprod. Biol. 20, 337–346.

Wilcoxon, F., 1992. Individual Comparisons by Ranking Methods, in: Kotz, S., Johnson, N.L. (Eds.), Breakthroughs in Statistics, Springer Series in Statistics. Springer New York, pp. 196–202. doi:10.1007/978-1-4612-4380-9_16

Wolfs, G.M., van Leeuwen, M., 1979. Electromyographic observations on the human uterus during labour. Acta Obstet. Gynecol. Scand. Suppl. 90, 1–61.

Wray, S., 1993. Uterine contraction and physiological mechanisms of modulation. Am. J. Physiol. 264, C1-18.

Yochum, M., Laforêt, J., Marque, C., 2016. An electro-mechanical multiscale model of uterine pregnancy contraction. Comput. Biol. Med. 77, 182–194. doi:10.1016/j.compbiomed.2016.08.001

Young, R.C., 2007. Myocytes, Myometrium, and Uterine Contractions. Ann. N. Y. Acad. Sci. 1101, 72–84. doi:10.1196/annals.1389.038

Zweig, M.H., Campbell, G., 1993. Receiver-operating characteristic (ROC) plots: a fundamental evaluation tool in clinical medicine. Clin. Chem. 39, 561–577.